REGULAR AND CHAOTIC DYNAMICS OF N-BEADS ON A RING

by

Bryan Cooley

A Dissertation Presented to the
FACULTY OF THE GRADUATE SCHOOL
UNIVERSITY OF SOUTHERN CALIFORNIA
In Partial Fulfillment of the
Requirements for the Degree
DOCTOR OF PHILOSOPHY
(Aerospace Engineering)

August 2006

Contents

List Of Tables

List Of Figures

Abstract

When N-beads slide along a frictionless hoop, their collision sequence gives rise to a dynamical system that can be studied via matrix products. It is of general interest to understand the distribution of velocities and the corresponding eigenvalue spectrum that a given collision sequence can produce. The problem is formulated for general N and some basic theorems are stated regarding the eigenvalues of the collision matrices and their products. The goal of this Ph.D. thesis is to study the case of three beads of masses m_1, m_2, m_3 in detail. Each collision sequence can be viewed as a billiard trajectory in a right triangle with non-standard reflection rules. Existence of families of periodic orbits are proven, and orbits that densely fill the triangle are computed. Eigenvalue distributions and position and velocity histograms are computed as a function of the restitution coefficient. Both periodic and dense collision sequences are discussed, and a series of conjectures based on computational evidence are formulated. Dense trajectories generated both from a chaotic collision sequence and a randomly ordered matrix sequence are compared via the eigenvalue distributions and autocorrelation matrices they produce.

The problem of three beads of masses m, $m-\epsilon$, $m+\epsilon$ is then studied for splitting parameter values $\epsilon \geq 0$. When $\epsilon = 0$ (three equal masses), the spectrum is discrete on the unit circle underlying the fact that the dynamics are regular [10]. For $\epsilon > 0$,

the eigenvalue spectrum produced by a deterministically chaotic trajectory is compared to spectra produced by two different stochastic problems. The first is the spectrum associated with the sequence of matrix products in which a random number algorithm is used to produce the matrix orderings. The second is the spectrum generated from a random walk process on the unit circle. We describe how to use the chaotic collision sequences as the basis for a random number generating algorithm. By an examination of both the runs and reverse arrangement tests, it is concluded that the degree of randomness produced by these sequences is equivalent to Matlab's **rand()** routine for generating random numbers.

Finally, the case where the masses are scaled so that $m_1 = 1/\epsilon$, $m_2 = 1$, $m_3 = 1 - \epsilon$, for $0 \leq \epsilon \leq 1$ is investigated. The singular limits $\epsilon = 0$ and $\epsilon = 1$ correspond to two equal mass beads colliding on the ring with a wall, and without a wall respectively. In both these cases, all solutions are periodic, and the eigenvalue distributions (around the unit circle) associated with the products of collision matrices are discrete. The regime which parametrically connects these two states, *i.e.* $0 < \epsilon < 1$ is examined, and it is shown that the eigenvalue distribution is generically uniform around the unit circle, which implies that the dynamics are no longer periodic. We characterize how the uniform spectrum collapses from continuous to discrete in the two singular limits $\epsilon \to 0$ and $\epsilon \to 1$. For the limit $\epsilon \to 0$, the distribution forms Gaussian peaks around the discrete limiting values ± 1, $\pm i$, with variances that scale in power law form as $\sigma^2 \sim \alpha\epsilon^\beta$. By contrast, as $\epsilon \to 1$, the variances converge to discrete values of ± 1 and follow a logarithmic power-law $\sigma^2 \sim \log(\epsilon^\beta)$.

Chapter 1

Introduction to Collision Theory

Consider the problem of two bodies colliding. If they collide during a very short time, the collision is called an "impact" for which the basic theory can be found, for example, in Hibbeler [12]. The line of impact is defined to be the line between the mass centers of the colliding particles. There are two general types of impacts: a central impact occurs when the two particles' mass centers travel along the line of impact, an oblique impact is when one or both of the mass centers is traveling at an angle with the line of impact. We summarize below the basic theory which leads to the formulation of the proposed Ph.D. thesis topic.

1.1 Central impacts

Consider first a central impact between two smooth particles as shown in figure 1.1. During the actual collision, which is typically assumed to be of infinitesimal duration, the two particles will deform, and an opposite but equal deformation impulse will be exerted on each particle. At maximum deformation, both particles will have zero relative motion and hence equal velocities. After maximum deformation, the two particles will return to

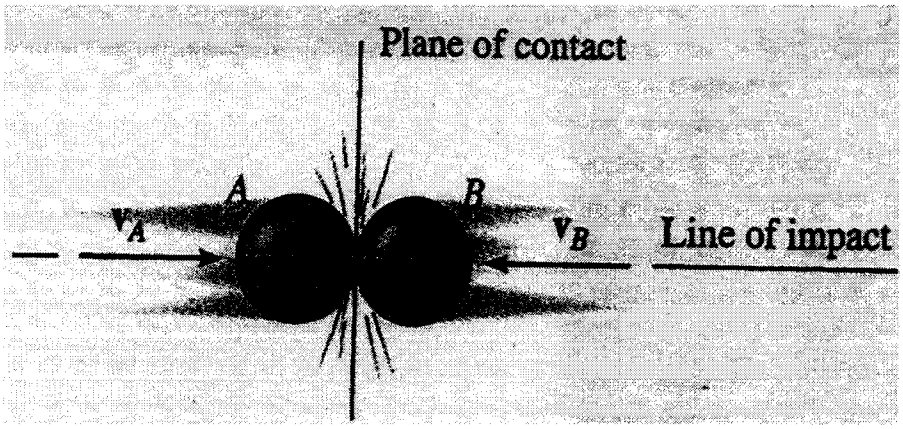

Figure 1.1: Central Collision

their original shape, and an opposite but equal restitution impulse will push the particles apart. Generally, the masses (m_A, m_B) and initial velocities $((v_A)_1, (v_B)_1)$ are known, but the velocities after the collision $((v_A)_2, (v_B)_2)$ are unknown. Thus, two equations must be used to solve for the unknown quantities. Using conservation of momentum on the system and noting that the internal impulses cancel, gives equation (1.1)

$$m_A(v_A)_1 + m_B(v_B)_1 = m_A(v_A)_2 + m_B(v_B)_2. \tag{1.1}$$

Applying the same principal to each particle individually during deformation and restitution where v is the common velocity of the particles at maximum deformation gives equations (1.2)-(1.5)

$$m_A(v_A)_1 - \int D dt = m_A v \tag{1.2}$$

$$m_A v - \int R dt = m_A(v_A)_2, \tag{1.3}$$

$$\int Ddt - m_B(v_B)_1 = m_B v, \tag{1.4}$$

$$\int Rdt - m_B v = m_B(v_B)_2. \tag{1.5}$$

The coefficient of restitution, r, is by definition the ratio of the restitution impulse to the deformation impulse

$$r = \frac{\int Rdt}{\int Ddt}. \tag{1.6}$$

Equations (1.2), (1.3), and (1.6) for particle A result in

$$r = \frac{v - (v_A)_2}{(v_A)_1 - v}. \tag{1.7}$$

Similarly, equations (1.4), (1.5), and (1.6) for particle B result in

$$r = \frac{(v_B)_2 - v}{v - (v_B)_1}. \tag{1.8}$$

Using equations (1.7)-(1.8), v can be eliminated to obtain an equation in terms of initial and final velocities

$$r = \frac{(v_B)_2 - (v_A)_2}{(v_A)_1 - (v_B)_1}. \tag{1.9}$$

Thus the coefficient of restitution is the ratio of relative velocity after an impact to that beforehand. From equation (1.6), we see that if R=D, then r=1, which corresponds to an elastic collision. If the particles remain stuck together (R=0), then r=0, which is the extreme case of an inelastic collision. General inelastic collisions are characterized by values of $0 < r < 1$.

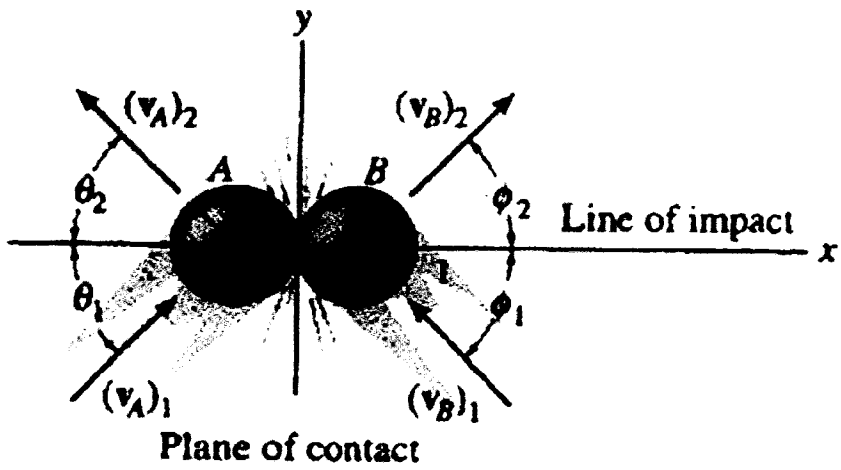

Figure 1.2: Oblique Collision

1.2 Oblique impacts

1.2.1 Symmetric particles

If the impact is oblique, velocities have direction as well as magnitude. The general case is shown in figure 1.2. If the x-axis is defined along the line of impact and the y-axis is perpendicular to that, then the impulses only occur in the x-direction. Conservation of momentum can be used on the system in the x-direction to obtain one equation, and the coefficient of restitution obtained from the relative velocity components along the x-axis gives a second equation. The final two equations are generated by conservation of momentum in the y-direction for each particle individually. Thus if initial velocities are known, these four equations can be used to solve for the four unknown final velocity components.

1.2.2 Non-symmetric particles

If the two colliding bodies are not symmetric particles, the bodies will generally not have the line connecting the mass centers coincident with the line of impact. These types of impacts are called eccentric impacts, and they often occur when a body is constrained to rotate about a fixed point. Assuming the body is smooth, the impulsive forces are still along the line of impact, but because of the offset from the mass centers, there are now moments. So, if the initial velocities are known, and one is solving for the final velocities, there needs to be two equations to solve for the two unknowns. These two equations are generated from the conservation of angular momentum and the definition of the coefficient of restitution. Proceeding as before, the resulting equations generated during deformation and restitution in figure 1.3 are

$$I_0(w_B)_1 + d\int Ddt = I_0\omega, \tag{1.10}$$

$$I_0\omega + d\int Rdt = I_0(\omega_B)_2, \tag{1.11}$$

where I_0 =moment of inertia of body B about the constrained point O

d =distance between the constrained point O and the line of impact. Substituting equations (1.10) and (1.11) into equation (1.6) and multiplying by $\frac{d}{d}$ results in

$$r = \frac{d\,(\omega_B)_2 - \omega}{d\,\omega - (\omega_B)_1} = \frac{(v_B)_2 - v}{v - (v_B)_1}. \tag{1.12}$$

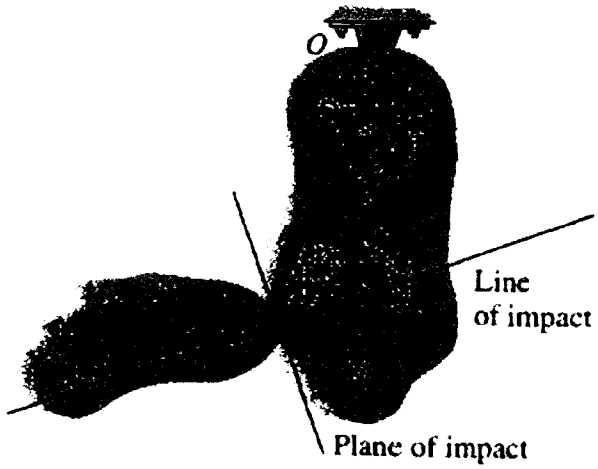

Figure 1.3: Eccentric Collision

Repeating the same procedure for particle A, one can generate an analogous equation.

$$r = \frac{d}{d}\frac{\omega - (\omega_A)_2}{(\omega_A)_1 - \omega} = \frac{v - (v_A)_2}{(v_A)_1 - v}. \tag{1.13}$$

Combining equations (1.12) and (1.13) and eliminating v, results in the familiar equation (1.9).

1.3 Impacts with friction

Keller [16] developed a method to obtain the post collision velocities if collisions occur with friction. Instead of an instantaneous impact, the impact is assumed to occur over a very small time period, t_c. From the equations of motion during the collision, the relative tangential velocity (slip velocity) is calculated at the point of contact. The time varying frictional force can then be obtained using this velocity and the law of friction, and the

integral of this force is the frictional impulse. These can then be used to obtain the velocities after a collision.

Using Keller's notation, two rigid bodies ($j = 1, 2$) collide at time $t' = 0$. The contact force exerted on body j during the collision from $t' = 0$ to $t' = t_c$ is $\frac{(-1)^j}{t_c} F(\frac{t'}{t_c})$. This results in the following equations of motion.

$$M_j \frac{dU_j}{dt'} = \frac{(-1)^j}{t_c} F(\frac{t'}{t_c}) + F_j^e(\frac{t'}{T}), \tag{1.14}$$

$$\frac{d(J_j \Omega_j)}{dt'} = \frac{(-1)^j}{t_c} R_j(\frac{t'}{T}) \times F(\frac{t'}{t_c}) + G_j^e(\frac{t'}{T}), \tag{1.15}$$

where M_j =mass of body j

J_j =central moment of inertia tensor for body j

$F_j^e(\frac{t'}{T})$ =external force applied at the body j's mass center

$G_j^e(\frac{t'}{T})$ =external torque on body j

$R_j(\frac{t'}{T})$ =vector from center of mass of body j to the point of contact

T =characteristic time on which external forces and torques vary

If $t = \frac{t'}{t_c}$, and $\epsilon = \frac{t_c}{T}$ (which tends to zero in the limit by definition of impact), equations (1.14)–(1.15) become

$$M_j \frac{dU_j}{dt} = (-1)^j F(t), \tag{1.16}$$

$$J_j \frac{d\Omega_j}{dt} = (-1)^j R_j \times F(t), \tag{1.17}$$

which hold only during the collision. Initial conditions are defined at $t = 0$ ($t' = 0$), and final conditions are defined at $t = 1$ ($t' = t_c$).

$$U_j(0) = U_j^- \qquad \Omega_j(0) = \Omega_j^-$$

$$U_j(1) = U_j^+ \qquad \Omega_j(1) = \Omega_j^+$$

Thus integrating equations (1.16)–(1.17) from $t = 0$ to $t = 1$ results in

$$[U_j] = U_j^+ - U_j^- = (-1)^j M_j^{-1} I \tag{1.18}$$

$$[\Omega_j] = \Omega_j^+ - \Omega_j^- = (-1)^j J_j^{-1}(R_j \times I) \tag{1.19}$$

where

$$I = \int_0^1 F(t)dt. \tag{1.20}$$

The contact force, F, can be split into normal and tangential components. The tangential part is due to friction, and is proportional to the normal force when sliding relative to one another.

$$F(t) = N(t)[\hat{n} + f(t)] \tag{1.21}$$

where N =normal component of F

$\hat{n}$ =unit normal to the surface at the point of contact

$f = -\mu\hat{u}_T$ by the law of friction

μ =coefficient of friction

$\hat{u}_T$ =unit vector of the tangential part of $u(t)$

The normal component of impulse exerted on body 2 up to time t is

$$\tau(t) = \hat{n} \cdot I = \int_0^t N(s)ds. \tag{1.22}$$

Keller proceeds to transform equations (1.20–1.22) into

$$(M_1^{-1} + M_2^{-1})\tau + \sum_{j=1,2} \hat{n} \cdot [(J_j^{-1}[R_j \times (\hat{n}\tau_0 - \mu \int_0^{\tau_0} \hat{u}_T(\tau')d\tau')]) \times R_j] = -u_N(0) \tag{1.23}$$

$$\frac{du_T}{d\tau} = -\mu(M_1^{-1} + M_2^{-1})\hat{u}_T(\tau) + (\sum_{j=1,2} (1 - n\hat{n}\cdot)[(J_j^{-1}[R_j \times (\hat{n} - \mu\hat{u}_T)]) \times R_j] \tag{1.24}$$

He then presents a way to solve equations 1.23–1.24 to obtain $u_T(\tau)$. This slip velocity can then be used in 1.18–1.19 and 1.21–1.22 to obtain the velocity jumps.

1.4 Iterated impact dynamics and the origin of randomness

So far, only single impacts have been discussed. However, systems that undergo repeated impacts present more interesting questions associated with the long time dynamics. Most studies of multi-particle systems assume that only two bodies collide at a time. Thus triple and higher collisions are ruled out due to the fact that they are typically rare "non-generic" events.

Murphy [22] uses conservation of momentum and energy to generate equations for the relative velocities of 3 elastic particles on a line:

$$\Delta v_i^{(j+1)} = \Delta v_i^{(j)} - 2\frac{\mu_{i,i+1}}{m_i}\Delta v_{i,i+1}^{(j)} \tag{1.25}$$

$$\Delta v_{i+1}^{(j+1)} = \Delta v_{i+1}^{(j)} + 2\frac{\mu_{i,i+1}}{m_{i+1}}\Delta v_{i,i+1}^{(j)} \tag{1.26}$$

He then points out how iterating these equations generates polynomials which can be transformed into the Chebyshev polynomials of the first kind. Using properties of these Chebyshev polynomials, he shows how the maximum number of collisions can be calculated. Along with Cohen, Murphy [23] goes one step further and proves how three identical elastic spheres in more than one dimension can collide a maximum of four times.

1.4.1 Inelastic collapse

McNamara and Young [20] use conservation of momentum and the definition of the coefficient of restitution (1.9) to generate equations for the velocities of equal masses:

$$v_1' = \frac{1}{2}(1-r)v_1 + \frac{1}{2}(1+r)v_2 \tag{1.27}$$

$$v_2' = \frac{1}{2}(1+r)v_1 + \frac{1}{2}(1-r)v_2 \tag{1.28}$$

Inelastic collapse is defined to be when the number of collisions between adjacent particles goes to infinity in a finite time such that the relative distances and velocities of the particles goes to zero. Using equations 1.27–1.28 they demonstrated using simulations how inelastic collapse occurs for three particles when the coefficient of restitution, $r <$

$r_c = 7 - 4\sqrt{3}$, and when r is greater, it takes more particles to cause inelastic collapse. They also showed that inelastic collapse is insensitive to initial conditions. In a separate work [21], they also demonstrate inelastic collapse of inelastic disks in two-dimensions starting from random initial conditions. Building upon this work, Zhou and Kadanoff [33] show that $0 \leq r < 7-4\sqrt{3}$ not only causes collapse of three particles in one-dimension, but the collapse is caused by an attractive fixed point, which causes the resulting orbit to be stable against small variations. They also show that in higher dimensions the collapse can be stable if $0 \leq r < 9 - 4\sqrt{5}$. Finally, Cipra *et al* [4] analyze the stability of periodic collision sequences as they collapse in one-dimension. Thus, "the occurrence of inelastic collapse depends on the number of particles present and the degree of inelasticity, as parameterized by the coefficient of restitution, r." [7]

1.4.2 Billiard systems

The collision system can also be viewed as a type of billiards problem. Constantin *et al* [7] convert the familiar three particles on a line to a two-dimensional billiard in a semi-enclosed space with unconventional reflection laws by viewing the relative separation space, see figure 1.4. Casting equations 1.27–1.28 in the form of equations 1.25–1.26, they arrive at a general equation for the relative velocities after a collision.

$$\Delta v_n^{'} = -r\Delta v_n \tag{1.29}$$

$$\Delta v_t^{'} = \Delta v_t + \frac{1}{2}(1+r)\Delta v_n \tag{1.30}$$

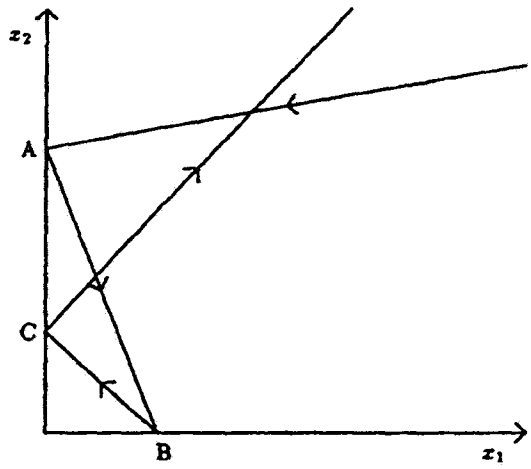

Figure 1.4: Trajectory in relative separation space

Δv_n and Δv_t are the velocity components normal and tangential to the collision axis. If the slope of the trajectory is defined as $m \equiv \Delta v_2/\Delta v_1$, then equations 1.29–1.30 can be expressed as

$$m' = -\frac{1}{r}(b+m) \quad when \quad x_1 = 0, x_2 \neq 0 \tag{1.31}$$

$$\frac{1}{m'} = -\frac{1}{r}(b+\frac{1}{m}) \quad when \quad x_1 \neq 0, x_2 = 0 \tag{1.32}$$

where $b = \frac{1}{2}(1+r)$. As seen in figure 1.4, a trajectory will alternate colliding with each axis unless it escapes. Thus iterative calculations of the slopes can be put in a recursive form. After some redefining of variables, Constantine arrives at

$$\mu_{n+2} = f(\mu_n) = -\eta\frac{\mu_n + 1}{\mu_n + 1 - \eta} \tag{1.33}$$

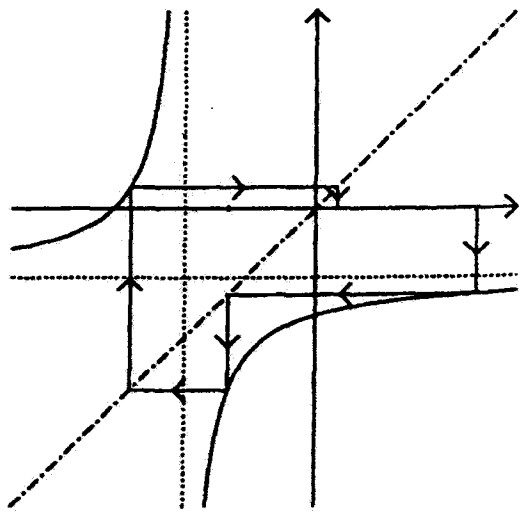

Figure 1.5: Plot of the recursive function $f(\mu)$

where $\mu_n = m_n/b$, $\eta = r/b^2$. This function describes a pair of hyperbolae seen in figure 1.5. Figure 1.5 can be used to determine regions of stability/instability, which indicate whether the particles collapse/escape.

Glashow and Mittag [10] investigate the system on a ring instead of a line. As such, the system is shown to be equivalent to a billiard ball in a triangular table. More generally, Gutkin [11] investigates two-dimensional billiards in closed polygons. Among other points, he states that two point masses on an interval are typically ergodic, but many simple questions remain about the ergodicity of polygonal billiards. He also discusses periodic orbits and various properties about these orbits. Cipra *et al* [5] also study periodic orbits and point out how they provide information on the density of states in the quantum system. These billiard problems are simple examples of chaotic systems that also have a rich family of periodic and quasi-periodic orbits embedded within their phase space.

Jepsen [13] studies nonequilibrium properties of equal mass particles in one-dimension with periodic boundary conditions, i.e. particles on a ring. He generates statistical formulas for the three particle problem and then extrapolates them to the many body system. He also uses the system's Poincaré cycle behavior to establish periodic trajectories and properties of them. This work is analogous to earlier research carried out by Tonks where it was established that, on a time average basis, a single species gas can obey statistical laws [29]. Zaslavsky [32] discusses how a system can exhibit dynamical, statistical, and chaotic tendencies. He demonstrates how classical billiard systems can have long flights, stickiness, trappings, and singular zones. Phase-space mappings can be used to quantify these interesting and diverse phenomena. He also points out how chaotic systems can possess a property of "persistence of nonequilibrium" where the dynamics never settles to a periodic or quasi-periodic orbit.

The topic of chaotic dynamics also has important connections to ergodic theory which deals with the long-term average behavior of systems. Since individual orbits in a chaotic system are exponentially unstable and hence difficult to track accurately for long times, one instead attempts to make statements about long-time averages. Boltzman's original ergodic hypothesis can be simply stated that time averages are equal to the space averages. More specifically, if the evolution of a system is given by $T : x \rightarrow x$, where T is a measure preserving transform, then this can be represented mathematically as

$$\lim_{N\rightarrow\infty} \frac{1}{N} \sum_{k=0}^{N-1} f(T^k x) = \int_X f d\mu \tag{1.34}$$

In other words, the "long-term time average along a single history (or orbit) should equal the average over all possible initial conditions, or, equivalently, the average at any other single moment over all possible histories." This can easily be seen by the simple example of rotations on a circle where $T_\alpha e^{2\pi i\theta} = e^{2\pi i(\theta+\alpha)}$. If α is rational, the orbit is periodic, and if α is irrational, the orbit is ergodic [25, 24]. This ergodicity is manifested by the fact that trajectories densely fill out the unit circle and the time average of the single trajectory equals the space average of all trajectories, namely π. A key result from ergodic theory is the Poincare Recurrence Theorem which states that almost every point in a volume preserving system must return arbitrarily close to its initial position. This is another manifestation of the fact that in ergodic systems, trajectories densely fill out their available space, a key point that will be used later in this thesis.

As briefly outlined above, the simple collision of particles becomes much more interesting when studied as a dynamical system in which repeated impacts occur. These systems, although deterministic in nature, exhibit statistical properties, and the long-time dynamics can exhibit ergodicity. Therefore, this rather simple dynamical system presents an ideal paradigm in which to study the origins of randomness in deterministic systems as well as to explore the connections between deterministic chaos and stochastic processes.

1.5 Summary of Ph.D. thesis

The thesis will be organized into four chapters. Chapter 1 introduces the background and history associated with the problem. Chapter 2 formulates the general problem of N-beads colliding on a ring. Chapter 3 explores the origins of randomness in the eigenvalue spectrum generated by a sequence of repeated collisions. Chapter 4 examines how the uniform eigenvalue distribution collapses from uniform to discrete as the singular limiting cases are approached by the splitting parameter. Details follow below.

Chapter 2: Iterated impact dynamics of N-beads on a ring

When N-beads slide along a frictionless hoop, their collision sequence gives rise to a dynamical system that can be studied via matrix products. It is of general interest to understand the distribution of velocities and the corresponding eigenvalue spectrum that a given collision sequence can produce. We formulate the problem for general N and state some basic theorems regarding the eigenvalues of the collision matrices and their products. The case of three beads of masses m_1, m_2, m_3 is studied in detail and we exploit the fact that each collision sequence can be viewed as a billiard trajectory in a right triangle with non-standard reflection rules. Families of periodic orbits are identified, as are orbits that densely fill the triangle. Eigenvalue distributions and position and velocity histograms are computed as a function of the restitution coefficient, and both periodic and dense collision sequences are discussed. Comparisons are made between the eigenvalue distributions associated with dense trajectories generated from a fixed collision sequence and spectra from matrix sequences generated from random orderings.

Chapter 3: Random number generation from chaotic impact collisions

The collision sequence produced by N-beads sliding on a frictionless hoop gives rise to a dynamical system that can be formulated as a string of matrix products [8, 10]. The matrices that form the product are written in the order in which the collisions unfold and their corresponding eigenvalues on the unit circle are treated as a discrete dynamical system. The problem of three beads of masses m, $m-\epsilon$, $m+\epsilon$ is studied in detail for splitting parameter values $\epsilon \geq 0$. When $\epsilon = 0$ (three equal masses), the spectrum is discrete on the unit circle underlying the fact that the dynamics are integrable [10]. For $\epsilon > 0$, the eigenvalue spectrum produced by a deterministically chaotic trajectory is compared to spectra produced by two different stochastic problems. The first is the spectrum associated with the sequence of matrix products in which a random number algorithm is used to produce the matrix orderings. The second is the spectrum generated from a random walk process on the unit circle. Autocorrelation coefficients for each of the models are compared.

Chapter 4: Chaotic diffusion from impact collisions on a ring

We consider the collision dynamics produced by three beads with masses (m_1, m_2, m_3) sliding without friction on a ring, where the masses are scaled so that $m_1 = 1/\epsilon$, $m_2 = 1$, $m_3 = 1-\epsilon$, for $0 \leq \epsilon \leq 1$. The singular limits $\epsilon = 0$ and $\epsilon = 1$ correspond to two equal mass beads colliding on the ring with a wall, and without a wall respectively. In both these cases, all solutions are periodic. We then examine the regime which parametrically connects these two states, i.e. $0 < \epsilon < 1$, and show that the eigenvalue distribution associated with products of collision matrices is uniform around the unit circle, which implies that the dynamics are no longer periodic. Special attention is focused on the two

singular limits $\epsilon \to 0$ and $\epsilon \to 1$ and it is shown precisely how the uniform spectrum collapses from continuous to discrete.

Chapter 2

Iterated impact dynamics of N-beads on a ring

2.1 Introduction

When N beads slide freely on a frictionless hoop, as shown in figure 2.1, their collision sequence gives rise to a dynamical system that is quite rich and not well understood. This is not surprising, since a detailed description of the impact between two objects, particularly with friction, involves many modeling assumptions as discussed in detail by Keller [16]. In the limit as the number of impacts gets large, these assumptions play an increasingly important role in the long time dynamics of the system. As described nicely in Sevryuk [26], it is a fundamental result that for N-particles colliding elastically on a *line*, the total number of collisions between particles for all initial conditions is finite and does not exceed a certain constant $C(N, m_1, m_2, \ldots, m_n)$ which can be bounded above by

$$C \leq 2\left[8N^2(N-1)\frac{m_{max}}{m_{min}}\right]$$

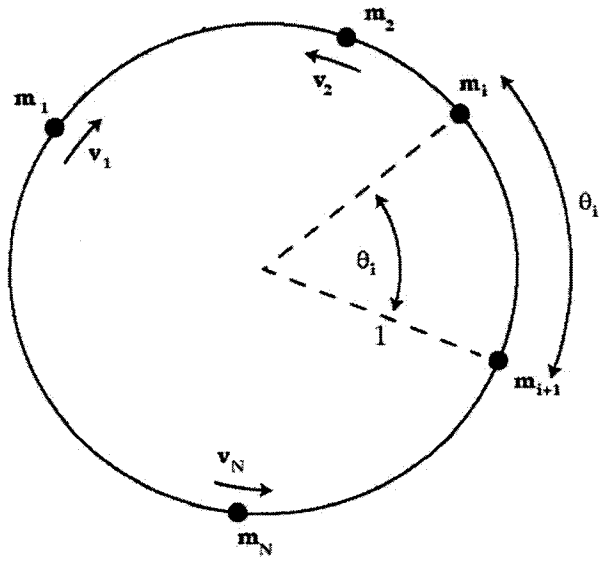

Figure 2.1: N-beads moving on a circular ring of unit radius. The beads stay ordered and each bead can only collide with one of its two neighboring beads.

where m_{max} is the largest mass and m_{min} is the smallest one. Murphy [22] examined the three particle case on a line in more detail and found, among other things, that the maximum number of collisions is the largest integer m such that

$$m_2 < (\mu_{12}\mu_{23})^{1/2}/\cos(\pi/(m-1)).$$

Here, m_2 is the mass of the central particle and μ_{12} and μ_{23} are the reduced masses of the left and right particle pairs. For elastic particles moving freely in space, the maximum number of collisions, $C(N)$, was first analyzed by Synge [28]. For N beads he obtained the bound

$$C(N) \geq \frac{1}{2}N(N-1).$$

He also proved that $C(3) = 3$ and $C(4) = 6$ for certain collision topologies. General multi-dimensional results are obtained by Murphy and Cohen [23] who prove that the maximum number of collisions of three identical beads in more than one-dimension is 4, with the conjecture that the maximum number for N beads in d-dimensions is independent of d, as long as $d \geq N - 1$.

By contrast, on a ring most initial conditions lead to an infinite number of collisions. Because of this, one is more interested in long-time properties of the dynamics which are influenced by the details of the collision assumptions one imposes. Glashow and Mittag [10] recently made the observation that the problem of three beads sliding on a frictionless ring with elastic collisions is equivalent to a standard billiard flow [18] in an acute triangular domain, where the interior angles of the triangle are functions of the masses. Earlier, Jepson [13] had calculated non-equilibrium properties of equal mass beads on a ring, particularly for the limit $N \to \infty$. If the collisions are *inelastic*, on a line (and presumably also on a ring), one has the possibility of finite-time collapse (inelastic collapse) of the system in 1D as studied by McNamara and Young [20], Constantin, Grossman, and Mungan [7], Zhou and Kadanoff [33], and clumping in 2D as studied in McNamara and Young [21]. Note that for three beads on a line, as treated in Constantin *et al* [7], since the problem can be formulated in terms of two relative distance variables and since the same 2 beads cannot collide twice in a row, a collision sequence corresponds to a string of the two relative distance variables going to zero in an alternating fashion. By contrast, for three beads on a ring, the collision sequence involves 3 relative distances and one does not know *a priori* what sequence will ensue for a given set of initial particle positions and velocities.

Other impact assumptions lead to different long time dynamics. For example, in two dimensions, a system of spinning discs was analysed by Broomhead and Gutkin [3] where the discs collide without slipping, and total energy is conserved. Such a collision assumption is an alternative way of introducing inelastic effects in the form of non-holonomic constraints. In general terms, all of these problems are versions and modifications of the original *Tonks gas of hard spheres* [29] first considered in 1936. Many related articles can be found in the collection edited by Lieb and Mattis [19]. We call this general class of problems *iterated impact* problems and our main concern is to analyze the long-time dynamics of such systems under various impact assumptions. We mention also the work of Whelan *et al* [31] who consider the iterated impact dynamics associated with two balls colliding in one dimension with gravity.

In this first section, we formulate the general problem as one of matrix products and we state some basic properties of the eigenvalues of the collision matrices and their products. Section 2 contains a description of the two-bead problem with arbitrary masses m_1, m_2, and restitution coefficient $r \in [0, 1]$. In section 3, the three-bead problem is treated. Both periodic and dense orbits are identified as trajectories in a right triangular billiard. In section 4, we describe the eigenvalue spectrum generated by periodic and dense trajectories and compare them with the spectrum generated from random matrix products, both for perfectly elastic collisions and inelastic ones (section 5).

This article is meant to elucidate some interesting questions in dynamics pertaining to the origins of randomness [32] using only elementary ideas in mechanics and mathematics, along with numerical algorithms that are simple, accurate, and can be quickly implemented on desktop systems. All of the computations shown in this paper were

performed on a laptop PC with Matlab scripts retaining double precision (16 digits) accuracy.

2.1.1 Collision assumptions

Our basic assumption in analyzing the general N-bead collision problem on a ring is that no triple or higher order collisions can occur, i.e. the dynamics unfolds through an iterated sequence of binary collisions between neighboring particles that necessarily retain their original ordering (i.e. beads cannot pass thru each other). A given mass, m_i $(2 \leq i \leq N-1)$, can only collide with its neighboring masses m_{i-1} and m_{i+1}, and cannot collide twice in a row with the same mass. In the absence of collisions, the velocities v_i, v_{i+1} and momenta $p_i = m_i v_i$, $p_{i+1} = m_{i+1} v_{i+1}$ remain unchanged. With collisions, if we first consider the perfectly elastic case, conservation of energy tells us that $KE = KE'$ i.e., that

$$m_i v_i^2 + m_{i+1} v_{i+1}^2 = m_i v_i'^2 + m_{i+1} v_{i+1}'^2$$

where v_i and v_{i+1} are the velocities of particles i and $i+1$ before collision, and v_i' and v_{i+1}' are their velocities after collision. This can be factored into

$$m_i(v_i - v_i')(v_i + v_i') = m_{i+1}(v_{i+1}' - v_{i+1})(v_{i+1} + v_{i+1}'). \tag{2.1}$$

Conservation of momentum yields

$$m_i v_i + m_{i+1} v_{i+1} = m_i v_i{}' + m_{i+1} v_{i+1}{}'$$

which can be factored into

$$m_i(v_i - v_i') = m_{i+1}(v_{i+1}' - v_{i+1}). \tag{2.2}$$

Dividing (2.1) by (2.2) gives us the relations between the relative velocities before and after collision

$$(v_i' - v_{i+1}') \equiv \Delta v_{i+1}' = -(v_i - v_{i+1}) \equiv -\Delta v_{i+1}. \tag{2.3}$$

If the collisions are inelastic, kinetic energy is lost upon each collision and we replace (2.3) with

$$\Delta v_{i+1}' = -r\Delta v_{i+1}, \tag{2.4}$$

where r is a coefficient of restitution, which for the purposes of this article has constant values lying in the range $0 \leq r \leq 1$. When $r = 1$ the collisions are perfectly elastic, otherwise they are inelastic.

2.1.2 N-bead collision matrix

Our goal is to track a given cluster of N-beads whose initial relative position vector, $\theta^{(0)}$, and initial velocity vector, $\mathbf{v}^{(0)}$, as depicted in figure 2.1, are

$$\theta^{(0)} = \begin{pmatrix} \theta_1^{(0)} \\ \theta_2^{(0)} \\ \vdots \\ \theta_N^{(0)} \end{pmatrix} \in \mathcal{R}^N, \quad \mathbf{v}^{(0)} = \begin{pmatrix} v_1^{(0)} \\ v_2^{(0)} \\ \vdots \\ v_N^{(0)} \end{pmatrix} \in \mathcal{R}^N.$$

After n collisions, the positions and velocities are

$$\theta^{(n)} = \begin{pmatrix} \theta_1^{(n)} \\ \theta_2^{(n)} \\ \vdots \\ \theta_N^{(n)} \end{pmatrix} \in \mathcal{R}^N, \quad \mathbf{v}^{(n)} = \begin{pmatrix} v_1^{(n)} \\ v_2^{(n)} \\ \vdots \\ v_N^{(n)} \end{pmatrix} \in \mathcal{R}^N.$$

Between the nth and $(n+1)$st collision, the ith bead moves freely:

$$\theta_i^{(n+1)} = v_i^{(n)} \cdot t + \theta_i^{(n)}$$

and since the hoop is closed, we have the constraint

$$\sum_{i=1}^{N} \theta_i^{(0)} = 2\pi.$$

Writing the pre- and postcollision velocities as vectors $\mathbf{v} \in \mathcal{R}^N$ and $\mathbf{v}' \in \mathcal{R}^N$ allows us to put the system in matrix form

$$\mathbf{v}' = \mathbf{M}_{i(i+1)}\mathbf{v}.$$

The collision $m_i \rightarrow m_{i+1}$ is thus governed by the $N \times N$ collision matrix $\mathbf{M_{i(i+1)}}$ where

$$\mathbf{M_{i(i+1)}} = \frac{1}{m_{i(i+1)}} \begin{pmatrix} m_{i(i+1)} & 0 & 0 & 0 & 0 & 0 & \dots \\ 0 & m_{i(i+1)} & 0 & 0 & 0 & 0 & \dots \\ \vdots & \vdots & \vdots & \vdots & \vdots & \vdots & \vdots \\ 0 & \dots & \mu_{i(i+1)} & \mu_{i+1} & 0 & 0 & \dots \\ 0 & \dots & \mu_i & \mu_{(i+1)i} & 0 & 0 & \dots \\ \vdots & \vdots & \vdots & \vdots & \vdots & \vdots & \vdots \\ 0 & 0 & 0 & \dots & \dots & \dots & m_{i(i+1)} \end{pmatrix}$$

with entries in the ith and $(i+1)$st row and columns given by

$$m_{i(i+1)} \equiv m_i + m_{(i+1)}; \quad \mu_{i(i+1)} \equiv m_i - r m_{(i+1)}; \quad \mu_{(i+1)i} \equiv m_{(i+1)} - r m_i;$$

$$\mu_i \equiv (1+r) m_i; \quad \mu_{(i+1)} \equiv (1+r) m_{(i+1)}.$$

Since the beads are on a ring, it is also possible for a collision to occur between m_1 and m_N, in which case the collision matrix is

$$\mathbf{M_{1N}} = \frac{1}{m_{1N}} \begin{pmatrix} \mu_{1N} & 0 & 0 & \dots & 0 & 0 & \mu_N \\ 0 & m_{1N} & 0 & \dots & 0 & 0 & 0 \\ 0 & 0 & m_{1N} & \dots & \dots & \dots & 0 \\ \vdots & \vdots & \vdots & \vdots & \vdots & \vdots & \vdots \\ \vdots & \vdots & \vdots & \vdots & \vdots & \vdots & \vdots \\ 0 & 0 & 0 & 0 & \dots & m_{1N} & 0 \\ \mu_1 & 0 & 0 & \dots & \dots & \dots & \mu_{N1} \end{pmatrix}.$$

The following properties of any collision matrix can be readily verified.

Proposition 1:

1. *Any two collision matrices are similar, hence have the same eigenvalues.*

2.

$$\mathrm{tr}\mathbf{M_{i(i+1)}} = \mathrm{tr}\mathbf{M_{1N}} \equiv \textstyle\sum_{j=1}^{N} \lambda_j = (N-1-r) \qquad (2.5)$$

$$\det \mathbf{M_{i(i+1)}} = \det \mathbf{M_{1N}} \equiv \Pi_{j=1}^{N} \lambda_j = -r \qquad (2.6)$$

3. *$\lambda = 1$ is an eigenvalue with algebraic multiplicity $N-1$ and $\lambda = -r$ is the remaining eigenvalue.*

4. For elastic collisions, each matrix is its own inverse, hence the eigenvalues are $\lambda = \pm 1$. If the masses are equal, the matrices are unitary.

The collision between masses m_i and m_j updates the velocity vector

$$\mathbf{v^{(n+1)}} = \mathbf{M_{ij}} \cdot \mathbf{v^{(n)}},$$

and a trajectory unfolds after n collisions from its intial velocity vector $\mathbf{v^{(0)}}$ to its final one $\mathbf{v^{(n)}}$ via the matrix equation

$$\mathbf{v^{(n)}} = \mathbf{M_{pq}} \cdots \mathbf{M_{kl}} \cdot \mathbf{M_{ij}} \cdot \mathbf{v^{(0)}}. \tag{2.7}$$

The indices on the matrices indicate that this is a sequence of collisions between m_i and m_j, m_k and m_l, ..., m_p and m_q which we denote $m_i \rightarrow m_j$, then $m_k \rightarrow m_l$, ..., and finally $m_p \rightarrow m_q$. *Valid* collision sequences for $N \geq 3$ are those in which no two particles collide two or more times in a row. Effectively this means that for the matrix products shown in eqn (2.7), identical matrices cannot be multiplied two or more times sequentially. The order in which these collisions occur is important, and generally speaking, if interchanged gives rise to a different trajectory. However, the following properties of the collision sequence *are* independent of the order.

Proposition 2: Let $\mathbf{M_n}$ denote the product of n collision matrices, i.e.

$$\mathbf{M_n} \equiv \underbrace{\mathbf{M_{pq}} \cdots \mathbf{M_{kl}} \cdot \mathbf{M_{ij}}}_{n-collisions}$$

1. $\det(\mathbf{M_n}) = \det(\mathbf{M_{pq}}) \ldots \det(\mathbf{M_{kl}}) \cdot \det(\mathbf{M_{ij}}) = (-r)^n = \Pi_{i=1}^{N} \lambda_i$

   where $(\lambda_1, \ldots, \lambda_N)$ *are the* N *eigenvalues of* $\mathbf{M_n}$

2. *The eigenvalues of the product* $\underbrace{\mathbf{M_{pq}} \cdots \mathbf{M_{kl}} \cdot \mathbf{M_{ij}}}_{n-collisions}$ *are independent of the order in which the matrices are multiplied, i.e. independent of the order in which the collisions occur.*

3. *Since* $\mathbf{M_n}$ *is a real matrix, if* $\lambda \in C$ *is a complex eigenvalue, then so is* λ^*.

These results follow from elementary matrix theory so we do not include proofs. The question arises as to whether *all* valid collision sequences are, in fact, realizable. An answer to this in the affirmative is obtained by noting that the matrix $\mathbf{M_n}$ is invertible. Hence we have the following proposition.

Proposition 3: (realizability of valid collision sequences) *Given an arbitrary final velocity vector* $\mathbf{v^{(n)}}$, *there exists an initial vector* $\mathbf{v^{(0)}}$ *such that* $\|\mathbf{v^{(0)}}\|^2 = \|\mathbf{v^{(n)}}\|^2$, $\mathbf{v^{(n)}} = \mathbf{M_n v^{(0)}}$, *and* $\mathbf{v^{(0)}} = \mathbf{M_n^{-1} v^{(n)}}$ *for any valid collision sequence.*

2.1.3 Closed orbits and periodic modes

We are now in a position to define what we call an *n-collision closed orbit* and an *n-collision periodic mode* for any finite n.

Definition: *An n-collision closed orbit associated with a valid N-bead collision sequence is one in which the initial position vector* $\theta^{(0)}$ *recurs after exactly n-collisions, i.e.* $\theta^{(0)} = \theta^{(n)}$. *An n-collision periodic mode is a closed orbit whose initial velocity vector recurs after exactly n-collisions. If we denote the initial velocity vector associated with such a mode as* $\mathbf{w}^{(0)}$, *then*

$$\mathbf{w}^{(n)} = \underbrace{\mathbf{M_{pq}} \cdots \mathbf{M_{kl}} \cdot \mathbf{M_{ij}}}_{n-matrices} \cdot \mathbf{w}^{(0)} = \mathbf{w}^{(0)} \tag{2.8}$$

The velocity vector associated with a periodic mode can be characterized as an eigenvector of a given matrix product.

Proposition 4: *For the n-collision periodic mode in equation (2.8),* $\mathbf{w}^{(0)} \in \mathcal{R}^N$ *is a right eigenvector of the* $N \times N$ *matrix* $\mathbf{M_{pq}} \cdots \mathbf{M_{kl}} \cdot \mathbf{M_{ij}}$, *with eigenvalue* $\lambda = 1$. *A given collision sequence can have at most N of these modes, in the case that* $\lambda = 1$ *is an eigenvalue of algebraic multiplicity N with geometric multiplicity N.*

An example of a closed orbit that is not periodic is shown by the closed loop generated from the first 5 collisions in figure 2.8. This mode, and all the others shown, are computed in Matlab with 16 digits of precision using a "shooting" algorithm which takes the initial position and the slope of the ray and propagates it forward using the appropriate reflection rules. There is no loss of accuracy in propagating the trajectory between collision since exact free-propagation formulas are used, and eigenvalues of the 3X3 collision matrix products for a given collision sequence can be computed to as high a degree of accuracy as desired - 16 digits of precision seemed sufficient for our purposes. This, of course, does

not address the issue of separation rate of two nearby orbits that may approach corners of the triangle giving divergent subsequent collision histories. Such questions of *stability* of orbits will be treated in a separate publication.

2.2 Two beads

Since the case $N = 2$ can be solved exactly and since two bead collisions are the fundamental interaction in the general N-bead problem, we consider this case in detail first.

2.2.1 Velocity distributions

After n collisions, the velocity vector $\mathbf{v^{(n)}}$ is given by

$$\mathbf{v^{(n)}} = \begin{pmatrix} v_1^{(n)} \\ v_2^{(n)} \end{pmatrix} = (\mathbf{M_{12}})^n \begin{pmatrix} v_1^{(0)} \\ v_2^{(0)} \end{pmatrix}$$

where

$$(\mathbf{M_{12}})^n = \left(\frac{1}{m_{12}}\right)^n \begin{bmatrix} \mu_{12} & \mu_2 \\ \mu_1 & \mu_{21} \end{bmatrix}^n$$

and we need to compute

$$\begin{bmatrix} \mu_{12} & \mu_2 \\ \mu_1 & \mu_{21} \end{bmatrix}^n .$$

Since we know that $\mathrm{tr}(\mathbf{M_{12}}) = 1 - r \equiv (\lambda_1 + \lambda_2)$ and $\det(\mathbf{M_{12}}) = -r \equiv \lambda_1 \cdot \lambda_2$, we obtain the eigenvalues of $\mathbf{M_{12}}$:

$$\lambda_1 = 1; \quad \lambda_2 = -r$$

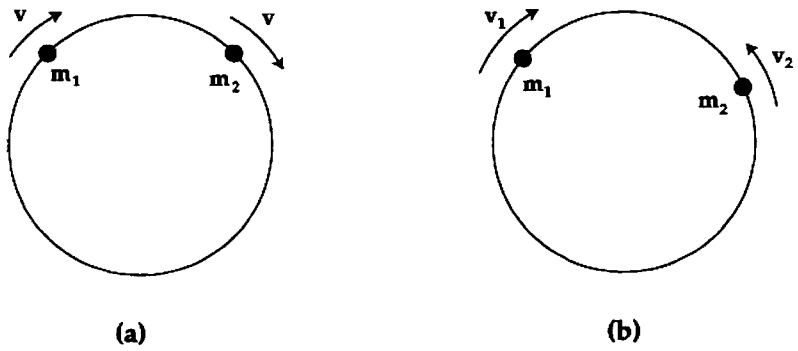

Figure 2.2: Normal modes for two-particle problem: (a) Uniformly translating mode $v = 1$; (b) Beating mode $v_1 = 1$, $v_2 = -m_1/m_2$.

with corresponding eigenvectors, or normal modes:

$$\mathbf{v}_1 = \begin{pmatrix} 1 \\ 1 \end{pmatrix} \quad \text{uniform translation,}$$

$$\mathbf{v}_2 = \begin{pmatrix} 1 \\ -\frac{m_1}{m_2} \end{pmatrix} \quad \text{beating}$$

These modes are shown in figure 2.2. Note that for elastic collisions ($r = 1$), the beating mode gives rise to a 2-collision periodic orbit since

$$\mathbf{v_2} = \mathbf{M_{12}} \cdot \mathbf{M_{12}} \cdot \mathbf{v_2} = -r\mathbf{M_{12}} \cdot \mathbf{v_2} = r^2\mathbf{v_2} = \mathbf{v_2}.$$

For inelastic collisions ($r < 1$) there are no n-collision periodic modes for any value of n.

The general solution can be obtained by diagonalizing $\mathbf{M_{12}}$:

$$\mathbf{M_{12}} = \mathbf{T}^{-1} \begin{pmatrix} 1 & 0 \\ 0 & -r \end{pmatrix} \mathbf{T}$$

giving

$$(\mathbf{M_{12}})^n = \mathbf{T}^{-1} \begin{pmatrix} 1 & 0 \\ 0 & (-r)^n \end{pmatrix} \mathbf{T}.$$

Here $\mathbf{T}$ is the invertible matrix whose rows are the eigenvectors of $\mathbf{M_{12}}$. Since a general initial velocity vector $\mathbf{v^{(0)}}$ can be written as a linear combination of the normal modes

$$\mathbf{v^{(0)}} = \alpha_1 \mathbf{v_1} + \alpha_2 \mathbf{v_2},$$

we know that after one collision, the new velocity vector becomes

$$\mathbf{v^{(1)}} = \alpha_1 \mathbf{M v_1} + \alpha_2 \mathbf{M v_2} = \alpha_1 \mathbf{v_1} - r\alpha_2 \mathbf{v_2},$$

while after two collisions, it is

$$\mathbf{v^{(2)}} = \alpha_1 \mathbf{M v_1} - r\alpha_2 \mathbf{M v_2} = \alpha_1 \mathbf{v_1} + r^2 \alpha_2 \mathbf{v_2}.$$

After n collisions, the velocity vector is

$$\mathbf{v^{(n)}} = \alpha_1 \mathbf{v_1} + (-r)^n \alpha_2 \mathbf{v_2},$$

We can always make the assumption, without loss of generality, that the total momentum is zero, i.e. $P \equiv \sum_{i=1}^{N} m_i v_i = 0$, which is equivalent to setting $\alpha_1 = 0$, i.e. eliminating the uniform translation. Also, we can assume $\alpha_2 > 0$. Then we have the simple relation

$$\mathbf{v^{(n)}} = (-r)^n \mathbf{v^{(0)}}.$$

For elastic collisions we can conclude that the velocities reverse sign upon collision, keeping their original magnitude. For inelastic collisions, the velocities reverse sign upon each collision and their magnitudes are driven monotonically to zero as $n \to \infty$.

2.2.2 Collision locations

If we denote the position of the nth collision by the vector $\mathbf{x}^{(n)}$ and the time between collision n and $n+1$ by $(\Delta t)^{(n)}$, then we have

$$\mathbf{x^{(n)}} = \mathbf{x^{(n-1)}} + (\Delta t)^{(n-1)} \mathbf{v^{(n-1)}}.$$

This gives a formula for $\mathbf{x^{(n)}}$ in terms of the initial positions and velocities:

$$\begin{aligned} \mathbf{x^{(n)}} &= \mathbf{x^{(0)}} + \left(\sum_{i=0}^{n-1} (\Delta t)^{(i)} \mathbf{M}^i \right) \mathbf{v^{(0)}} \\ &= \mathbf{x^{(0)}} + (\Delta t)^{(0)} \mathbf{v^{(0)}} + \left(\sum_{i=1}^{n-1} (\Delta t)^{(i)} \mathbf{M}^i \right) \mathbf{v^{(0)}} \end{aligned} \tag{2.9}$$

We know that

$$|v_1^{(i)}|(\Delta t)^{(i)} + |v_2^{(i)}|(\Delta t)^{(i)} = 2\pi \quad (i \geq 1)$$

which gives a formula for $(\Delta t)^{(i)}$

$$(\Delta t)^{(i)} = \frac{2\pi}{(|v_1^{(i)}| + |v_2^{(i)}|)} = \frac{2\pi}{\alpha_2 r^i (1 + \frac{m_1}{m_2})} \tag{2.10}$$

Substituting this back into (2.9) then yields

$$\mathbf{x^{(n)}} = \mathbf{x^{(1)}} + \beta \sum_{i=1}^{n-1} (-1)^i \mathbf{v^{(0)}}$$

where $\beta = 2\pi/\alpha_2(1 + \frac{m_1}{m_2})$. Hence

$$\mathbf{x}^{(1)} = \mathbf{x}^{(3)} = \mathbf{x}^{(5)} = \ldots \qquad \text{(n odd)}$$

$$\mathbf{x}^{(2)} = \mathbf{x}^{(4)} = \mathbf{x}^{(6)} = \ldots \quad = \mathbf{x}^{(1)} - \beta \mathbf{v}^{(0)} \qquad \text{(n even)}$$

Remarks

1. From this final formula we can conclude that collisions can only occur at 2 locations: $\mathbf{x^{(1)}}$ and $\mathbf{x^{(2)}}$;

2. For $r < 1$, the time between collisions (as shown in eqn (2.10)) continues to increase.

3. If our assumption that $P = 0$ is relaxed and we put back in a drift velocity, then, in general, the collision points will densely cover the circle.

Finally, notice that in terms of the relative distance variables $\theta_1(t)$ and $\theta_2(t)$, where $\theta_1(t) + \theta_2(t) = 2\pi$, the dynamics can be viewed conveniently as in figure 2.3. Figure 2.3(a) is a 'one-dimensional' billiard where the variables evolve on the hypotenuse of a

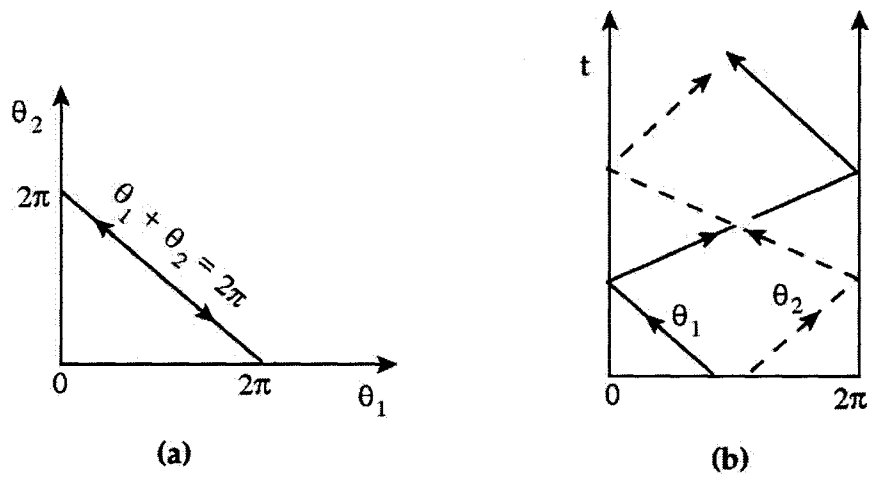

Figure 2.3: Two particles on a ring viewed as a 'one-dimensional' billiard system. (a) Evolution on the hypotenuse of a right triangle; (b) Worldlines of each bead in a vertical strip (θ_1 solid; θ_2 dashed)

right triangle, while figure 2.3(b) shows the "worldlines" of each bead. Collisions are depicted when the trajectory hits one of the sides of the vertical strip.

2.3 Three beads

We now consider the case of three beads of masses $m_1 \neq m_2 \neq m_3$ in detail. Comparisons are made with the case of equal masses where the particles are identical and simply reverse direction upon collision giving trivial dynamics. Periodic orbits as well as ones that are dense are identified.

2.3.1 Collision matrices

The dynamics of the particle system unfolds through a sequence of binary collisions between pairs m_1 and m_2; m_2 and m_3; m_1 and m_3, which gives rise to the three collision matrices $\mathbf{M_{12}}$, $\mathbf{M_{23}}$, $\mathbf{M_{13}}$:

$$\mathbf{M_{12}} = \frac{1}{m_{12}} \begin{pmatrix} \mu_{12} & \mu_2 & 0 \\ \mu_1 & \mu_{21} & 0 \\ 0 & 0 & m_{12} \end{pmatrix}$$

$$\mathbf{M_{23}} = \frac{1}{m_{23}} \begin{pmatrix} m_{23} & 0 & 0 \\ 0 & \mu_{23} & \mu_3 \\ 0 & \mu_2 & \mu_{32} \end{pmatrix}$$

$$\mathbf{M_{13}} = \frac{1}{m_{13}} \begin{pmatrix} \mu_{13} & 0 & \mu_3 \\ 0 & m_{13} & 0 \\ \mu_1 & 0 & \mu_{31} \end{pmatrix}$$

with $m_{ij} = m_i + m_j$, $\mu_{ij} = m_i - rm_j$, $\mu_i = (1 + r)m_i$. The problem is more complex than the two-bead case since it is not *a priori* clear what the collision sequence will be for any given initial velocity vector, hence the ordering of the matrix products as in equation (2.8) is not immediately available. The dynamical variables are $(\theta_1(t), \theta_2(t), \theta_3(t))$ with the constraint $\theta_1 + \theta_2 + \theta_3 = 2\pi$. As such, each dynamical collision sequence can be viewed as a trajectory moving in a right triangle with sides $\theta_1 \in [0, 2\pi]$ and $\theta_2 \in [0, 2\pi]$. A trajectory hitting the bottom leg $\theta_2 = 0$ represents a collision between m_2 and m_3,

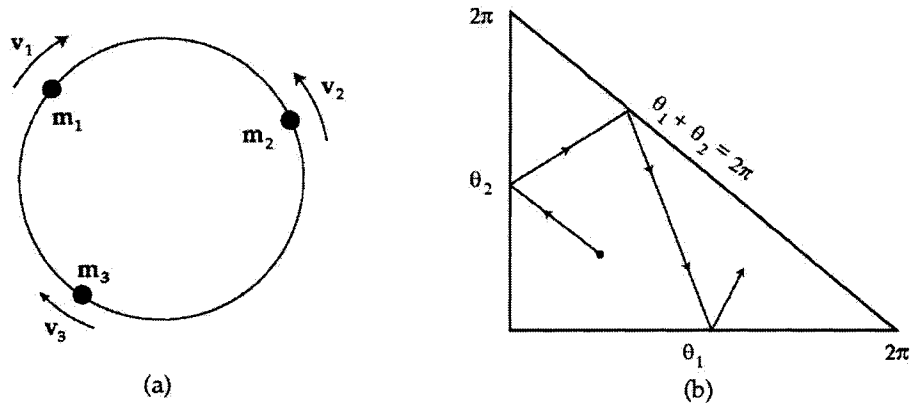

Figure 2.4: (a) Three particle motion on a ring; (b) Viewed as a trajectory in a right triangle.

a trajectory hitting the side $\theta_1 = 0$ represents a collision between m_1 and m_2, while a trajectory hitting the hypotenuse ($\theta_3 = 0$) represents a collsion between m_1 and m_3 as shown in figure 2.4.

Question: Are there collision sequences that give rise to trajectories that densely fill the triangle as $n \to \infty$? A related question is whether there are sequences that give rise to velocity distributions that densely take on values in the allowable range $v \in [v_{min}, v_{max}]$ as $n \to \infty$. These trajectories would clearly not be n-collision periodic modes for any finite n.

From a billiard dynamics perspective, what makes this problem interesting is that the reflection laws associated with the "billiard" description are non-standard [18]. As opposed to the standard billiard in a right triangle, as studied in Cipra *et al* [5] where the angle in equals the angle out, here, the reflection angles are velocity dependent. This was pointed out in Constantin *et al* [7] who were interested in the problem of inelastic

collapse on a line. In general terms, if we define velocity differences between bead i and bead j by

$$\Delta v_i = v_j - v_i$$

and if we adopt Constantin *et al*'s [7] definition of slope before collision as

$$m = \Delta v_2 / \Delta v_1,$$

then the following reflection formulas give the slopes m' after collision:

$$\begin{aligned}
\text{1-2 collision: m'=} \quad & -\tfrac{m+b_1}{r} \\
\text{2-3 collision: m'=} \quad & -\tfrac{rm}{1+mb_2} \\
\text{1-3 collision: m'=} \quad & \tfrac{\Delta v_2 + b_3 \Delta v_3}{\Delta v_1 + \frac{m_3 b_3 \Delta v_3}{m_1}}
\end{aligned}$$

where

$$\begin{aligned}
b_1 &= m_1(1+r)/(m_1+m_2) \\
b_2 &= m_2(1+r)/(m_2+m_3) \\
b_3 &= m_1(1+r)/(m_1+m_3).
\end{aligned}$$

2.3.2 Periodic trajectories

It is useful to first consider some special modes, such as those shown in figure 2.5. Figure 2.5(a) represents the case of uniform translation, 2.5(b) are the degenerate cases of three particles colliding simultaneously, while 2.5(c) represents a single closed loop state which

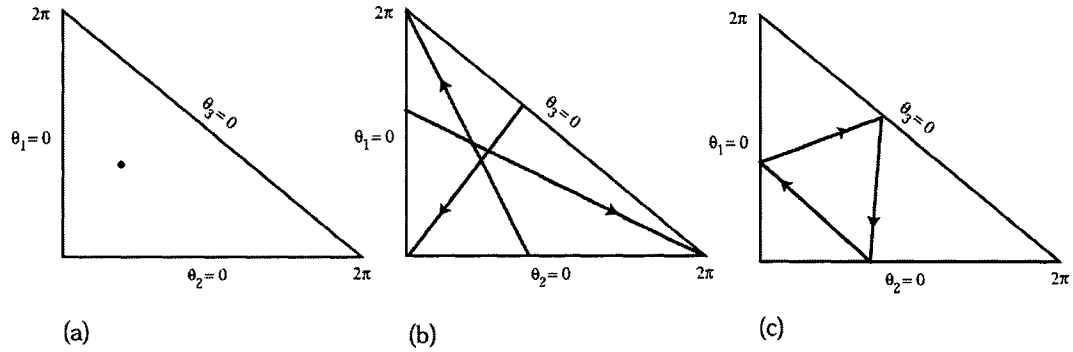

Figure 2.5: Normal modes for the three particle problem: (a) Uniformly translating mode; (b) Degenerate two-particle mode; (c) Three-particle beating mode.

is a 3-collision periodic mode. Several computed examples of these 3-collision periodic modes are shown in figure 2.6. Their existance is proven in this section. Note that to be a periodic mode, the loop must be closed (i.e. the relative positions return to their original state) and the initial slope and final slopes must match (i.e. the velocities return to their original states). They are obtained by a 'shooting method' type algorithm which takes the initial position and slope of a ray and propagates it forward using the reflection rules described previously. After 3 reflections, the ray path is compared with its initial path and, for a closed loop, if the position and slope do not coincide, adjustments are made to the initial positions and slopes until a closed loop is obtained. When closed loops are prevalent, the shooting method works well and identification of loops, as shown in figure 2.6, is straightforward.

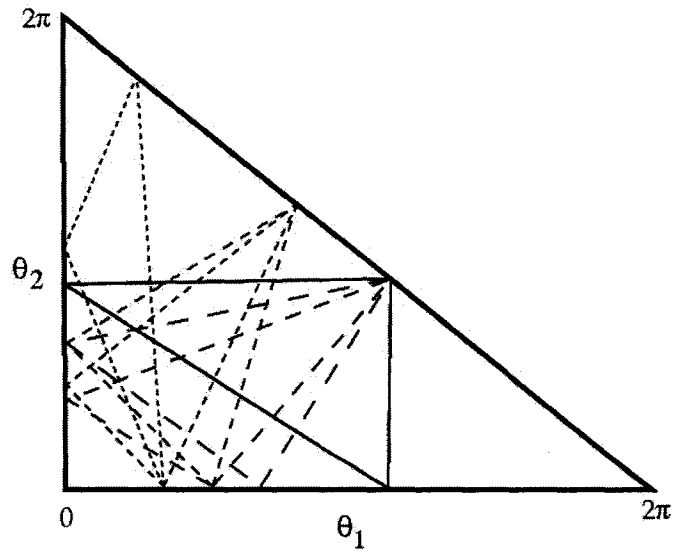

Figure 2.6: 3-collision periodic modes for various initial conditions and $r = 1$.

We represent a given collision sequence, such as a single loop mode where m_1 and m_2 collide, then m_2 and m_3 collide, then m_1 and m_3 collide as $m_1 \rightarrow m_2$; $m_2 \rightarrow m_3$; $m_1 \rightarrow m_3$. The matrix iteration proceeds as

$$\begin{aligned} \mathbf{v^{(1)}} &= \mathbf{M_{12}} \cdot \mathbf{v^{(0)}} \\ \mathbf{v^{(2)}} &= \mathbf{M_{23}} \cdot \mathbf{v^{(1)}} = \mathbf{M_{23}M_{12}} \cdot \mathbf{v^{(0)}} \\ \mathbf{v^{(3)}} &= \mathbf{M_{13}} \cdot \mathbf{v^{(2)}} = \mathbf{M_{13}M_{23}M_{12}} \cdot \mathbf{v^{(0)}} = \mathbf{v^{(0)}}. \end{aligned}$$

If we write $\mathbf{M_{123}} \equiv \mathbf{M_{13}M_{23}M_{12}}$ then

$$\mathbf{v^{(3n)}} = (\mathbf{M_{123}})^n \cdot \mathbf{v^{(0)}}$$

and the only new velocities generated are those intermediate states $\mathbf{v^{(1)}}$ and $\mathbf{v^{(2)}}$. Eigenvalues of $\mathbf{M_{ij}}$ are given by

$$\lambda_1 = 1 \quad ; \lambda_2 = 1 \quad ; \lambda_3 = -r$$

with corresponding eigenvectors

$$\mathbf{M_{12}}: \quad \xi_1 = \begin{pmatrix} 1 \\ 1 \\ 0 \end{pmatrix}, \quad \xi_2 = \begin{pmatrix} 0 \\ 0 \\ 1 \end{pmatrix}, \quad \xi_3 = \begin{pmatrix} 1 \\ -m_1/m_2 \\ 0 \end{pmatrix};$$

$$\mathbf{M_{23}}: \quad \xi_1 = \begin{pmatrix} 0 \\ 1 \\ 1 \end{pmatrix}, \quad \xi_2 = \begin{pmatrix} 1 \\ 0 \\ 0 \end{pmatrix}, \quad \xi_3 = \begin{pmatrix} 0 \\ 1 \\ -m_2/m_3 \end{pmatrix};$$

$$\mathbf{M_{13}}: \quad \xi_1 = \begin{pmatrix} 1 \\ 0 \\ 1 \end{pmatrix}, \quad \xi_2 = \begin{pmatrix} 0 \\ 1 \\ 0 \end{pmatrix}, \quad \xi_3 = \begin{pmatrix} -m_3/m_1 \\ 0 \\ 1 \end{pmatrix}.$$

For the three bead problem, we can now characterize the eigenvalues of the matrix M_n, for general n.

Proposition 5: *Let* $\mathbf{M_n}$ *be the product of* n *collision matrices for the three bead problem, with eigenvalues denoted* $\lambda_1^{(n)}$, $\lambda_2^{(n)}$, $\lambda_3^{(n)}$.

1. *The product of the three eigenvalues is given by*

$$\det(\mathbf{M_n}) = \lambda_1^{(n)} \cdot \lambda_2^{(n)} \cdot \lambda_3^{(n)} = (-1)^n \tag{2.11}$$

2. *The eigenvalues of* $\mathbf{M_n}$ *lie on the unit circle, i.e.*

$$|\lambda_j^{(n)}|^2 = 1, \quad j = 1, 2, 3. \tag{2.12}$$

3. *One eigenvalue of* $\mathbf{M_n}$ *is given by* $\lambda_1^{(n)} = (-1)^n$, *while the other two are complex conjugates*

$$\lambda_2^{(n)} = \lambda^{(n)}; \quad \lambda_3^{(n)} = \lambda^{(n*)} \tag{2.13}$$

with $|\lambda^{(n)}|^2 = 1$.

Proof:

1. $\det(\mathbf{M_n}) = \underbrace{\det(\mathbf{M_{pq}}) \ldots \det(\mathbf{M_{kl}}) \det(\mathbf{M_{ij}})}_{n-determinants} = (-1)^n$ *by Proposition 2(i).*
2. *The eigenvalues of* $\mathbf{M_n}$ *are given by*

$$\mathbf{M_n x} = \lambda \mathbf{x} \Rightarrow < \mathbf{M_n x}, \mathbf{M_n x} > = < \lambda \mathbf{x}, \lambda \mathbf{x} > = |\lambda|^2 < \mathbf{x}, \mathbf{x} > .$$

Hence,

$$|\lambda|^2 = \|\mathbf{M_n x}\|^2 / \|\mathbf{x}\|^2.$$

But

$$\|\mathbf{M_n v^{(0)}}\|^2 = \|\mathbf{v^{(n)}}\|^2 = \|\mathbf{v^{(0)}}\|^2 \Rightarrow \|\mathbf{M_n v^{(0)}}\|^2 / \|\mathbf{v^{(0)}}\|^2 = 1.$$

Letting $\mathbf{v^{(0)}} = \mathbf{x}$ *then gives* $|\lambda|^2 = 1$.

3. *From (1) we know* $\lambda_1^{(n)} \cdot \lambda_2^{(n)} \cdot \lambda_3^{(n)} = (-1)^n$. *Since* $\mathbf{M_n}$ *is real, if* λ *is an eigenvalue, so is* λ^*. *Hence, either all three eigenvalues are real, or one is real while the other two are complex conjugates lying on the unit circle. If* n *is even, this means the eigenvalues are* $1, 1, 1$ *or* $1, -1, -1$. *If one is real and the other two are complex conjugates, then the real eigenvalue is* 1. *If* n *is odd, this means the eigenvalues are* $-1, 1, 1$ *or* $-1, -1, -1$. *If one is real and the other two are complex conjugates, then the real eigenvalue is* -1.

We can now prove the existence of periodic modes for the three bead problem:

Proposition 6: (Existence of periodic modes) *For the three bead problem, when* n *is even,* $\lambda = 1$ *is an eigenvalue of* $\mathbf{M_n}$, *hence there exists a right eigenvector* $\mathbf{w^{(0)}}$ *such that* $\mathbf{M_n w^{(0)}} = \mathbf{w^{(0)}}$. *When* n *is odd,* $\lambda = -1$ *is an eigenvalue of* $\mathbf{M_n}$, *hence there exists a right eigenvector* $\mathbf{v^{(0)}}$ *such that* $\mathbf{M_n} \cdot \mathbf{M_n v^{(0)}} = \mathbf{v^{(0)}}$. *In both cases, these eigenvectors represent periodic modes associated with the underlying collision sequence forming* $\mathbf{M_n}$ *and* $\mathbf{M_n} \cdot \mathbf{M_n}$ *respectively.*

Examples of some higher order periodic modes can be found by implimenting a similar shooting algorithm as the one used for computing the lower order modes. We show in figure 2.7 several 6-collision periodic modes. 6-collision periodic modes unfold via the

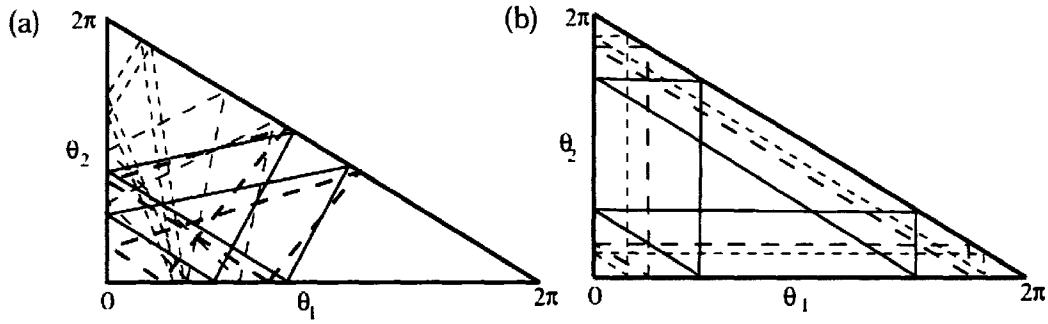

Figure 2.7: Double loop modes (6 collisions) for various initial conditions and $r = 1$ generated with Matlab script retaining 16 decimal places accuracy.

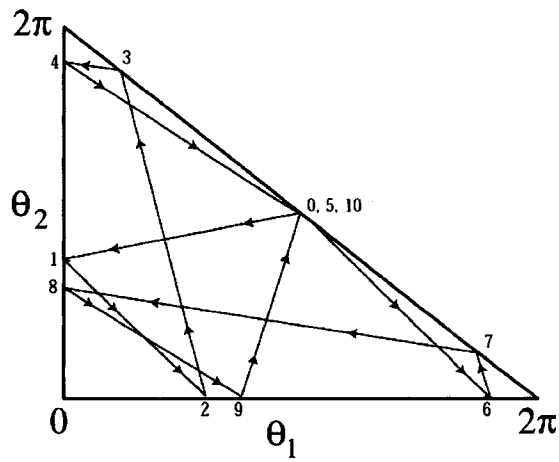

Figure 2.8: Triple loop mode (ten collisions) for $r = 1$. The numbering 0 through 10 indicates the sequence in which the collisions take place. 0 to 5 is a closed loop but not periodic, 0 to 10 is a periodic loop.

collision sequence $m_1 \rightarrow m_2$; $m_2 \rightarrow m_3$; $m_1 \rightarrow m_3$; $m_1 \rightarrow m_2$; $m_2 \rightarrow m_3$; $m_1 \rightarrow m_3$ before repeating. The governing matrix iteration equation is

$$\mathbf{v^{(6n)}} = (\mathbf{M_{123}})^{2n} \cdot \mathbf{v^{(0)}}$$

The trajectories shown in figure 2.7(b) are trajectories that begin perpendicular to a side. It is a general result of Cipra *et al* [5] that for standard billiard reflection laws in a right triangle, almost all trajectories of this type are periodic. In figure 2.8 we show a 10-collision periodic mode. This triple loop mode unfolds via the collision sequence $m_1 \rightarrow m_2$; $m_2 \rightarrow m_3$; $m_1 \rightarrow m_3$; $m_1 \rightarrow m_2$; $m_1 \rightarrow m_3$; $m_2 \rightarrow m_3$; $m_1 \rightarrow m_3$; $m_1 \rightarrow m_2$; $m_2 \rightarrow m_3$; $m_1 \rightarrow m_3$ before repeating. The governing matrix iteration equation is

$$\mathbf{v^{(10n)}} = (\mathbf{M_{1-10}})^{n} \cdot \mathbf{v^{(0)}}$$

The numbering 0 through 10 indicates the collision sequence, with 0 through 5 being a closed loop mode which is not periodic, while 0 through 10 is a periodic mode.

2.3.3 Dense trajectories

The higher the order of the loop, the more delicate it is to find the initial conditions that realize it. In general, for three unequal masses, it is possible to find collision sequences that densely fill the triangle, as shown in figure 2.9 for masses $m_1 = 1$, $m_2 = 5$, and $m_3 = 10$. After approximately 2000 collisions, the right triangle is effectively filled.

We are now in a position to formulate two conjectures regarding the density of orbits in the right triangular billiard domain.

Conjecture 1: (Density of periodic trajectories) *Consider the case of three unequal masses* $m_1 \neq m_2 \neq m_3$ *undergoing elastic collisions on a ring. The periodic orbits are dense in the right triangle* $\mathbf{T} = \{\theta = (\theta_1, \theta_2), 0 < \theta_1 < 2\pi; 0 < \theta_2 < 2\pi; \theta_1 + \theta_2 = 2\pi\}$, *i.e. given any point* $\theta^* \in \mathbf{T}$, *there exists an n-periodic mode passing through every* ϵ*-neighborhood of* θ^*, *for arbitrarily small* ϵ.

Conjecture 2: (Existence of dense non-periodic trajectories) *Consider the case of three unequal masses* $m_1 \neq m_2 \neq m_3$ *undergoing elastic collisions on a ring. There exists dense non-periodic orbits in the right triangle* $\mathbf{T} = \{\theta = (\theta_1, \theta_2), 0 < \theta_1 < 2\pi; 0 < \theta_2 < 2\pi; \theta_1 + \theta_2 = 2\pi\}$, *i.e. given any point* $\theta^* \in \mathbf{T}$, *there exists a non-periodic orbit passing through every* ϵ*-neighborhood of* θ^*, *for arbitrarily small* ϵ.

Both of these conjectures are depicted in figure 2.10. Thus, the numerical simulations indicate that the periodic modes and the non-periodic modes co-exist on 'equal footing' in the triangular billiard - either family of orbits is capable of densely filling the triangle. It is, of course, quite difficult to distinguish between an n-periodic mode with n large and a non-periodic trajectory using any numerical method, no matter how accurate, due to the finite precision associated with any computation.

2.4 Eigenvalue distribution

In this section we describe the eigenvalue distribution associated with a given sequence of collisions, both for the cases that correspond to periodic orbits (ordered sequences), as well as orbits that are not periodic. The eigenvalue distributions associated with dense

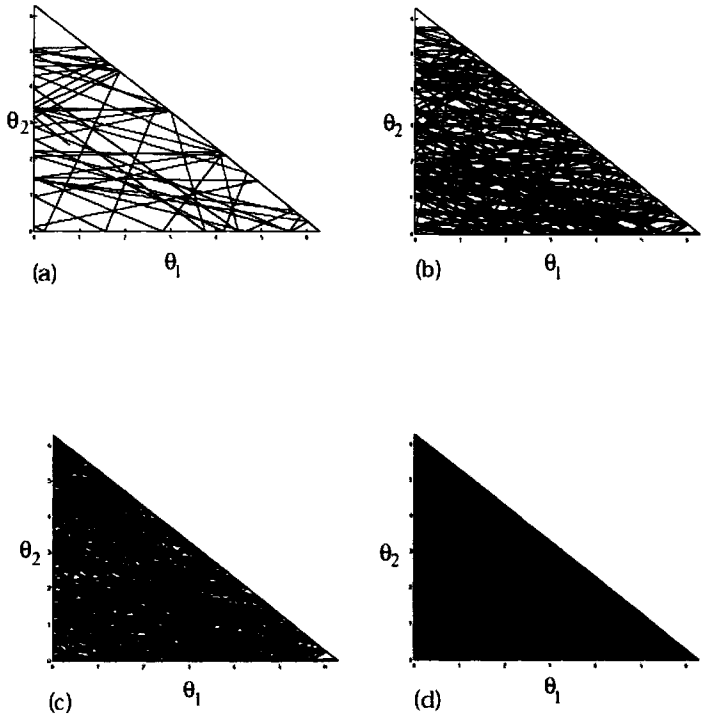

Figure 2.9: Trajectory that densely fills the triangle: (a) 50 collisions; (b) 200 collisions; (c) 400 collisions; (d) 2000 collisions.

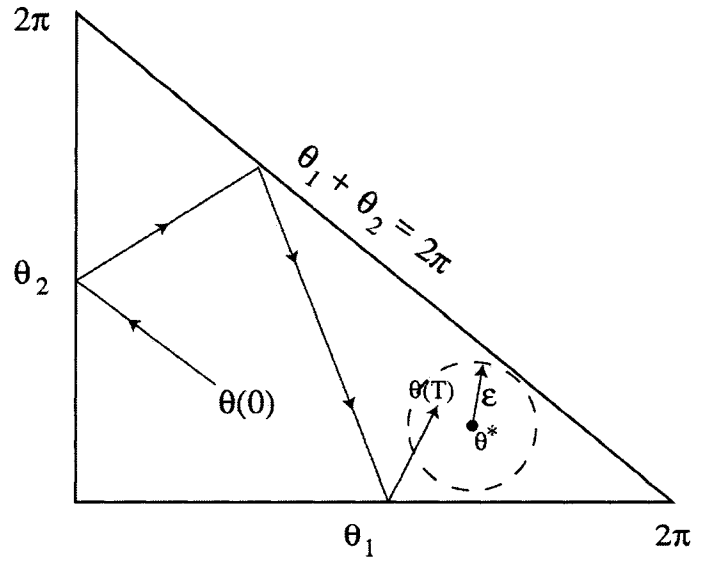

Figure 2.10: A trajectory which passes into an ϵ-neighborhood of an arbitrary point θ^* after sufficiently long time. Conjecture 1 posits the existence of periodic orbits with this property. Conjecture 2 posits the existence of non-periodic orbits with this property.

trajectories are compared with those generated from random sequences of matrix products. We start by focusing on the cases that generate periodic orbits, and we examine the eigenvalue distribution produced by their matrix products. We start by focusing on the cases that generate periodic orbits, and we examine the eigenvalue distribution produced by their matrix products. In related work of Shudo [27], the algorithmic complexity of the eigenvalue sequence of a nonintegrable Hamiltonian system is examined.

2.4.1 Ordered sequences

Several closed periodic loops were shown in figures 2.6, 2.7, and 2.8. Special initial conditions are required to generate these trajectories, which also defines a specific collision sequence, hence an ordering of matrix products. It is interesting to plot the distribution of eigenvalues as the number of collisions gets large (ideally, goes to infinity). Since eigenvectors are not pre-multiplying the matrix products, the eigenvalue distributions only depend on the specific collision sequence. Note, however, that by Proposition 2(2), it is only the specific collision matrices in the product that determines the eigenvalue distribution, not the ordering in which they occur. We have chosen three cases to focus our discussion:

Case 1: $m_1 = m_2 = m_3 = 1$ (trivial dynamics);

Case 2: $m_1 = 1, m_2 = 2, m_3 = 1$ (effective two-bead dynamics);

Case 3: $m_1 = 1, m_2 = 5, m_3 = 10$ (three-bead dynamics).

For perfectly elastic collisions, one of the eigenvalues, say $\lambda_3 = (-1)^n$. By equation (2.13), the other two are complex conjugates lying on the unit circle. The periodic case 1, shown in figure 2.11, results in a simple distribution of eigenvalues with the four discrete values:

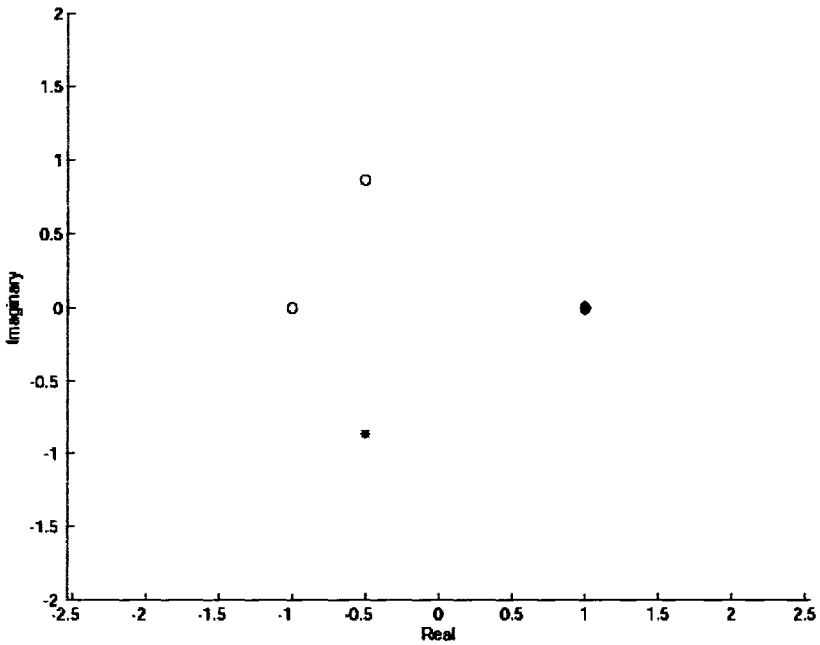

Figure 2.11: Eigenvalue spectrum associated with case 1 for an ordered sequence of 400 collsions.

$\pm 1; -\frac{1}{2} \pm i\sqrt{3}/2$. We know from Proposition 1 that in this case, each collision matrix is unitary. The next case is also quite simple, with very sparse eigenvalue distribution around the unit circle, as shown in figure 2.12. Figure 2.13 shows the spectrum from case 3 associated with an ordered sequence of collisions, also giving rise to a sparse distribution around the unit circle. This should be contrasted with case 3, shown in figure 2.14, for the collision sequence associated with the dense trajectory of figure 2.9. The eigenvalue distribution is effectively dense around the unit circle after 2000 collisions.

2.4.2 Random sequences

We contrast the previous cases with those that are generated from matrix products with collision matrices chosen from a random ordering. A random number generator is used

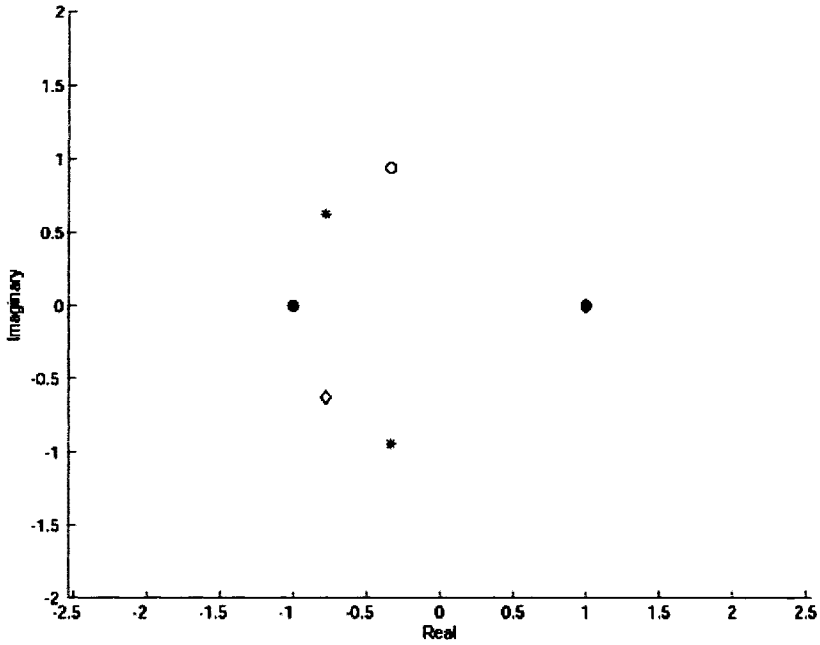

Figure 2.12: Eigenvalue spectrum associated with case 2 for an ordered sequence of 400 collsions.

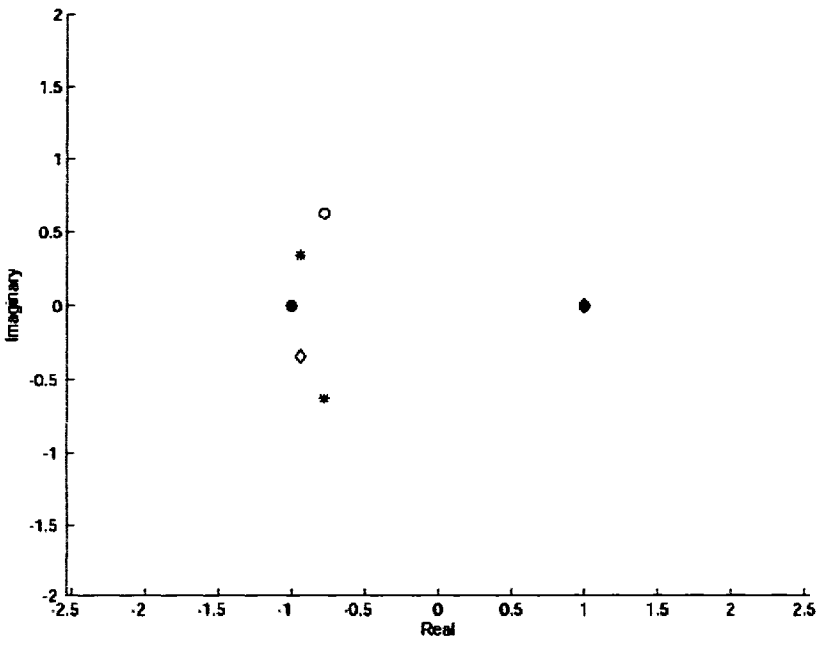

Figure 2.13: Eigenvalue spectrum associated with case 3 for an ordered sequence of 400 collsions.

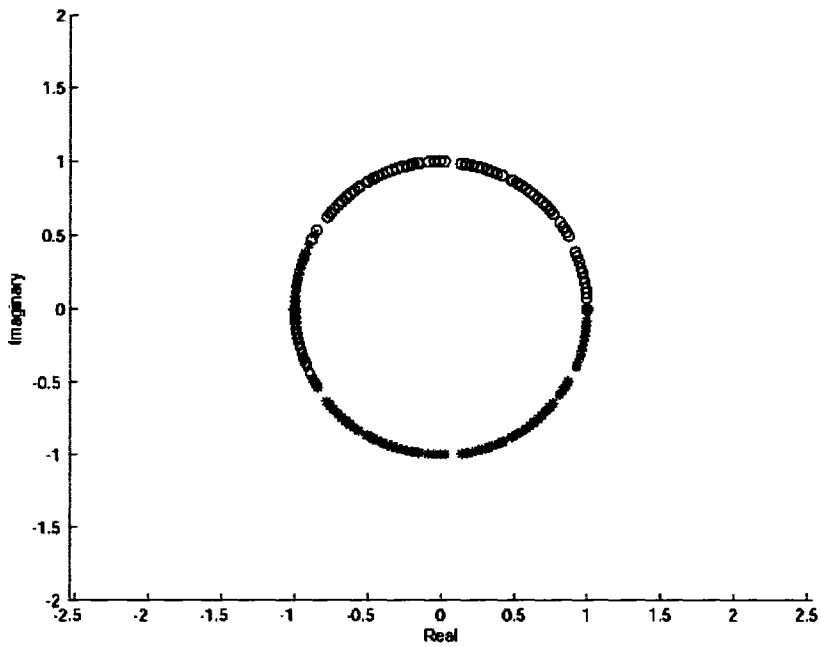

Figure 2.14: Eigenvalue spectrum associated with case 3 for the dense collision sequence shown in figure 2.9 after 400 collsions.

to choose one of the three collision matrices to form a product of up to 2000 matrices. The only rule is that no two collision matrices can be multiplied twice in a row. The three eigenvalues of the products are plotted after each matrix multiplication. Since each matrix has (at most) three eigenvalues and we track up to 2000 collsions, at most 6000 eigenvalues are plotted. The eigenvalue distribution from case 1 again reduces to the four discrete values: $\pm 1; -\frac{1}{2} \pm i\sqrt{3}/2$ shown in figure 10, despite the fact that the matrix ordering is random. The eigenvalues from case 2 begin to fill the unit circle densely, as shown in figure 2.15. This should be contrasted with the ordered case shown in figure 2.12 for the same choice of masses. Case 3 best depicts a dense distribution as shown in figure 2.16 for a typical run of 2000 collisions. The eigenvalue distribution for case 3 shown in figure 2.14 is similar to those generated from a random ordering of matrix

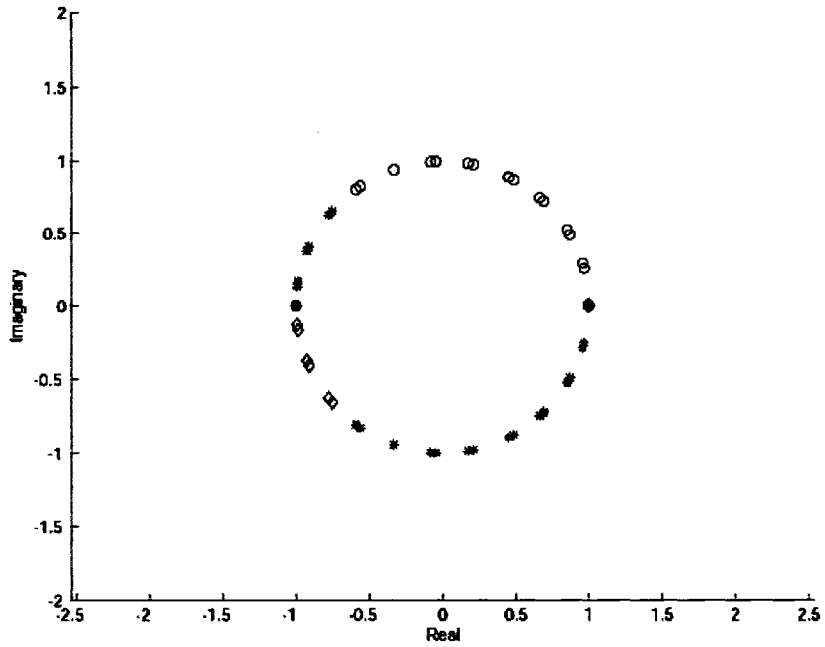

Figure 2.15: Eigenvalue spectrum associated with case 2 for a random sequence of 400 collsions.

products — both densely fill the unit circle after roughly 2000 collisions. We examine this last case in more detail in the next section.

2.4.3 Dense trajectory

With masses taken to be $m_1 = 1$, $m_2 = 5$, $m_3 = 10$, and with initial velocities $v_1 = -1$, $v_2 = 1$, $v_3 = -1$, and initial positions $\theta_1 = \pi/4$, $\theta_2 = 3\pi/4$, $\theta_3 = \pi$, the right triangle, as shown in figure 2.9, is densely filled by a trajectory. Since this sequence is not periodic and not randomly generated, a 'shooting method' was used to generate the trajectory. To examine whether this mass distribution uniformly distributes the positions and velocities, we plot histograms for these variables. Thirty-two bins were used with 2000 collisions, as shown below in figure 2.17(a),(b) for particle 1; figure 2.18(a),(b) for particle 2, and

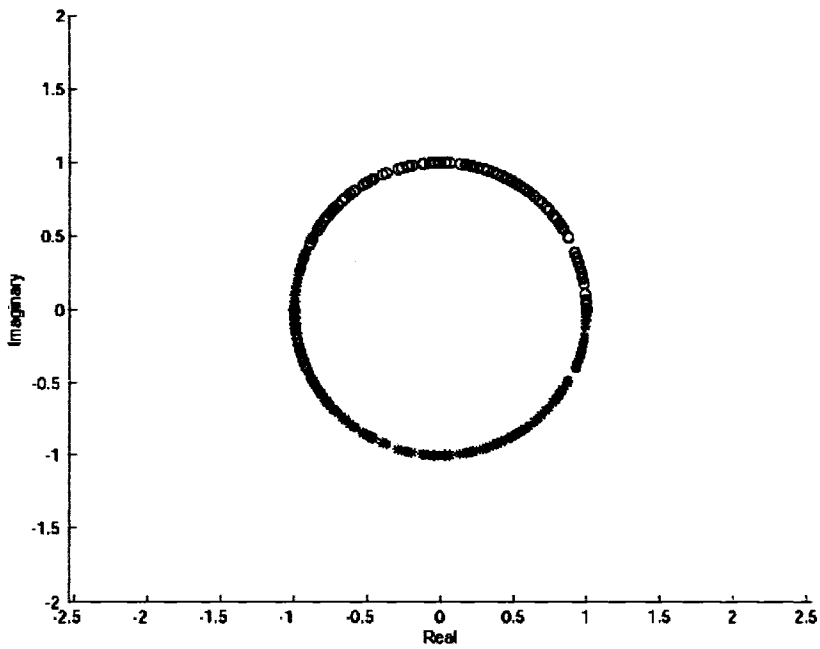

Figure 2.16: Eigenvalue spectrum associated with case 3 for a random sequence of 400 collsions.

figure 2.19(a),(b) for particle 3. The position histograms show relative positions and therefore, since they are taken at the collision time, will always have one relative distance equaling zero, causing the zero bin to be taller than the others. All show a relatively even distribution among the other bins, a conclusion enforced by choosing smaller and smaller bin sizes and increasing the number of collisions.

Conjecture 3: (Spectral density for elastic collisions) *Consider the case of three unequal masses* $m_1 \neq m_2 \neq m_3$ *undergoing elastic collisions on a ring. Given any* $\lambda_0 \in \mathcal{C}, |\lambda_0| = 1$, *there exists an eigenvalue* $\lambda \in \mathcal{C}, |\lambda| = 1$ *of* $\mathbf{M_n}$ *such that* $|\lambda - \lambda_0| < \epsilon$ *for* ϵ *arbitrarily small, for some n. See figure 2.20.*

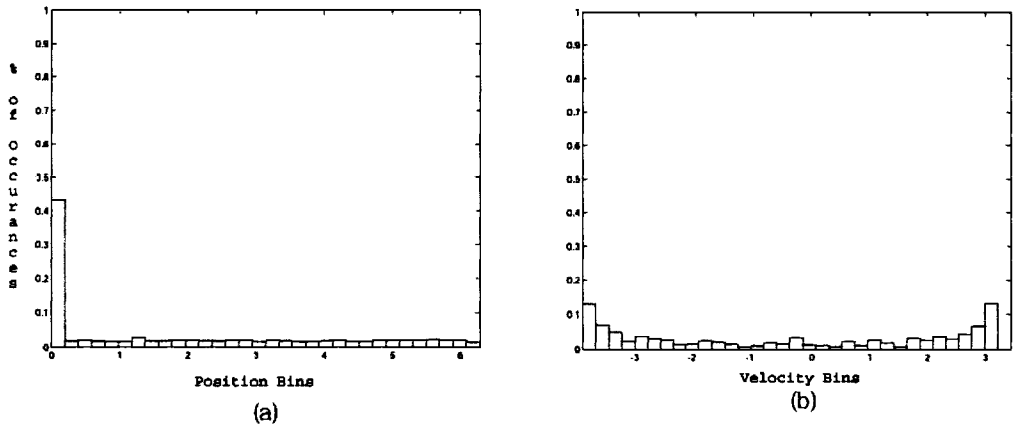

Figure 2.17: 32 bin histograms for particle 1, case 3, dense collision sequence with 2000 collisions. (a) Position histogram; (b) Velocity histogram.

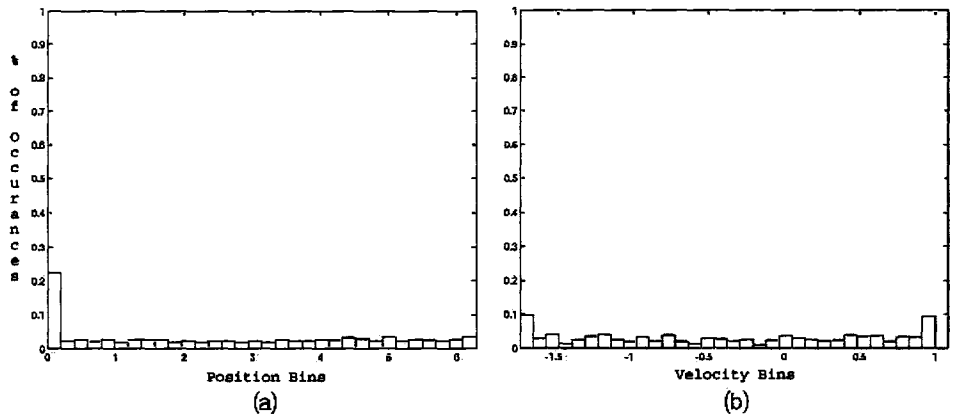

Figure 2.18: 32 bin histograms for particle 2, case 3, dense collision sequence with 2000 collisions. (a) Position histogram; (b) Velocity histogram.

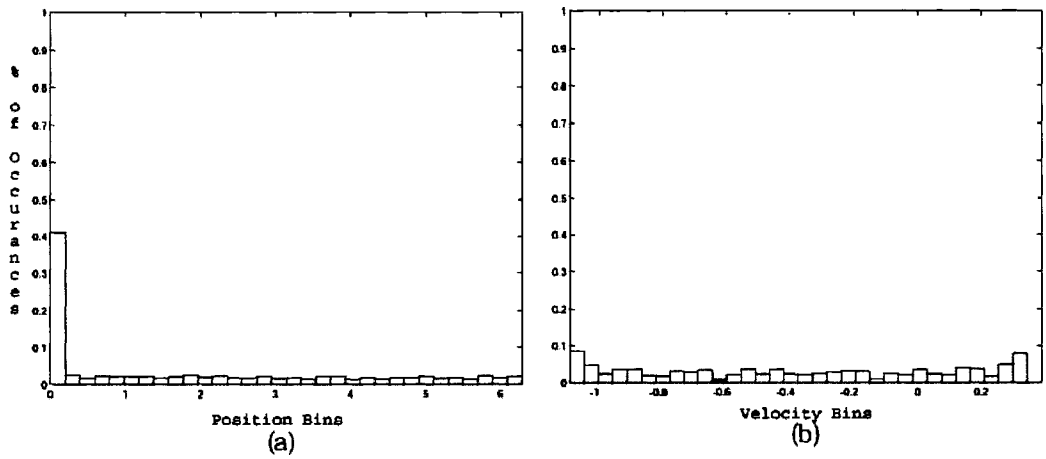

Figure 2.19: 32 bin histograms for particle 3, case 3, dense collision sequence with 2000 collisions. (a) Position histogram; (b) Velocity histogram.

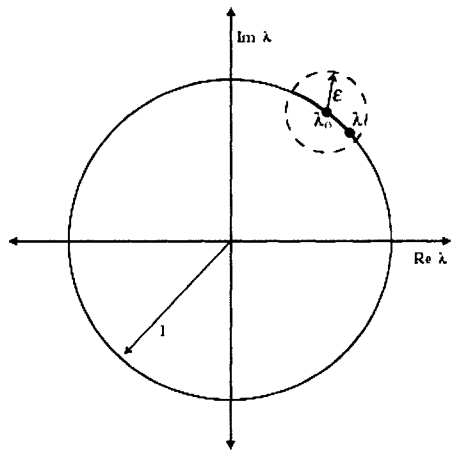

Figure 2.20: There exists an eigenvalue λ of M_n in any ϵ-neighborhood of an arbitrary point λ_0 on the unit circle.

2.4.4 Autocorrelation spectrum

We now examine the spectral sequences $\{\theta^{(1)}, \theta^{(2)}, ..., \theta^{(n)}\}$ as a discrete time series. We compare the deterministically chaotic sequence of collisions with randomly generated sequences. The two time-series are shown in figure 2.21, one corresponding to each of the two processes. To render the sequence associated with the chaotic process stationary, we form the first difference:

$$\begin{aligned} \hat{\theta}^{(i)} &\equiv \theta^{(i+1)} - \theta^{(i)} \\ &= \{\theta^{(2)} - \theta^{(1)}, \theta^{(3)} - \theta^{(2)}, ..., \theta^{(n)} - \theta^{(n-1)}\}. \end{aligned}$$

Autocorrelation coefficients measure the degree of correlation between observations in a time series that are k steps apart. The autocorrelation coefficients (r_k) can be caluclated as follows:

$$c_k = \frac{1}{N} \sum_{t=1}^{N-k} (x_t - \bar{x}) \tag{2.14}$$

$$r_k = c_k / c_0. \tag{2.15}$$

Plotting the autocorrelation coefficients versus the lag k gives the autocorrelation spectrum, as shown in figure 2.22. Typically, only values of k up to $N/4$ are used and most fall between the bounds $\pm 2/\sqrt{N}$. The autocorrelation matrix $\mathbf{P}$ is constructed as

$$\mathbf{P} = \begin{pmatrix} 1 & r_1 & r_2 & r_3 & \cdots & \cdots & r_k \\ r_1 & 1 & r_1 & r_2 & r_3 & \cdots & r_{k-1} \\ r_2 & r_1 & 1 & r_1 & r_2 & \cdots & r_{k-2} \\ \vdots & \vdots & \vdots & \vdots & \vdots & \vdots & \vdots \\ \vdots & \vdots & \vdots & \vdots & \vdots & \vdots & \vdots \\ r_k & r_{k-1} & r_{k-2} & \cdots & \cdots & \cdots & 1 \end{pmatrix}$$

The matrix is hermitian and thus has only positive real eigenvalues. The eigenvalues (histogrammed) are shown in figure 2.23 along with the corresponding Gaussian fits to the data. Our conjecture based on the comparisons between these two systems is formulated below.

Conjecture 4: (Statistical equivalence of chaotic and random spectral sequences) *The time series (appropriately filtered to render it stationary) generated from the spectrum associated with a chaotic collision sequence of matrices is statistically indistinguishable from that generated from a sequence of randomly ordered collision matrices.*

2.4.5 Inelastic collisions

If the coefficient of restitution is reduced from unity making the collisions inelastic, the eigenvalues no longer lie on the unit circle. We focus again on the same three cases. We first show case 1 for $r = 0.99$ and $r = 0.7$ where the collision sequences are ordered. Figure

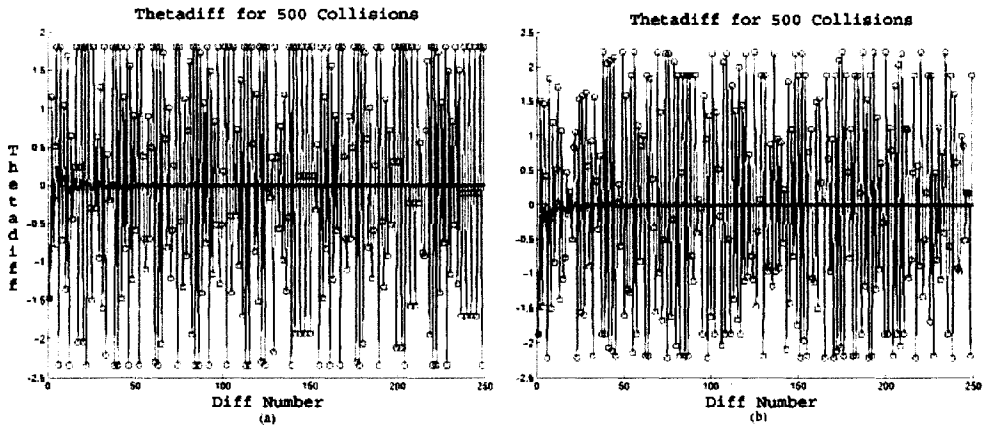

Figure 2.21: Time series associated with the chaotic spectral sequence and a random spectral sequence. (a) First order differenced spectral timeseries associated with a chaotic collision sequence; (b) Spectral timeseries associated with a random sequence of collision matrices.

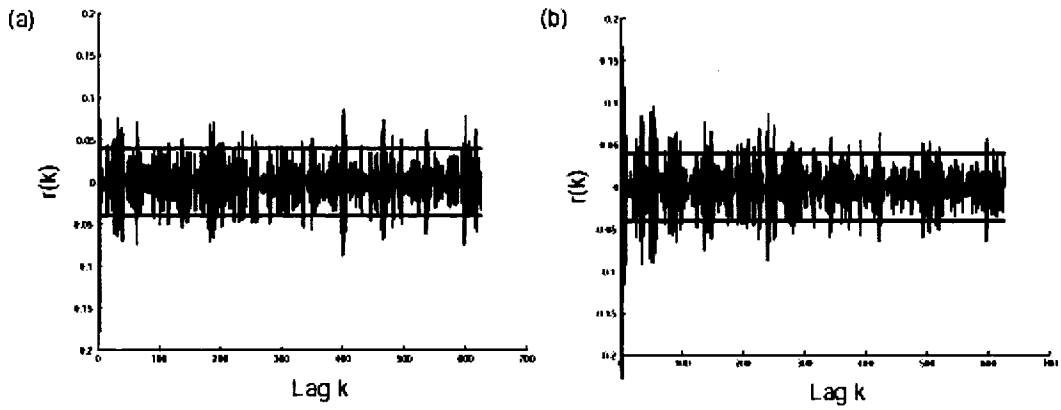

Figure 2.22: Autocorrelation coefficients for the two different processes. (a) Chaotic process; (b) Random matrix process.

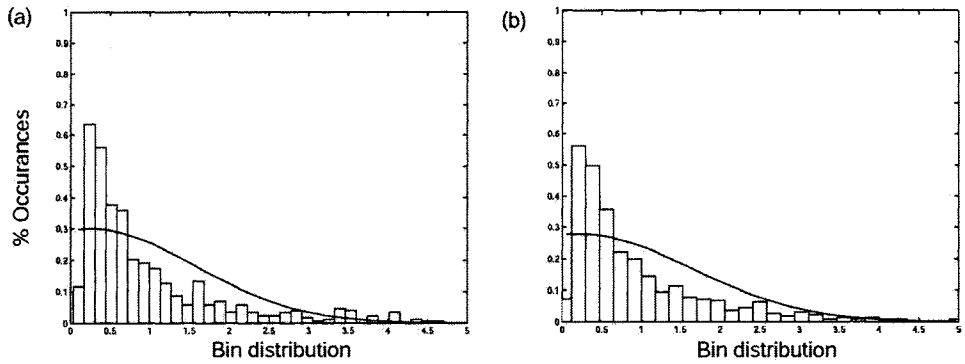

Figure 2.23: Histograms and Gaussian fits for the eigenvalues of the P matrix for the two processes. (a) Chaotic process; (b) Random matrix process.

2.24 (a),(b) shows that the eigenvalues move inward off the unit circle but otherwise stay on fixed rays in the complex plane. Case 2 with the same two values of r, again for ordered sequences, is shown in figure 2.25(a),(b). Again, the eigenvalues move inward with ray angles well defined, as are those of case 3 shown in figure 2.26(a),(b) for ordered sequences. Figures 2.27 and 2.28 depict cases 2 and 3 when the matrix products are randomly ordered. In both cases, the spectrum fills out more completely with just 400 collisions. With smaller values of r, the spectrum collapses more quickly to the axes. Figure 2.29 shows case 3 for the dense sequence of collisions, as in figure 2.14. The similarities between the spectrum associated with the dense trajectory and the one generated with a random ordering are clear.

Conjecture 5: (Spectral density for inelastic collisions) *Consider the case of three unequal masses* $m_1 \neq m_2 \neq m_3$ *undergoing inelastic collisions on a ring. Given any* $\lambda_0 \in C, |\lambda| < 1$, *there exists an eigenvalue* $\lambda \in C$ *of* $\mathbf{M_n}$ *such that* $|\lambda - \lambda_0| < \epsilon$ *for* ϵ *arbitrarily small, for some n. See figure 2.30.*

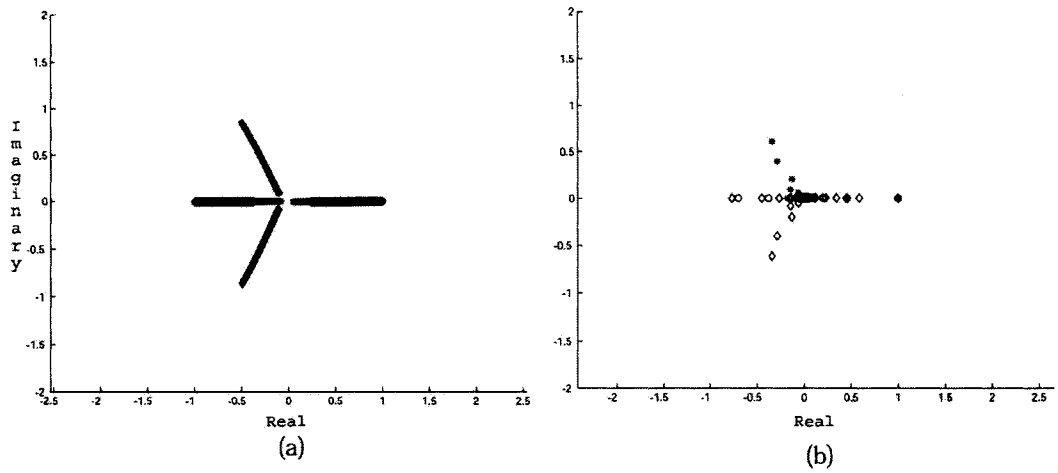

Figure 2.24: Inelastic eigenvalue spectrum for case 1, 400 ordered collisions. (a) $r = 0.99$; (b) $r = 0.7$.

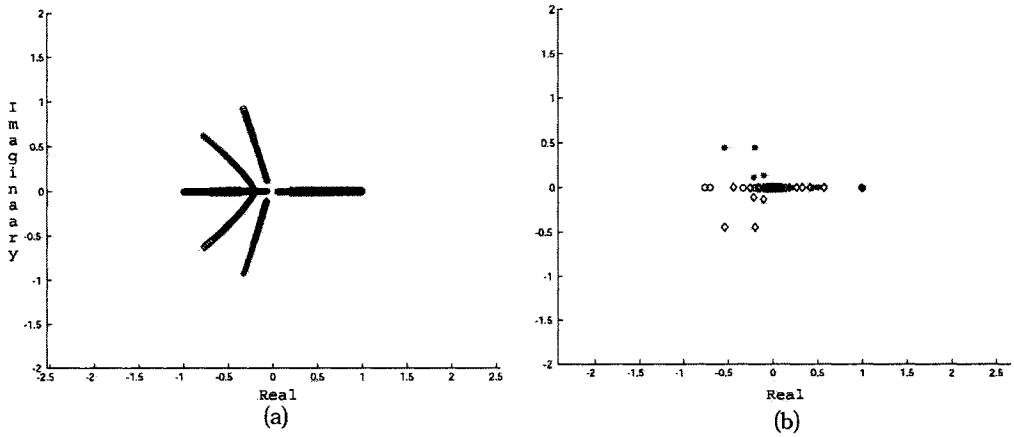

Figure 2.25: Inelastic eigenvalue spectrum for case 2, 400 ordered collisions. (a) $r = 0.99$; (b) $r = 0.7$.

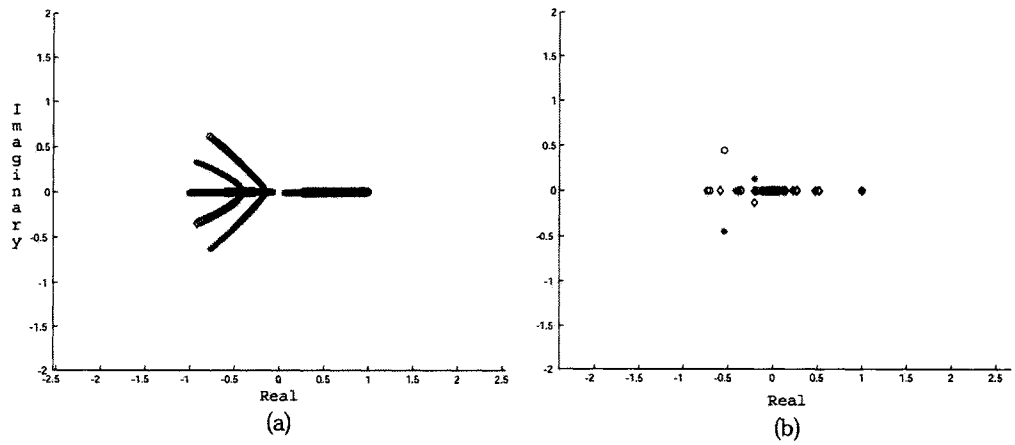

Figure 2.26: Inelastic eigenvalue spectrum for case 3, 400 ordered collisions. (a) $r = 0.99$; (b) $r = 0.7$.

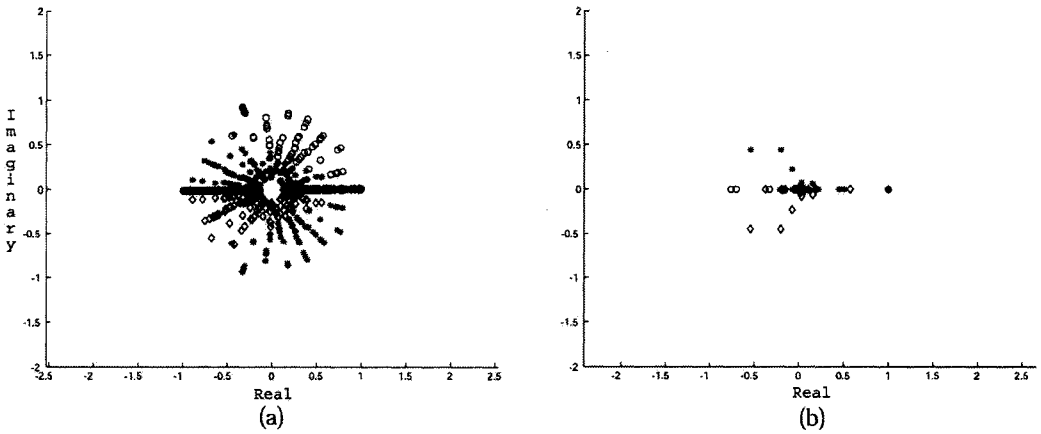

Figure 2.27: Inelastic eigenvalue spectrum for case 2, 400 random collisions. (a) $r = 0.99$; (b) $r = 0.7$.

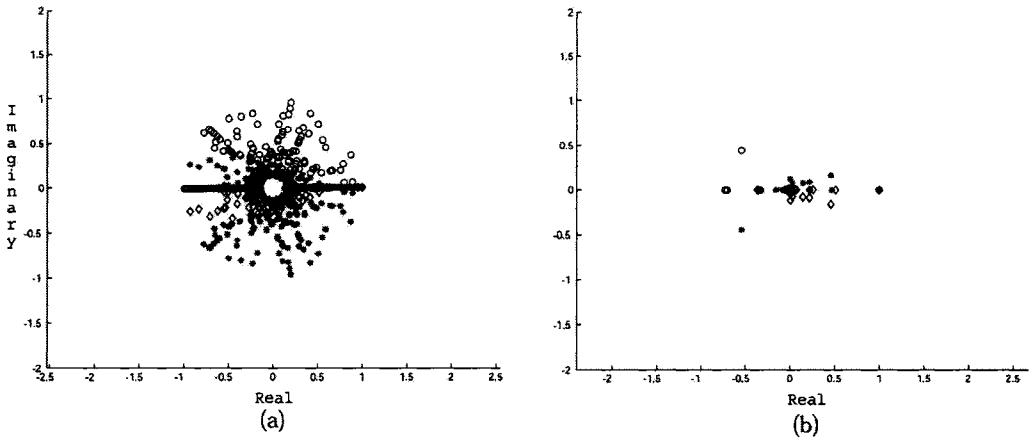

Figure 2.28: Inelastic eigenvalue spectrum for case 3, 400 random collisions. (a) $r = 0.99$; (b) $r = 0.7$.

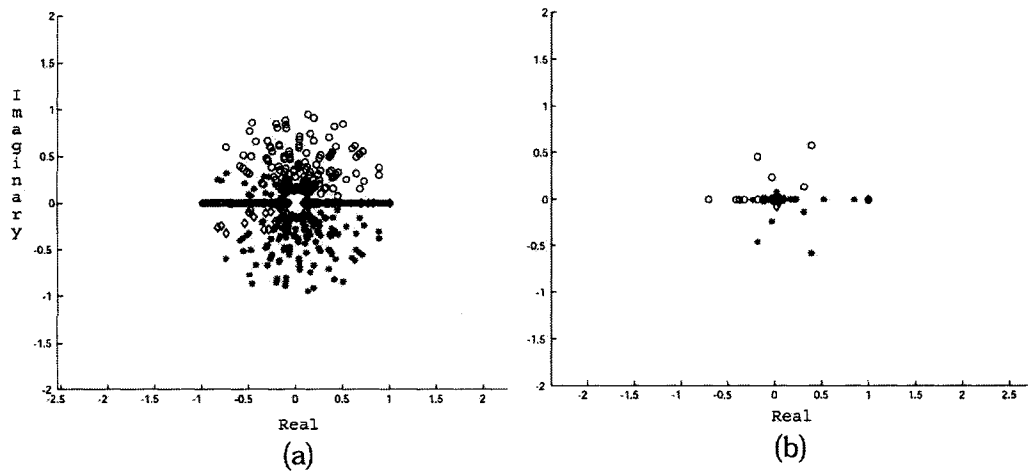

Figure 2.29: Inelastic eigenvalue spectrum for case 3, dense trajectory, 400 collisions. (a) $r = 0.99$; (b) $r = 0.7$.

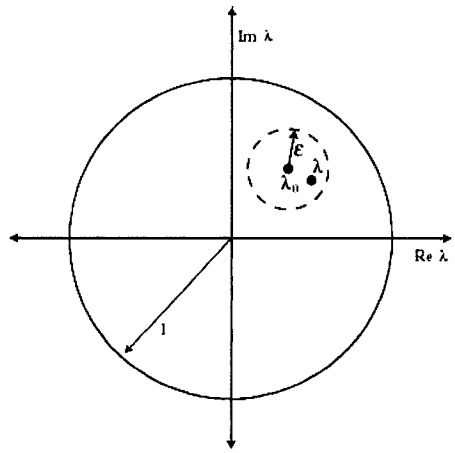

Figure 2.30: Dense spectrum inside the unit circle. There exists an eigenvalue λ of M_n in every ϵ-neighborhood of λ_0 inside the unit circle, for inelastic collisions.

2.5 Discussion

Although special mass values and initial conditions for three beads on a ring can generate ordered dynamics, the more typical case is one in which a dense distribution of particle positions and velocities is achieved. The canonical case for this arises when $m1 \neq m2 \neq m3$ which we have described in some detail. Analysis of the eigenvalue distributions associated with sequences of matrix products is the key tool in analyzing the long-time dynamics associated with these iterated impact problems. Asking how many collisions it takes for the eigenvalue spectrum to be indistinguishable from a random one is similar to asking how many shuffles it takes to mix a deck of cards [17] which leads to the separate and intriguing question of whether the 3-bead collision problem, because of its computational simplicity, could be useful as the basis for a random number generation algorithm that would be competitive with the host of pseudo-random routines currently in use [6]. Given a "seed" collision between two of the three beads (say m_1 and m_2), the subsequent chaotic sequence of collisions can be encoded as a string of 0's and 1's

by assigning a 0 or 1 to each of the two upcoming collision possibilities (say assign 0 if the collision is between m_2 and m_3, and assign 1 if it is between m_1 and m_3). After a long sequence of collisions, the string of 0's and 1's can be thought of as a binomial representation of a random number. Random numbers could be numerically generated this way quickly and accurately to any desired precision and the system has a simple mechanical analogue.

The correspondence between chaotic deterministic systems and random ones is, of course, a classical topic about which much has been written [32]. We believe that these iterated impact problems are ideal ones in which to pin down similarities and differences — simple enough to prove theorems, yet rich enough, for general N, to exhibit a wide range of behavior and this article is meant to give an overview of this interesting topic in nonlinear dynamics.

Chapter 3

Random number generation from chaotic impact collisions

3.1 Introduction

When three masses (m_1, m_2, m_3) slide without friction on a ring, in the absence of collisions, their velocities, v_i, and momenta, $p_i = m_i v_i$, remain unchanged. Before and after a binary collision, conservation of energy and momentum allows us to write the system conveniently in matrix form [8]

$$\mathbf{v}' = \mathbf{M_{ij}}\mathbf{v}, \tag{3.1}$$

where $\mathbf{v} \in \mathcal{R}^3$, $\mathbf{v}' \in \mathcal{R}^3$ are the pre and post-collision velocities, and $\|\mathbf{v}\|^2 = \|\mathbf{v}'\|^2$. $\mathbf{M_{ij}}$ are the collision matrices $\mathbf{M_{12}}$, $\mathbf{M_{23}}$, $\mathbf{M_{13}}$, given explicitly as

$$\mathbf{M}_{12} = \frac{1}{m_{12}} \begin{pmatrix} \mu_{12} & \mu_2 & 0 \\ \mu_1 & \mu_{21} & 0 \\ 0 & 0 & m_{12} \end{pmatrix}$$

$$\mathbf{M}_{23} = \frac{1}{m_{23}} \begin{pmatrix} m_{23} & 0 & 0 \\ 0 & \mu_{23} & \mu_3 \\ 0 & \mu_2 & \mu_{32} \end{pmatrix}$$

$$\mathbf{M}_{13} = \frac{1}{m_{13}} \begin{pmatrix} \mu_{13} & 0 & \mu_3 \\ 0 & m_{13} & 0 \\ \mu_1 & 0 & \mu_{31} \end{pmatrix}$$

with $m_{ij} = m_i + m_j$, $\mu_{ij} = m_i - m_j$, $\mu_i = 2m_i$.

A collision between masses m_i and m_j updates the velocity vector on the nth collision:

$$\mathbf{v^{(n+1)}} = \mathbf{M_{ij}} \cdot \mathbf{v^{(n)}},$$

and a trajectory unfolds after n collisions from its initial velocity vector $\mathbf{v^{(0)}}$ to its final one $\mathbf{v^{(n)}}$ via the linear matrix equation

$$\mathbf{v^{(n)}} = \underbrace{\mathbf{M_{pq}} \cdots \mathbf{M_{kl}} \cdot \mathbf{M_{ij}}}_{n-collisions} \cdot \mathbf{v^{(0)}} \equiv \mathbf{M_n} \cdot \mathbf{v^{(0)}}. \tag{3.2}$$

The indices on the matrices indicate that this is a sequence of collisions between m_i and m_j, m_k and m_l, ..., m_p and m_q which we denote $m_i \rightarrow m_j$, then $m_k \rightarrow m_l$, ..., and finally $m_p \rightarrow m_q$. *Valid* collision sequences are those in which no two particles collide two or more times in a row. Effectively this means that for the matrix products shown in eqn (3.2), identical matrices cannot be multiplied two or more times sequentially. The order in which these collisions occur is important, and generally speaking, if interchanged

gives rise to a distinct trajectory. A string of n collision matrices associated with a given trajectory is denoted by the matrix $\mathbf{M_n} \in \mathcal{R}^{3X3}$.

In this paper we study the system $m_1 = m$, $m_2 = m - \epsilon$, $m_3 = m + \epsilon$ for values of the splitting parameter $\epsilon \geq 0$. In particular, we consider the eigenvalue spectrum generated by a sequence of n collisions. For $\epsilon = 0$ (the case of three equal masses), we prove that the spectrum is discrete, underlying the fact that the dynamics are regular – we start by summarizing relevant aspects of this problem. For $\epsilon > 0$, we study the eigenvalue spectrum as a dynamical system generated by a chaotic trajectory and we compare it with spectra produced by two known stochastic problems. The first is the eigenvalue spectrum associated with a sequence of matrix products where a random number algorithm is used to produce the matrix orderings. The second is the spectrum generated from a discrete random walk model on the unit circle. Computations of the eigenvalues of the $3X3$ matrices are performed using Matlab's **eig** routine and can be done quickly on a standard desktop machine with high precision (typically 16 digits accuracy). In the final section, we use the chaotic collision sequences as the basis for a random number generating algorithm and we investigate its properties using the runs and reverse order tests.

3.1.1 Properties of the collision matrices

We summarize here the main features of the collision matrices:

Proposition 1:

1. *The eigenvalues of* $\mathbf{M_{ij}}$ *are given by* $\lambda_1 = 1$, $\lambda_2 = 1$, $\lambda_3 = -1$;

2. *The corresponding unit eigenvectors are given by*

$$\mathbf{M_{12}}: \quad \xi_1 = \frac{1}{\sqrt{2}}\begin{pmatrix} 1 \\ 1 \\ 0 \end{pmatrix}; \quad \xi_2 = \begin{pmatrix} 0 \\ 0 \\ 1 \end{pmatrix}; \quad \xi_3 = \frac{1}{\sqrt{1+\frac{m_1^2}{m_2^2}}}\begin{pmatrix} 1 \\ -\frac{m_1}{m_2} \\ 0 \end{pmatrix}$$

$$\mathbf{M_{23}}: \quad \xi_1 = \frac{1}{\sqrt{2}}\begin{pmatrix} 0 \\ 1 \\ 1 \end{pmatrix}; \quad \xi_2 = \begin{pmatrix} 1 \\ 0 \\ 0 \end{pmatrix}; \quad \xi_3 = \frac{1}{\sqrt{1+\frac{m_2^2}{m_3^2}}}\begin{pmatrix} 0 \\ 1 \\ -\frac{m_2}{m_3} \end{pmatrix}$$

$$\mathbf{M_{13}}: \quad \xi_1 = \frac{1}{\sqrt{2}}\begin{pmatrix} 1 \\ 0 \\ 1 \end{pmatrix}; \quad \xi_2 = \begin{pmatrix} 0 \\ 1 \\ 0 \end{pmatrix}; \quad \xi_3 = \frac{1}{\sqrt{1+\frac{m_3^2}{m_1^2}}}\begin{pmatrix} -\frac{m_3}{m_1} \\ 0 \\ 1 \end{pmatrix}$$

3. $\mathbf{M_{ij}}$ *can be diagonalized:* $\mathbf{M_{ij}} = \mathbf{T_{ij}} D \mathbf{T_{ij}}^{-1}$

$$\textit{where } D = \begin{pmatrix} 1 & 0 & 0 \\ 0 & 1 & 0 \\ 0 & 0 & -1 \end{pmatrix}; \quad \mathbf{T_{12}} = \begin{pmatrix} \frac{1}{\sqrt{2}} & 0 & \frac{1}{\sqrt{1+\frac{m_1^2}{m_2^2}}} \\ \frac{1}{\sqrt{2}} & 0 & \frac{-\frac{m_1}{m_2}}{\sqrt{1+\frac{m_1^2}{m_2^2}}} \\ 0 & 1 & 0 \end{pmatrix};$$

$$\mathbf{T_{23}} = \begin{pmatrix} 0 & 1 & 0 \\ \frac{1}{\sqrt{2}} & 0 & \frac{1}{\sqrt{1+\frac{m_2^2}{m_3^2}}} \\ \frac{1}{\sqrt{2}} & 0 & \frac{-\frac{m_2}{m_3}}{\sqrt{1+\frac{m_2^2}{m_3^2}}} \end{pmatrix}; \quad \mathbf{T_{13}} = \begin{pmatrix} \frac{1}{\sqrt{2}} & 0 & \frac{-\frac{m_3}{m_1}}{\sqrt{1+\frac{m_3^2}{m_1^2}}} \\ 0 & 1 & 0 \\ \frac{1}{\sqrt{2}} & 0 & \frac{1}{\sqrt{1+\frac{m_3^2}{m_1^2}}} \end{pmatrix}$$

4. *The eigenvectors form a orthonormal basis for* $\mathcal{R}^3$.

Our analysis will focus primarily on the product of n collision matrices, $\mathbf{M_n} \in \mathcal{R}^{\mathbf{3X3}}$, whose three eigenvalues we denote $\lambda_j^{(n)} \in \mathbf{C}$, (j=1,2,3). The following proposition characterizes the eigenvalues of $\mathbf{M_n}$.

Proposition 2:

1. *If* $\mathbf{M_n}$ *is the product of* n *collision matrices, then*

$$\det(\mathbf{M_n}) = \lambda_1^{(n)} \cdot \lambda_2^{(n)} \cdot \lambda_3^{(n)} = (-1)^n$$

2. *The eigenvalues of* $\mathbf{M_n}$ *lie on the unit circle, i.e.*

$$|\lambda_j^{(n)}|^2 = 1, \quad j = 1, 2, 3.$$

3. *One eigenvalue of* $\mathbf{M_n}$ *is given by* $\lambda_1^{(n)} = (-1)^n$, *while the other two are complex conjugates*

$$\lambda_2^{(n)} = \lambda^{(n)}; \quad \lambda_3^{(n)} = \lambda^{(n*)}$$

with $|\lambda^{(n)}|^2 = 1$.

The proof can be found in [8] and is not included.

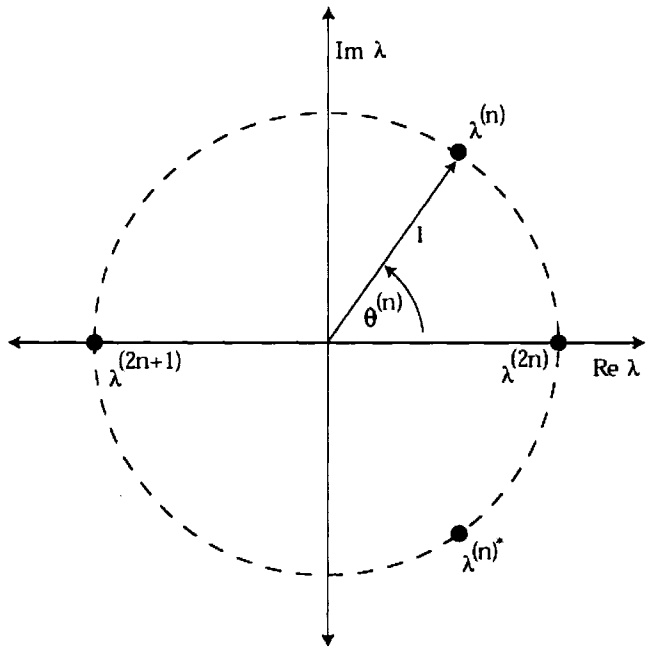

Figure 3.1: Eigenvalue spectrum of $\mathbf{M_n}$ on the unit circle.

3.1.2 Rotation map on S^1

Our main interest is in studying the eigenvalue sequence $\lambda^{(1)}, \lambda^{(2)}, ..., \lambda^{(n)}$ as the collisions unfold. It is more convenient instead to represent the sequence in terms of its corresponding angle variables around the unit circle, $\theta^{(1)}, \theta^{(2)}, ..., \theta^{(n)}$, where $\theta^{(n)} \in [0, 2\pi]$, with

$$\theta^{(n)} = \cos^{-1}(\lambda_r^{(n)}) = \sin^{-1}(\lambda_i^{(n)}).$$

The spectrum associated with $\mathbf{M_n}$ is shown in figure 3.1.

It is convenient to introduce the rotation map $\mathcal{R}(\alpha_{n+1})$ on the unit circle $S^1 = \{z \in \mathcal{C}; |z| = 1\}$ defined by

$$\mathcal{R}(\alpha_{n+1}) \equiv \exp 2\pi i(\theta_{n+1} - \theta_n) = \exp 2\pi i \alpha_{n+1}$$

where $\alpha_{n+1} = (\theta_{n+1} - \theta_n)$. The map is *non-autonomous* (in contrast to the standard autonomous rotation map described in [15]) since the rotation angle depends on the time-step n. It is natural to define the notions of *topological transitivity* and *minimality* as follows [15]:

Definition 1: Consider the dynamical system on S^1 generated by the rotation map $\mathcal{R}(\alpha_{n+1})$. The map is *topologically transitive* if there exists an θ_0 such that the sequence $\{\mathcal{R}(\alpha_{n+1})\}$ is dense on S^1.

Definition 2: The dynamical system is *minimal* if the orbit of every point is dense, i.e. there are no proper closed invariant sets.

3.2 Mass splitting perturbations

It is useful to write the collision matrices as expansions in powers of the *splitting parameter* ϵ:

$$\mathbf{M}_{12}^{(\epsilon)} = \begin{pmatrix} \frac{\epsilon}{2m}\left(\frac{1}{1-\frac{\epsilon}{2m}}\right) & \left(1-\frac{\epsilon}{m}\right)\left(\frac{1}{1-\frac{\epsilon}{2m}}\right) & 0 \\ \left(\frac{1}{1-\frac{\epsilon}{2m}}\right) & -\frac{\epsilon}{2m}\left(\frac{1}{1-\frac{\epsilon}{2m}}\right) & 0 \\ 0 & 0 & 1 \end{pmatrix} = \mathbf{M}_{12}^{(0)} + \frac{\epsilon}{2m}\mathbf{M}_{12}^{(1)} + \ldots$$

$$\sim \begin{pmatrix} 0 & 1 & 0 \\ 1 & 0 & 0 \\ 0 & 0 & 1 \end{pmatrix} + \frac{\epsilon}{2m}\begin{pmatrix} 1 & -1 & 0 \\ 1 & -1 & 0 \\ 0 & 0 & 0 \end{pmatrix} + O((\tfrac{\epsilon}{2m})^2)$$

$$\mathbf{M}_{23}^{(\epsilon)} = \begin{pmatrix} 1 & 0 & 0 \\ 0 & -\frac{\epsilon}{m} & 1+\frac{\epsilon}{m} \\ 0 & 1-\frac{\epsilon}{m} & \frac{\epsilon}{m} \end{pmatrix} = \mathbf{M}_{23}^{(0)} + \frac{\epsilon}{2m}\mathbf{M}_{23}^{(1)}$$

$$= \begin{pmatrix} 1 & 0 & 0 \\ 0 & 0 & 1 \\ 0 & 1 & 0 \end{pmatrix} + \frac{\epsilon}{2m}\begin{pmatrix} 0 & 0 & 0 \\ 0 & -2 & 2 \\ 0 & -2 & 2 \end{pmatrix}$$

$$\mathbf{M}_{13}^{(\epsilon)} = \begin{pmatrix} -\frac{\epsilon}{2m}\left(\frac{1}{1+\frac{\epsilon}{2m}}\right) & 0 & \left(1+\frac{\epsilon}{m}\right)\left(\frac{1}{1+\frac{\epsilon}{2m}}\right) \\ 0 & 1 & 0 \\ \left(\frac{1}{1+\frac{\epsilon}{2m}}\right) & 0 & \frac{\epsilon}{2m}\left(\frac{1}{1+\frac{\epsilon}{2m}}\right) \end{pmatrix} = \mathbf{M}_{13}^{(0)} + \frac{\epsilon}{2m}\mathbf{M}_{13}^{(1)} + \ldots$$

$$\sim \begin{pmatrix} 0 & 0 & 1 \\ 0 & 1 & 0 \\ 1 & 0 & 0 \end{pmatrix} + \frac{\epsilon}{2m}\begin{pmatrix} -1 & 0 & 1 \\ 0 & 0 & 0 \\ -1 & 0 & 1 \end{pmatrix} + O((\tfrac{\epsilon}{2m})^2)$$

We now define the rotation map $\mathcal{R}^{(\epsilon)}(\alpha_{n+1})$ as the one generated by the sequential application of the collision matrices $\mathbf{M_{ij}}$.

Conjecture 1: The map $\mathcal{R}^{(\epsilon)}(\alpha_{n+1})$ for $\epsilon > 0$ is topologically transitive but not minimal.

3.2.1 Discrete spectrum for $\epsilon = 0$

The case of equal masses is special – upon collision, the velocities reverse but otherwise remain unchanged. In this section, we prove that the spectrum produced by an arbitrary sequence of collisions is discrete on the unit circle reflecting the fact that the dynamics for this case is simple and regular. The collision matrices are given identically as

$$\mathbf{M_{12}^{(0)}} = \begin{pmatrix} 0 & 1 & 0 \\ 1 & 0 & 0 \\ 0 & 0 & 1 \end{pmatrix}; \quad \mathbf{M_{23}^{(0)}} = \begin{pmatrix} 1 & 0 & 0 \\ 0 & 0 & 1 \\ 0 & 1 & 0 \end{pmatrix}; \quad \mathbf{M_{13}^{(0)}} = \begin{pmatrix} 0 & 0 & 1 \\ 0 & 1 & 0 \\ 1 & 0 & 0 \end{pmatrix}.$$

This gives rise to a very regular eigenvalue spectrum for any valid sequence of collision matrices.

Proposition 3: *For the case of three equal masses ($\epsilon = 0$), the following properties hold for the collision matrices:*

1. $\mathbf{M_{ij}^{(0)}} = \mathbf{M_{ij}^{(0)}}^T$, *i.e. each collision matrix is symmetric.*
   $\left(\mathbf{M_{ij}^{(0)}}\right)^2 = I$, *i.e. each collision matrix is its own inverse and unitary.*
2. $\mathbf{M_{ij}^{(0)}} \cdot \mathbf{M_{ik}^{(0)}} \cdot \mathbf{M_{jk}^{(0)}} = \mathbf{M_{ik}^{(0)}}$
3. $\mathbf{M_{ij}^{(0)}} \cdot \mathbf{M_{ik}^{(0)}} \cdot \mathbf{M_{ij}^{(0)}} = \mathbf{M_{jk}^{(0)}}$
4. $\mathbf{M_{ij}^{(0)}} \cdot \mathbf{M_{jk}^{(0)}} \cdot \mathbf{M_{ij}^{(0)}} = \mathbf{M_{ik}^{(0)}}$
5. *The eigenvalues produced by the product of any two distinct collision matrices are* $\lambda_1 = 1$, $\lambda_2 = e^{\frac{2i\pi}{3}}$, $\lambda_3 = e^{\frac{4i\pi}{3}}$

6. *The eigenvalues produced by any valid sequence of three collision matrices are* $\lambda_1 = 1$, $\lambda_2 = 1$, $\lambda_3 = -1$.

Proof:

1. $$\left(\mathbf{M}_{\mathbf{ij}}^{(0)}\right)^2 = \begin{pmatrix} 0 & 1 & 0 \\ 1 & 0 & 0 \\ 0 & 0 & 1 \end{pmatrix} \cdot \begin{pmatrix} 0 & 1 & 0 \\ 1 & 0 & 0 \\ 0 & 0 & 1 \end{pmatrix} = \begin{pmatrix} 1 & 0 & 0 \\ 0 & 1 & 0 \\ 0 & 0 & 1 \end{pmatrix}$$

$$\left(\mathbf{M}_{\mathbf{jk}}^{(0)}\right)^2 = \begin{pmatrix} 1 & 0 & 0 \\ 0 & 0 & 1 \\ 0 & 1 & 0 \end{pmatrix} \cdot \begin{pmatrix} 1 & 0 & 0 \\ 0 & 0 & 1 \\ 0 & 1 & 0 \end{pmatrix} = \begin{pmatrix} 1 & 0 & 0 \\ 0 & 1 & 0 \\ 0 & 0 & 1 \end{pmatrix}$$

$$\left(\mathbf{M}_{\mathbf{ik}}^{(0)}\right)^2 = \begin{pmatrix} 0 & 0 & 1 \\ 0 & 1 & 0 \\ 1 & 0 & 0 \end{pmatrix} \cdot \begin{pmatrix} 0 & 0 & 1 \\ 0 & 1 & 0 \\ 1 & 0 & 0 \end{pmatrix} = \begin{pmatrix} 1 & 0 & 0 \\ 0 & 1 & 0 \\ 0 & 0 & 1 \end{pmatrix}$$

2. $$\mathbf{M}_{\mathbf{ij}}^{(0)} \cdot \mathbf{M}_{\mathbf{ik}}^{(0)} \cdot \mathbf{M}_{\mathbf{jk}}^{(0)} = \begin{pmatrix} 0 & 1 & 0 \\ 1 & 0 & 0 \\ 0 & 0 & 1 \end{pmatrix} \cdot \begin{pmatrix} 0 & 0 & 1 \\ 0 & 1 & 0 \\ 1 & 0 & 0 \end{pmatrix} \cdot \begin{pmatrix} 1 & 0 & 0 \\ 0 & 0 & 1 \\ 0 & 1 & 0 \end{pmatrix}$$

$$= \begin{pmatrix} 0 & 0 & 1 \\ 0 & 1 & 0 \\ 1 & 0 & 0 \end{pmatrix} = \mathbf{M}_{\mathbf{ik}}^{(0)}$$

3. $$\mathbf{M}_{ij}^{(0)} \cdot \mathbf{M}_{ik}^{(0)} \cdot \mathbf{M}_{ij}^{(0)} = \begin{pmatrix} 0 & 1 & 0 \\ 1 & 0 & 0 \\ 0 & 0 & 1 \end{pmatrix} \cdot \begin{pmatrix} 0 & 0 & 1 \\ 0 & 1 & 0 \\ 1 & 0 & 0 \end{pmatrix} \cdot \begin{pmatrix} 0 & 1 & 0 \\ 1 & 0 & 0 \\ 0 & 0 & 1 \end{pmatrix}$$
$$= \begin{pmatrix} 1 & 0 & 0 \\ 0 & 0 & 1 \\ 0 & 1 & 0 \end{pmatrix} = \mathbf{M}_{jk}^{(0)}$$

4. $$\mathbf{M}_{ij}^{(0)} \cdot \mathbf{M}_{jk}^{(0)} \cdot \mathbf{M}_{ij}^{(0)} = \begin{pmatrix} 0 & 1 & 0 \\ 1 & 0 & 0 \\ 0 & 0 & 1 \end{pmatrix} \cdot \begin{pmatrix} 1 & 0 & 0 \\ 0 & 0 & 1 \\ 0 & 1 & 0 \end{pmatrix} \cdot \begin{pmatrix} 0 & 1 & 0 \\ 1 & 0 & 0 \\ 0 & 0 & 1 \end{pmatrix}$$
$$= \begin{pmatrix} 0 & 0 & 1 \\ 0 & 1 & 0 \\ 1 & 0 & 0 \end{pmatrix} = \mathbf{M}_{ik}^{(0)}$$

5. $$\mathbf{M}_{ij}^{(0)} \cdot \mathbf{M}_{jk}^{(0)} = \mathbf{M}_{jk}^{(0)} \cdot \mathbf{M}_{ik}^{(0)} = \mathbf{M}_{ik}^{(0)} \cdot \mathbf{M}_{ij}^{(0)} = \begin{pmatrix} 0 & 0 & 1 \\ 1 & 0 & 0 \\ 0 & 1 & 0 \end{pmatrix}$$

$$\mathbf{M}_{ij}^{(0)} \cdot \mathbf{M}_{ik}^{(0)} = \mathbf{M}_{jk}^{(0)} \cdot \mathbf{M}_{ij}^{(0)} = \mathbf{M}_{ik}^{(0)} \cdot \mathbf{M}_{jk}^{(0)} = \begin{pmatrix} 0 & 1 & 0 \\ 0 & 0 & 1 \\ 1 & 0 & 0 \end{pmatrix}$$

$$|(\mathbf{M}_{ij}^{(0)} \cdot \mathbf{M}_{jk}^{(0)}) - \lambda I| = \begin{vmatrix} -\lambda & 0 & 1 \\ 1 & -\lambda & 0 \\ 0 & 1 & -\lambda \end{vmatrix} = \lambda^3 - 1 = 0$$

$$|(\mathbf{M}_{\mathbf{ij}}^{(0)} \cdot \mathbf{M}_{\mathbf{ik}}^{(0)}) - \lambda I| = \begin{vmatrix} -\lambda & 1 & 0 \\ 0 & -\lambda & 1 \\ 1 & 0 & -\lambda \end{vmatrix} = \lambda^3 - 1 = 0$$

$\lambda = \{1, e^{\pm\frac{2\pi i}{3}}\}$

6. *From (1)-(4), any valid sequence of three collisions, gives a single collision matrix.*

   Therefore,

$$|\mathbf{M}_{\mathbf{ij}}^{(0)} - \lambda I| = \begin{vmatrix} -\lambda & 1 & 0 \\ 1 & -\lambda & 0 \\ 0 & 0 & (1-\lambda) \end{vmatrix} = (1-\lambda)(\lambda^2 - 1) = 0$$

$$|\mathbf{M}_{\mathbf{jk}}^{(0)} - \lambda I| = \begin{vmatrix} (1-\lambda) & 0 & 0 \\ 0 & -\lambda & 1 \\ 0 & 1 & -\lambda \end{vmatrix} = (1-\lambda)(\lambda^2 - 1) = 0$$

$$|\mathbf{M}_{\mathbf{ik}}^{(0)} - \lambda I| = \begin{vmatrix} -\lambda & 0 & 1 \\ 0 & (1-\lambda) & 0 \\ 1 & 0 & -\lambda \end{vmatrix} = (1-\lambda)(\lambda^2 - 1) = 0$$

$\lambda = \{1, \pm 1\}$

The spectrum of $\mathbf{M}_{\mathbf{n}}^{(0)}$ can now be fully characterized.

Proposition 4: *The eigenvalue spectrum generated by* $\mathbf{M}_{\mathbf{n}}^{(0)}$, $(n = 1, 2, 3, ...)$, *is discrete on the unit circle and is made up of* $\{1, -1, e^{\frac{2\pi i}{3}}, e^{\frac{4\pi i}{3}}\}$, *as shown in figure 3.2. The rotation map* $\mathcal{R}^{(0)}(\alpha_{n+1})$ *is not topologically transitive.*

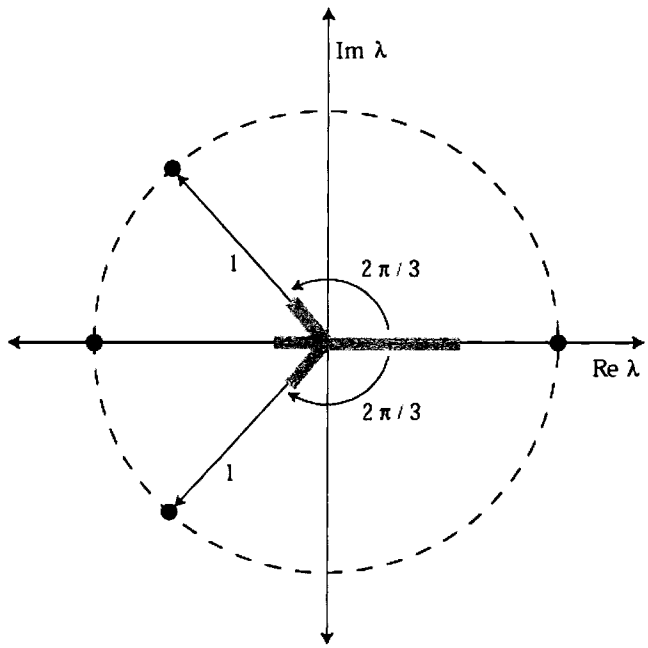

Figure 3.2: Eigenvalue distribution of $\mathbf{M_n}$ on the unit circle in the complex λ-plane for $\epsilon = 0$. Shaded areas are histograms showing the distribution of the eigenvalues among the four values. 50% of the eigenvalues are unity, while the others are evenly distributed among the other three values.

Proof: For $n = 1$, the eigenvalues of $\mathbf{M_1^{(0)}}$ are given by Proposition 1. For $n = 2$, Proposition 3(5) gives the spectrum. For $n = 3$, Proposition 3(6) gives the spectrum. For $n = 4$, let $\mathbf{M_4^{(0)}} = \mathbf{M_3^{(0)}} \cdot \mathbf{M_{ij}^{(0)}}$. By Proposition 3(2),(3),(4), since $\mathbf{M_3^{(0)}}$ is the product of three collision matrices, it is itself a collision matrix. Hence $\mathbf{M_3^{(0)}} \cdot \mathbf{M_{ij}^{(0)}}$ is the product of two collision matrices whose spectrum is characterized in Proposition 3(5). etc.

3.2.2 Splitting the spectrum: $\epsilon > 0$

By contrast, a typical spectrum for $\epsilon > 0$ is shown in figure 3.3. The eigenvalues are relatively evenly distributed around the unit circle (± 1 are not shown). For $\epsilon > 0$,

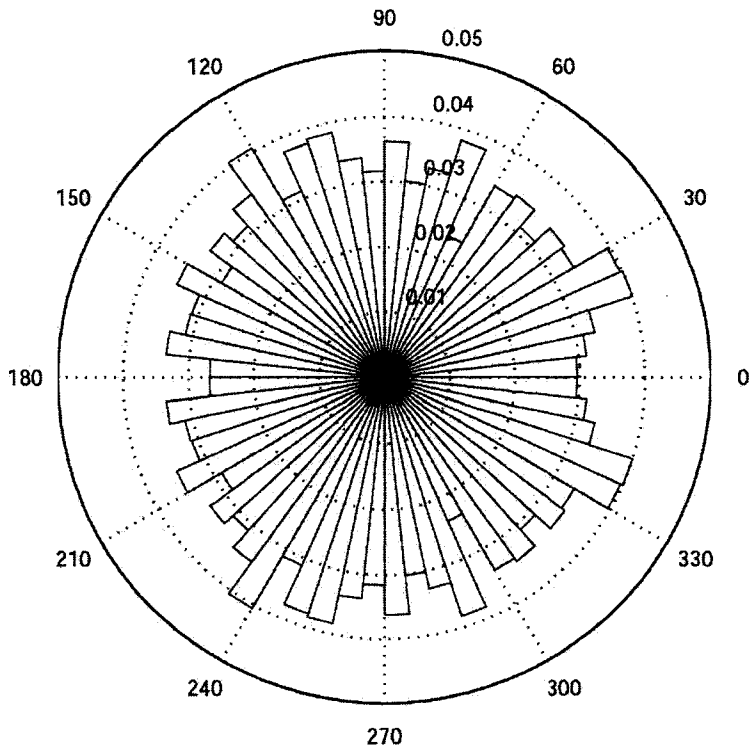

Figure 3.3: Eigenvalue distribution on the unit circle in the complex λ-plane for a chaotic trajectory after $n = 10,000$ collisions.

large enough values of n typically produce distributions around the circle that are close to uniform (excluding ± 1), as long as we have not locked onto a periodic orbit. The existence of periodic orbits is proven in [8].

3.3 Random matrix sequences

We now examine the spectrum generated by a sequence of collision matrices when the ordering is generated randomly. To generate the random sequence, we initiate the string of matrices forming $\mathbf{M_n}$ with one of the three collision matrices $\mathbf{M_{12}^{(\epsilon)}}$, $\mathbf{M_{23}^{(\epsilon)}}$, $\mathbf{M_{13}^{(\epsilon)}}$. The next matrix in the sequence must be one of the other two. A uniformly distributed random

number between 0 and 1 is generated using Matlab's rand(1) routine to produce a random variable, then round(rand(1)) produces $x_i = \{0, 1\}$. This is then used to determine which of the two available collision matrices to apply next. This algorithm is used at each of the n steps in constructing $\mathbf{M_n}$ and producing the discrete sequence $\{\theta^{(1)}, \theta^{(2)}, ..., \theta^{(n)}\}$.

3.3.1 Convergence to the sample mean

First we investigate properties of the random variable x_i generated by Matlab's rand() routine. Consider the sample mean, μ_n, associated with the string of 0's and 1's, i.e.

$$\mu_n = \frac{1}{n}\sum_{i=1}^{n} x_i,$$

which is itself a random variable $\in [0, 1]$. By the Central Limit Theorem [2], we know that $\mu_n \to 1/2$ as $n \to \infty$ and that the distribution around the mean is Gaussian

$$p(\mu_n) = \frac{1}{\sqrt{2\pi\sigma_n^2}} \exp\left[-\frac{(\mu_n - \frac{1}{2})^2}{2\sigma_n^2}\right], \tag{3.3}$$

with $\sigma_n^2 \sim 1/n$. Suppose we take j trials, i.e. form j strings of 0's and 1's, each randomly generated. The sample mean associated with the jth trial is denoted

$$\mu_n^{(j)} = \frac{1}{n}\sum_{i=1}^{n} x_i^{(j)}, \tag{3.4}$$

where $x_i^{(j)} = \{0, 1\}$. Figure 3.4 shows the convergence properties of $\mu_n^{(j)}$. In particular, we generate $j = 500$ random trials (only 5 are shown), resulting in a sample mean $\mu_j^{(n)}$ for each n. Each of the trials converges to $1/2$ as $n \to \infty$, as expected. To study the

convergence rate, we show histograms in the same figure, corresponding to the three values $n = 100, 1000, 2000$. Each is very nearly a Gaussian distribution which gets tighter around $1/2$ as n increases. The first four statistical moments and measures of skewness and kurtosis can be calculated to determine how close the data is to being perfectly normal:

$$\begin{aligned}
\text{First moment (mean)}:\mu_n &= \frac{1}{j}\sum_{j=1}^{500}\mu_n^{(j)} \\
\text{Second moment (variance)}:\sigma_n^2 &= \frac{1}{j}\sum_{j=1}^{500}(\mu_n^{(j)} - \mu_n)^2 \\
\text{Third moment (skewness)}:\mu_n^{(''')} &= \frac{1}{j}\sum_{j=1}^{500}(\mu_n^{(j)} - \mu_n)^3 \\
\text{Fourth moment (kurtosis)}:\mu_n^{(''''')} &= \frac{1}{j}\sum_{j=1}^{500}(\mu_n^{(j)} - \mu_n)^4 \\
\text{measure of skewness}:\gamma_1 &= \frac{\mu_n^{(''')}}{\sigma_n^3} \\
\text{measure of kurtosis}:\gamma_2 &= \frac{\mu_n^{(''''')}}{\sigma_n^4}
\end{aligned}$$

Perfectly Gaussian data would give values $\mu = \frac{1}{2}$, $\gamma_1 = 0$ (perfect symmetry about the mean), $\gamma_2 = 3$ (measures the degree of peakness). For $n = 100$, the values are $\gamma_1 = -.0190$, $\gamma_2 = 2.4920$, for $n = 1000$ they are $\gamma_1 = .0779$, $\gamma_2 = 2.7939$, while for $n = 2000$, they are $\gamma_1 = -.0597$, $\gamma_2 = 2.7462$. Figure 3.4(b) shows the variance as a function of n, indicating clear power law behavior of the form $\nu \sim .2599n^{-1.0022}$.

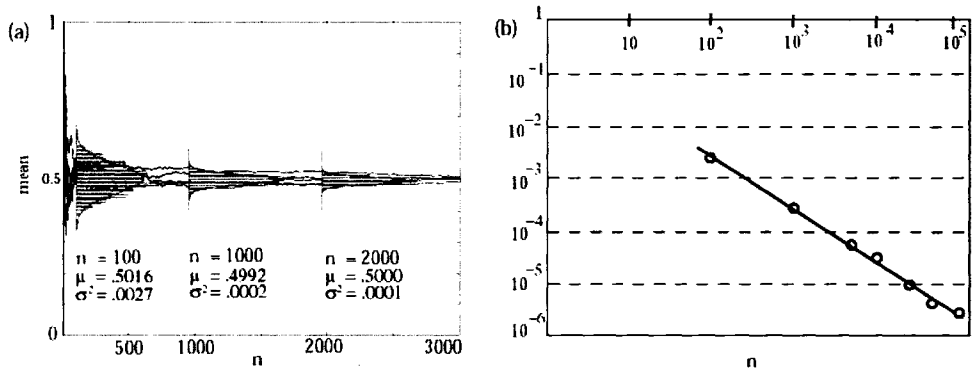

Figure 3.4: Convergence properties: (a) Five runs from the Matlab random number generator on $[0,1]$ showing convergence to 0.5 as a function of n; (b) Variance as a function of n. The slope of the line is -1.0022.

3.4 Time-series analysis of the spectra

We now examine the spectral sequences $\{\theta^{(1)}, \theta^{(2)}, ..., \theta^{(n)}\}$ as a discrete time series. We compare the deterministically chaotic sequence of collisions with randomly generated sequences. Then, we implement a random walk model [2] on the unit circle using the random process

$$\theta_t = \theta_{t-1} \pm \rho\tilde{\theta}_t \tag{3.5}$$

where $\tilde{\theta}_t$ is a randomly generated number and ρ is a parameter which determines the mean and variance of the process. Three time-series are shown in figure 3.5, one corresponding to each of the three processes. To render the sequence associated with the chaotic process stationary, we form the first difference,

$$\begin{aligned} \hat{\theta}^{(i)} &\equiv \theta^{(i+1)} - \theta^{(i)} \\ &= \{\theta^{(2)} - \theta^{(1)}, \theta^{(3)} - \theta^{(2)}, ..., \theta^{(n)} - \theta^{(n-1)}\}. \end{aligned}$$

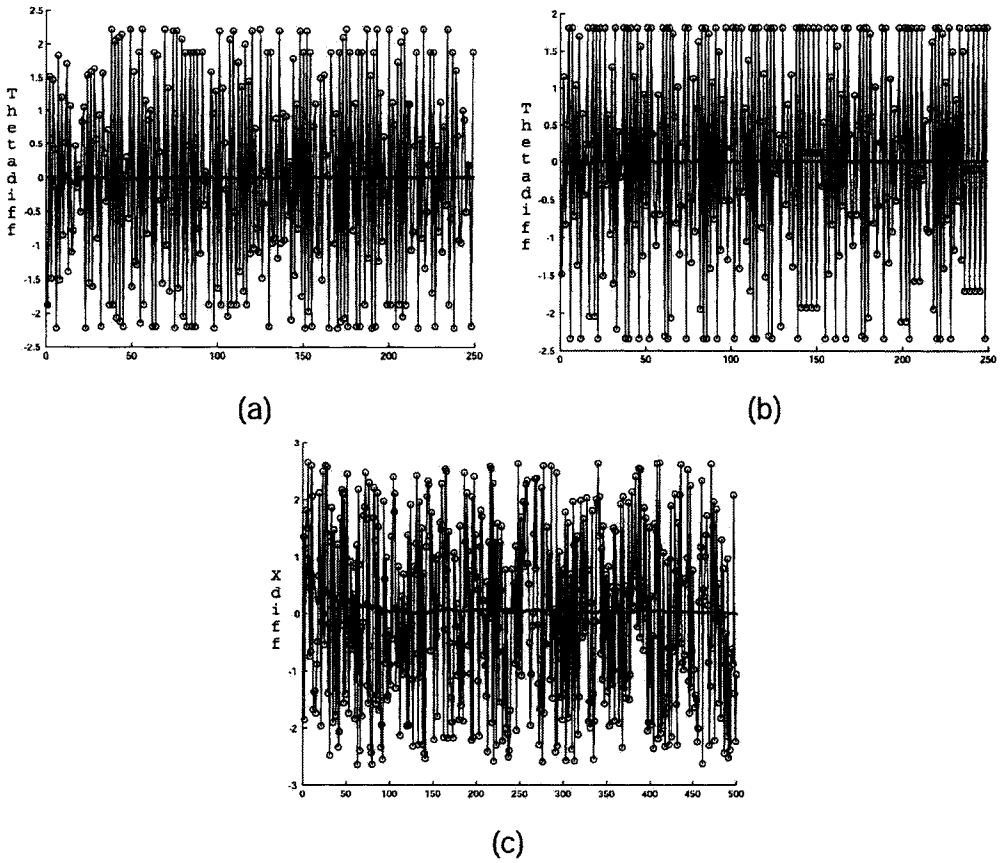

Figure 3.5: Time series associated with the first order differenced spectral sequence. (a) Chaotic process; (b) Random matrix process; (c) Random walk model.

We choose values of the parameter ρ so that the mean and standard deviation of the random walk model are comparable to the other two processes.

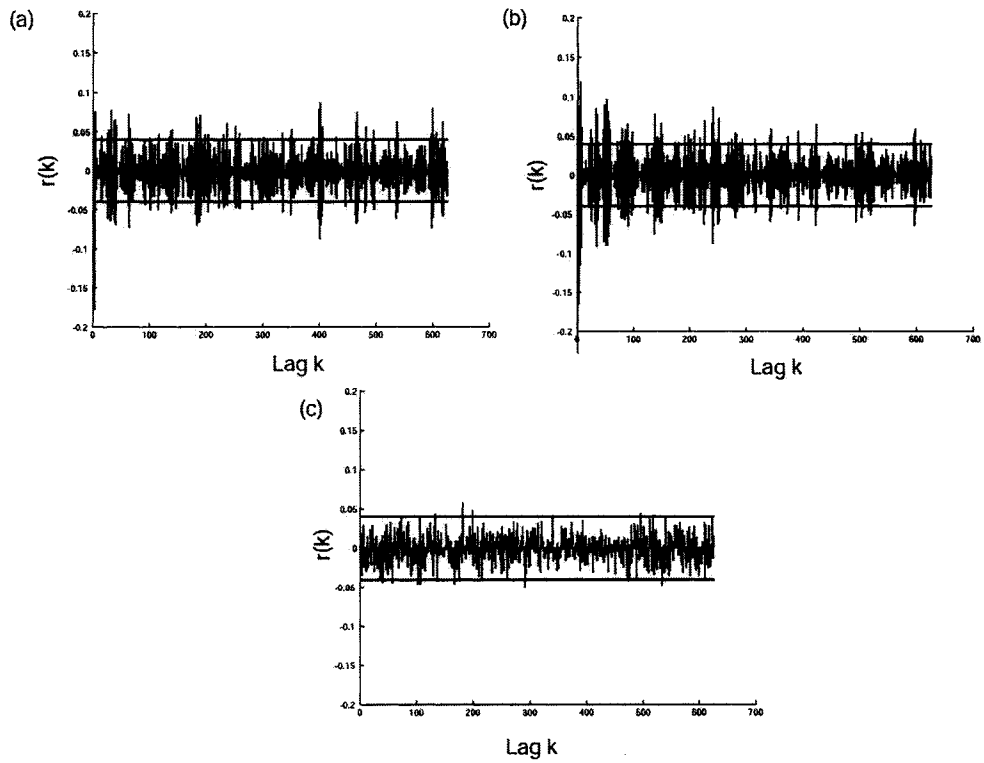

Figure 3.6: Autocorrelation coefficients. (a) Chaotic process; (b) Random matrix process; (c) Random walk model.

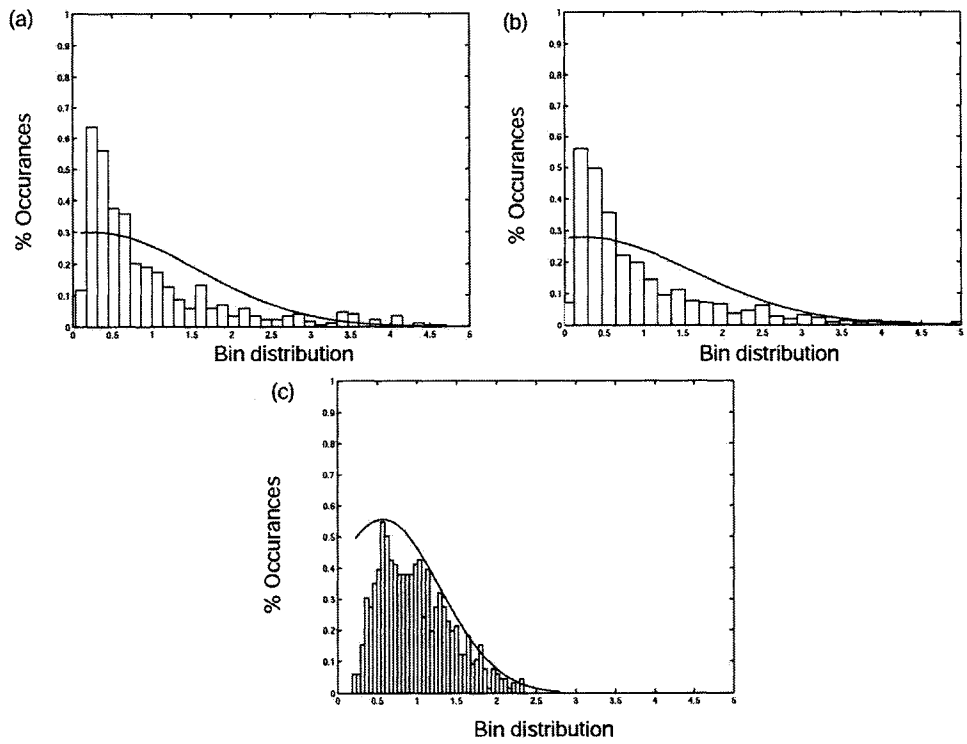

Figure 3.7: Histograms and Gaussian fits for eigenvalues of the P matrix. (a) Chaotic process; (b) Random matrix process; (c) Random walk model.

3.4.1 Autocorrelation coefficients

Autocorrelation coefficients measure the degree of correlation between observations in a time series that are k steps apart. The autocorrelation coefficients (r_k) can be calculated as follows:

$$c_k = \frac{1}{N}\sum_{t=1}^{N-k}(x_t - \bar{x}) \tag{3.6}$$

$$r_k = c_k/c_0. \tag{3.7}$$

Plotting the autocorrelation coefficients versus the lag k gives the autocorrelation spectrum, as shown in figure 3.6. Typically, only values of k up to $N/4$ are used and most fall between the bounds $\pm 2/\sqrt{N}$. The autocorrelation matrix $\mathbf{P}$ is constructed as

$$\mathbf{P} = \begin{pmatrix} 1 & r_1 & r_2 & r_3 & \cdots & \cdots & r_k \\ r_1 & 1 & r_1 & r_2 & r_3 & \cdots & r_{k-1} \\ r_2 & r_1 & 1 & r_1 & r_2 & \cdots & r_{k-2} \\ \vdots & \vdots & \vdots & \vdots & \vdots & \vdots & \vdots \\ \vdots & \vdots & \vdots & \vdots & \vdots & \vdots & \vdots \\ r_k & r_{k-1} & r_{k-2} & \cdots & \cdots & \cdots & 1 \end{pmatrix}$$

The matrix is hermitian and thus has only positive real eigenvalues. The eigenvalues (histogrammed) are shown in figure 3.7 along with the corresponding Gaussian fits to the data. We note that a purely linear Gaussian random process is fully specified by its

first and second moments and that the autocorrelations alone cannot distinguish random from chaotic signals.

3.5 On the generation of random numbers

Given the fact that the three mass system for $\epsilon > 0$ generates a dense spectrum on the unit circle and, in addition, is simple to code and fast to run on desktop computers, we consider in this section the use of the iterated impact problem as a basis for an effective random number generating algorithm [6]. Consider the real number $\chi^{(N)}$ obtained from the binary expansion

$$\chi^{(N)} = \sum_{n=1}^{N} \alpha_n / 2^n. \tag{3.8}$$

Suppose the coefficients $\alpha_1, \alpha_2, \ldots, \alpha_N$ are a string of 0's and 1's generated by a random process, giving rise to a random number $\chi^{(N)} \in [0, 1]$. Our goal is to characterize the properties of $\chi^{(N)}$. Histograms generated from ensembles of 50,000 realizations of this process are shown in figure 3.8. For example, figure 3.8(a) shows the distribution of 50,000 numbers with coefficients generated from Matlab's **rand()** routine. The mean and variance in this case are given by $\mu = 0.499175$, $\sigma = 0.288962$. Figures 3.8(b) and (c) show the corresponding histograms when the coefficients are generated by the three mass chaotic collision sequences. In figure 3.8(b), the three mass values are generated randomly (using Matlab's rand()) for each of the 50,000 realizations, using fixed initial velocities. The string of 0's and 1's is generated according to the following rules. Suppose the masses are arranged in a clockwise ordering m_1, m_2, m_3. Starting with a given collision (say between m_1 and m_2), the next collision can only be one of two possibilities. Either it

takes place between the two masses oriented one position clockwise to the previous one (an m_2, m_3 collision), or it is oriented counterclockwise to it (an m_1, m_3 collision). If the collision is clockwise to the previous one at the nth step, we assign a 1 to the coefficient α_n, otherwise we assign a 0 to it. In order to eliminate possible biasing, we alternate the assignment of 0's and 1's to clockwise and counterclockwise collisions as the string unfolds. For each realization, we produce a string of 58 coefficients, and we drop the first 38 in the string and use the remaining 20 to produce the random number associated with that string. The mean and variance corresponding to figure 3.8(b) is $\mu = 0.500982$, $\sigma = 0.27864$. Figure 3.8(c) is the histogram generated in the same way as that in figure 3.8(b), but with fixed masses and randomly generated initial velocities. The mean and variance in this case is $\mu = 0.523840$, $\sigma = 0.269250$.

The question arises as to whether the three processes described above for generating random numbers perform similarly when subjected to standard statistical tests for randomness, the most common being the *runs* test and the *reverse arrangement* test [1]. A *run* is defined as a sequence of identical observations (say all 0's) that is followed and preceeded by a different observation (i.e. a 1). The number of runs that occurs in a sequence of N observations gives an indication of whether or not the results are independent observations of the same random variable. To define a *reverse arrangement*, consider a sequence of N observations of a random variable χ, with each observation denoted X_n, where $n = 1, 2, 3, \ldots, N$. Count the number of times in a string that $X_i > X_j$ for $i < j$. Each such inequality is called a reverse arrangement and the total number of reverse arrangements in a given string of observations is denoted $\mathcal{A}$. Since each of these two tests is standard in the statistical literature, we do not describe them further but

	Matlab Rand	Rand Mass	Rand Vel
μ	0.499175	0.500982	0.523840
σ	0.288962	0.278642	0.269250
run_1	89	93	88
run_2	106	95	95
run_3	110	101	84
run_4	102	94	98
run_5	97	99	97
arr_1	2510	2362	2502
arr_2	2468	2537	2560
arr_3	2611	2310	2398
arr_4	2651	2550	2317
arr_5	2307	2285	2310

Table 3.1: Results of runs test and reverse arrangement test for $\alpha = 0.02$ confidence. Each of the strings are taken from an ensemble of 50,000 data points.

refer the reader to [1]. We note that, in general, the reverse arrangement test is more powerful than the runs test for detecting monotonic trends in a sequence of observations but not good for detecting fluctuating trends, hence the two are complementary and are commonly used in conjunction with each other to test for randomness. Table 3.1 shows the results of both tests from strings of random numbers generated by each of the three methods described earlier, using 5 distinct strings of $N = 200$ observations from the 50,000 runs for the runs test and $N = 100$ observations for the reverse arrangement test. To pass the tests at the $\alpha = 0.02$ confidence level, all of the numbers for the runs test shown in table 3.1 must lie between 84 and 117 (see table A.6 in [1]) and all of those for the reverse arrangement test must lie between 2083 and 2866 (see table A.7 in [1]). Our conclusion from these tests is that each of the three methods of generating random numbers passes the independence hypothesis at the $\alpha = 0.02$ confidence level, thus performs equally well with respect to these measures.

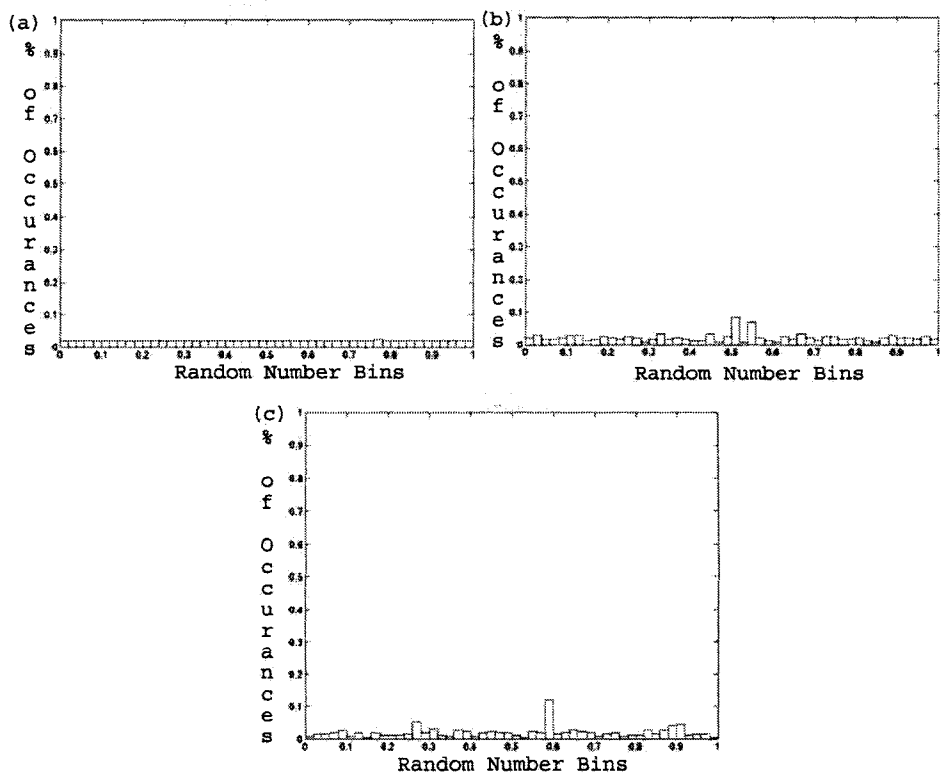

Figure 3.8: Histograms of random number distributions between 0 and 1 for 50,000 runs. (a) Coefficients generated by Matlab's Rand() routine; (b) Coefficients generated by chaotic collision sequence with randomly generated mass distributions; (c) Coefficients generated by chaotic collision sequence with random initial velocities, fixed masses.

3.6 Conclusions

The three mass collision problem, with unequal mass values, typically generates a chaotic collision sequence whose spectrum can be viewed as a non-autonomous rotation map on the unit circle which is topologically transitive but not minimal. When viewed from a nonlinear time series perspective [14], the spectral sequences are similar to two canonical random problems, the first being a random walk on the unit circle, the second being a spectral sequence generated from a string of matrix products with random orderings. Because of the relative simplicity of the model and the speed with which sequences can be generated on standard laptop computers, it is natural to use the three mass collision problem as the basis for a random number generating algorithm. This is explored and we conclude on the basis of an examination of the autocorrelation spectra and the runs and reverse arrangement tests (standard statistical tests) that the sequences generated this way produce equivalent levels of pseudo-randomness as Matlab's **rand()** algorithm. While differences in the levels of randomness may well emerge from applications of more delicate tests (an indication of this might be the differences evident in the histograms shown in figure 3.8 — figure 3.8(a) shows a very smooth distribution, while figures 3.8(b) and 3.8(c) show a more jagged distribution), we should point out that no pseudo-random number generating algorithm [6] is capable of passing *all* tests of randomness. It seems logical to use algorithms currently in use as benchmarks and to require that proposed new algorithms perform equally well when subjected to standard statistical testing. In this regard, we have tried to identify the simplest possible chaotic system (from the point of view of computational speed as well as coding complexity) for use in a random number

generating scheme, and the one described in this paper has many attractive features that we are currently exploring.

Chapter 4

Chaotic diffusion from impact collisions on a ring

4.1 Introduction

We consider the problem of three beads with masses (m_1, m_2, m_3) moving on a frictionless hoop undergoing a sequence of perfectly elastic collisions. In this paper we scale the masses so that $m_1 = 1/\epsilon$, $m_2 = 1$, $m_3 = 1 - \epsilon$, for the parameter range $0 \leq \epsilon \leq 1$. Formally, setting $\epsilon = 0$ yields $m_1 = \infty$, $m_2 = m_3 = 1$, the problem of a stationary wall and two unit masses on a periodic ring. Setting $\epsilon = 1$ yields $m_1 = m_2 = 1$, $m_3 = 0$, which corresponds to the case of two unit masses on a ring with no wall. Both cases are shown in figure 4.1. In this paper, we explore the regime $0 < \epsilon < 1$ that parametrically connects the two limit cases and examine the effect of the wall on the long time dynamics of the system, paying particular attention to the two singular limits $\epsilon \to 0$, $\epsilon \to 1$.

For $\epsilon \sim 0$, the three masses are unequal and finite, with $\infty > m_1 >> m_2 > m_3$, but since m_1 is large compared to the other two, the wall (m_1) can slowly diffuse from its initial position under the repeated impacts from the other beads. The problem is analogous to that of classical Brownian motion [30], hence we would expect that the mean square value

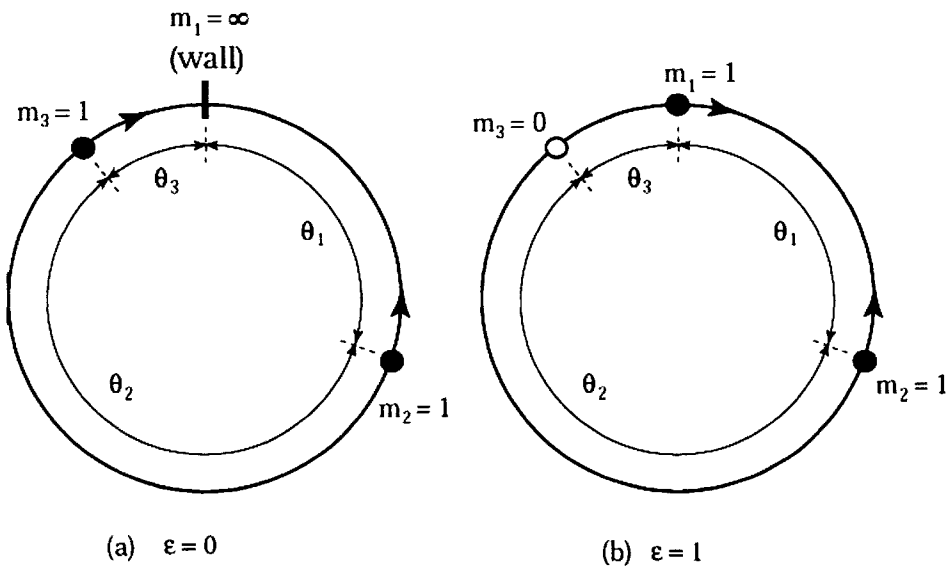

Figure 4.1: The singular limits of three beads of masses $m_1 = 1/\epsilon$, $m_2 = 1$, $m_3 = 1 - \epsilon$, sliding without friction on a circular hoop undergoing a sequence of perfectly elastic collisions. (a) $\epsilon = 0$: Two equal beads and a wall; (b) $\epsilon = 1$: Two equal beads and no wall.

of the displacement of the wall should increase linearly with the number of collisions, i.e. $< s^2 > \approx \beta n$. The precise coefficient β is usually expressed as $\beta = \frac{2kT}{f}$, where f is the friction coefficient of the medium, T is the absolute temperature, and k is Boltzmann's constant.

However there are some difficulties with this analogy. First, there is no direct way to relate the properties of the medium, f and T, with the mass parameter ϵ, nor is there an obvious interpretation of the Boltzmann constant for the three bead problem. Hence, macroscopic properties associated with the bead dynamics, such as the mean square displacement of the wall, are difficult to obtain theoretically. Furthermore, there is no *a priori* reason to assume that these features should be independent of ϵ. Equally relevant is the fact that the three bead problem is an extremely low-dimensional dynamical system,

whereas the setting for most classical Brownian studies are very high dimensional, in statistical regimes where ergodicity is assumed. At the other extreme, for $\epsilon \sim 1$, one has two unequal masses colliding with a third very light mass $m_1 > m_2 >> m_3 > 0$, a singular perturbation from the two bead problem. Thus, the parameter ϵ formally connects the two regimes that can be analyzed completely.

The problem can be formulated cleanly in terms of velocities as follows.[9] Before and after each binary collision, conservation of energy and momentum for the system of beads allows us to write the system in matrix form as

$$\mathbf{v}' = \mathbf{M_{ij}}\mathbf{v}, \tag{4.1}$$

where $\mathbf{v} \in \mathcal{R}^3$, $\mathbf{v}' \in \mathcal{R}^3$ are the pre and post-collision velocities, and $\|\mathbf{v}\|^2 = \|\mathbf{v}'\|^2$. $\mathbf{M_{ij}}$ are the collision matrices $\mathbf{M_{12}}$, $\mathbf{M_{23}}$, $\mathbf{M_{13}}$, given explicitly as

$$\mathbf{M_{12}} = \frac{1}{m_{12}} \begin{pmatrix} \mu_{12} & \mu_2 & 0 \\ \mu_1 & \mu_{21} & 0 \\ 0 & 0 & m_{12} \end{pmatrix};$$

$$\mathbf{M_{23}} = \frac{1}{m_{23}} \begin{pmatrix} m_{23} & 0 & 0 \\ 0 & \mu_{23} & \mu_3 \\ 0 & \mu_2 & \mu_{32} \end{pmatrix};$$

$$\mathbf{M_{13}} = \frac{1}{m_{13}} \begin{pmatrix} \mu_{13} & 0 & \mu_3 \\ 0 & m_{13} & 0 \\ \mu_1 & 0 & \mu_{31} \end{pmatrix}$$

with $m_{ij} = m_i + m_j$, $\mu_{ij} = m_i - m_j$, $\mu_i = 2m_i$.

A collision between masses m_i and m_j updates the velocity vector on the nth collision:

$$\mathbf{v^{(n+1)}} = \mathbf{M_{ij}} \cdot \mathbf{v^{(n)}},$$

and a trajectory unfolds after n collisions from its initial velocity vector $\mathbf{v^{(0)}}$ to its final one $\mathbf{v^{(n)}}$ via the linear matrix equation

$$\mathbf{v^{(n)}} = \underbrace{\mathbf{M_{pq}} \cdots \mathbf{M_{kl}} \cdot \mathbf{M_{ij}}}_{n-collisions} \cdot \mathbf{v^{(0)}} \equiv \mathbf{M_n} \cdot \mathbf{v^{(0)}}. \tag{4.2}$$

The indices on the matrices indicate that this is a sequence of collisions between m_i and m_j, m_k and m_l, ..., m_p and m_q which we denote $m_i \rightarrow m_j$, then $m_k \rightarrow m_l$, ..., and finally $m_p \rightarrow m_q$. *Valid* collision sequences are those in which no two particles collide two or more times in a row, which means that for the matrix products shown in eqn (4.2), identical matrices cannot be multiplied two or more times sequentially. A string of n collision matrices associated with a given trajectory is denoted by the matrix $\mathbf{M_n} \in \mathcal{R}^{3X3}$.

To set the stage, we summarize the properties of the collision matrices and their products.

Proposition 1 (Properties of the collision matrices):

1. *The eigenvalues of* $\mathbf{M_{ij}}$ *are given by* $\lambda_1 = 1$, $\lambda_2 = 1$, $\lambda_3 = -1$;

2. The corresponding unit eigenvectors are given by

$$\mathbf{M_{12}}: \quad \xi_1 = \begin{pmatrix} 1 \\ 1 \\ 0 \end{pmatrix}; \quad \xi_2 = \begin{pmatrix} 0 \\ 0 \\ 1 \end{pmatrix}; \quad \xi_3 = \begin{pmatrix} 1 \\ -\frac{m_1}{m_2} \\ 0 \end{pmatrix}$$

$$\mathbf{M_{23}}: \quad \xi_1 = \begin{pmatrix} 0 \\ 1 \\ 1 \end{pmatrix}; \quad \xi_2 = \begin{pmatrix} 1 \\ 0 \\ 0 \end{pmatrix}; \quad \xi_3 = \begin{pmatrix} 0 \\ 1 \\ -\frac{m_2}{m_3} \end{pmatrix}$$

$$\mathbf{M_{13}}: \quad \xi_1 = \begin{pmatrix} 1 \\ 0 \\ 1 \end{pmatrix}; \quad \xi_2 = \begin{pmatrix} 0 \\ 1 \\ 0 \end{pmatrix}; \quad \xi_3 = \begin{pmatrix} -\frac{m_3}{m_1} \\ 0 \\ 1 \end{pmatrix}$$

3. $\mathbf{M_{ij}}$ *can be diagonalized:* $\mathbf{M_{ij}} = \mathbf{T_{ij}} D \mathbf{T_{ij}}^{-1}$

$$\textit{where } D = \begin{pmatrix} 1 & 0 & 0 \\ 0 & 1 & 0 \\ 0 & 0 & -1 \end{pmatrix}; \quad \mathbf{T_{12}} = \begin{pmatrix} 1 & 0 & 1 \\ 1 & 0 & -\frac{m_1}{m_2} \\ 0 & 1 & 0 \end{pmatrix};$$

$$\mathbf{T_{23}} = \begin{pmatrix} 0 & 1 & 0 \\ 1 & 0 & 1 \\ 1 & 0 & -\frac{m_2}{m_3} \end{pmatrix}; \quad \mathbf{T_{13}} = \begin{pmatrix} 1 & 0 & -\frac{m_3}{m_1} \\ 0 & 1 & 0 \\ 1 & 0 & 1 \end{pmatrix}$$

4. The eigenvectors form a orthonormal basis for $\mathcal{R}^3$.

Proposition 2 (Properties of the products of collision matrices):

1. *If* $\mathbf{M_n}$ *is the product of* n *collision matrices, then*

$$\det(\mathbf{M_n}) = \lambda_1^{(n)} \cdot \lambda_2^{(n)} \cdot \lambda_3^{(n)} = (-1)^n$$

2. *The eigenvalues of* $\mathbf{M_n}$ *lie on the unit circle, i.e.*

$$|\lambda_j^{(n)}|^2 = 1, \quad j = 1, 2, 3.$$

3. *One eigenvalue of* $\mathbf{M_n}$ *is given by* $\lambda_1^{(n)} = (-1)^n$, *while the other two are complex conjugates*

$$\lambda_2^{(n)} = \lambda^{(n)}; \quad \lambda_3^{(n)} = \lambda^{(n*)}$$

with $|\lambda^{(n)}|^2 = 1$.

The main tool we use in this paper is an examination of the eigenvalue spectrum associated with the sequence of collision matrices $\mathbf{M_n}$ as the collisions unfold, i.e. for $n = 1, 2, 3, \ldots$. In particular, we consider $\bigcup_n \lambda^{(n)}$ where $\lambda^{(n)} \in \mathcal{C}$ is the complex eigenvalue of $\mathbf{M_n}$ on the unit circle shown in figure 4.2. We will examine this spectral sequence for the parameter range $0 \leq \epsilon \leq 1$, paying particular attention to the singular regimes $\epsilon \sim 0$ and $\epsilon \sim 1$ and how the spectrum *collapses* in the limits $\epsilon \to 0$, $\epsilon \to 1$. This will be contrasted with the spectral distribution for a "typical" value of ϵ far from these two limiting cases.

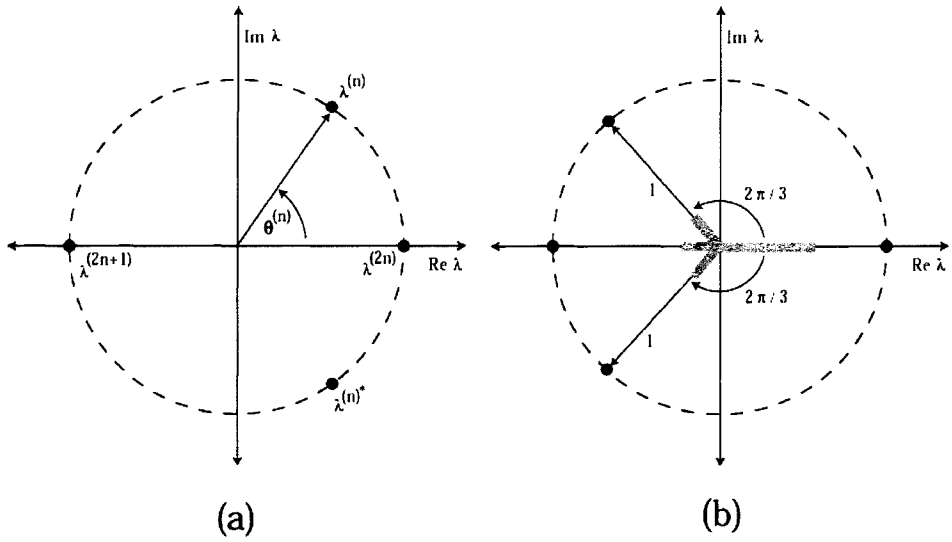

Figure 4.2: Eigenvalue spectrum on the unit circle associated with $\mathbf{M_n}$. (a) The eigenvalues of $\mathbf{M_n}$, for each n, lie at ± 1 and $\lambda^{(n)} \in \mathcal{C}$ and $\lambda^{(n)^*}$; (b) Spectral distribution of $\mathbf{M_n}$, $n = 1, ..., \infty$, for the special case of three beads of equal mass. Half of the eigenvalues are unity, while the other half are evenly divided among the three values shown as indicated by the grey histogram bars.

The spectral distributions of $\mathbf{M_n}$ for the case of equal masses that are well understood [8, 9]. The eigenvalues of $\mathbf{M_{2n+1}}$ are $(-1, 1, 1)$, while the eigenvalues of $\mathbf{M_{2n}}$ are $(1, \lambda, \lambda^*)$, where $\lambda = \exp(2\pi i/3)$ and $\lambda^* = \exp(4\pi i/3)$. Hence, half of the eigenvalues are unity, while the other half are evenly distributed among the three values $\{\exp(2\pi i/3), -1, \exp(4\pi i/3)\}$ as shown in figure 4.2. By contrast, the spectral distribution for a generic case of unequal masses is more complicated. As in the case of equal masses, the eigenvalues of $\mathbf{M_{2n+1}}$ are always $(-1, 1, 1)$. Those of $\mathbf{M_{2n}}$ are now given by $(1, \lambda(n), \lambda^*(n))$, i.e. the complex conjugate eigenvalues are now functions of n. We show a typical spectral distribution for up to $n = 10,000$ collisions in figure 4.3 after removing the eigenvalues at ± 1. As one can see, the distribution is relatively uniform around the circle and gets more uniform if

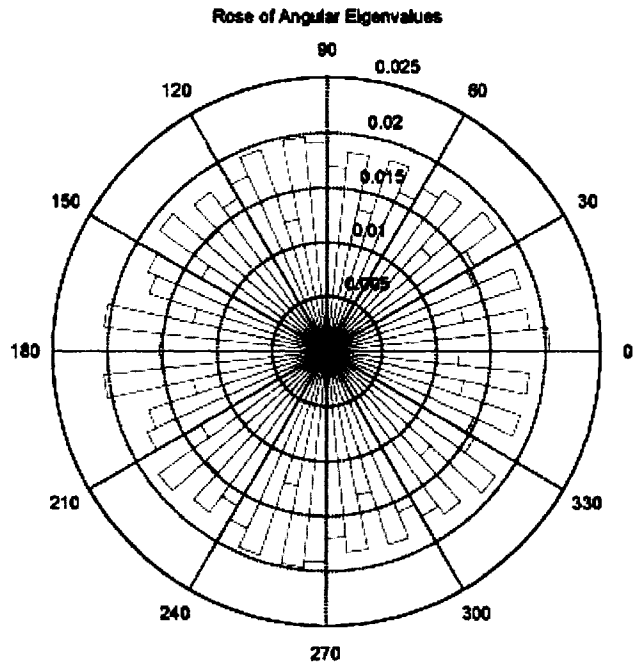

Figure 4.3: Computed histogram of the spectral distribution associated with $\mathbf{M_n}$ for $\epsilon = 0.5$ and 1000 collisions. The eigenvalues at ± 1 have been removed in order to more clearly see the uniformity around the circle.

one takes more collisions. The goal of this paper is to characterize how the distribution collapses to a point spectrum in the limits $\epsilon \to 0$ and $\epsilon \to 1$.

We finish this introductory section by noting that the use of relative angle variables $(\theta_1, \theta_2, \theta_3)$ with constraint $\theta_1 + \theta_2 + \theta_3 = 2\pi$ as shown in figure 4.1, allows us to recast the problem as a billiards problem in a right triangle and a particular collision sequence can then be represented as a trajectory made up of straight line segments inside the triangle. This point of view and results based on it was first advocated in [10] and was further exploited in [9]. Hence, one can restate the goal of this paper as one of quantifying the spectral distributions produced by a chaotic billiard system in a right triangular domain

and to study how the spectrum collapses to a point spectrum in the case when the billiard system becomes integrable.

4.2 Limiting cases

In this section we describe the spectral distributions of the products of collision matrices, $\mathbf{M_n}$, for the two limiting cases $\epsilon = 0$ and $\epsilon = 1$.

4.2.1 $\epsilon = 1$: Two beads with no wall

When $\epsilon = 1$, the system effectively becomes a two bead case with two equal masses $(m_1 = 1, m_2 = 1, m_3 = 0)$ as shown in figure 4.1. The collision matrices $\mathbf{M_{ij}}$ reduce to the following:

$$\mathbf{M_{12}} = \begin{pmatrix} 0 & 1 & 0 \\ 1 & 0 & 0 \\ 0 & 0 & 1 \end{pmatrix}; \quad \mathbf{M_{23}} = \begin{pmatrix} 1 & 0 & 0 \\ 0 & 1 & 0 \\ 0 & 2 & -1 \end{pmatrix}; \quad \mathbf{M_{13}} = \begin{pmatrix} 1 & 0 & 0 \\ 0 & 1 & 0 \\ 2 & 0 & -1 \end{pmatrix}$$

Since there is no third particle $(m_3 = 0)$, M_{12} is the only pertinent collision matrix and this can be reduced to simply the 2 X 2 sub-matrix

$$\mathbf{M_{12}} = \begin{pmatrix} 0 & 1 \\ 1 & 0 \end{pmatrix}.$$

After n collisions, the velocity vector $\mathbf{v^{(n)}}$ is given by

$$\mathbf{v^{(n)}} = \begin{pmatrix} v_1^{(n)} \\ \\ v_2^{(n)} \end{pmatrix} = (\mathbf{M_{12}})^n \begin{pmatrix} v_1^{(0)} \\ \\ v_2^{(0)} \end{pmatrix}.$$

The eigenvalues of $\mathbf{M_{12}}$ are

$$\lambda_1 = 1; \quad \lambda_2 = -1$$

with corresponding eigenvectors, or normal modes:

$$\mathbf{v_t} = \begin{pmatrix} 1 \\ \\ 1 \end{pmatrix} \quad \text{uniform translation,}$$

$$\mathbf{v_b} = \begin{pmatrix} 1 \\ \\ -1 \end{pmatrix} \quad \text{beating.}$$

Note that the beating mode gives rise to a 2-collision periodic orbit since

$$\mathbf{v_b} = \mathbf{M_{12}} \cdot \mathbf{M_{12}} \cdot \mathbf{v_b} = (-1)\mathbf{M_{12}} \cdot \mathbf{v_b} = (-1)^2 \mathbf{v_b} = \mathbf{v_b}.$$

The general solution can be obtained by diagonalizing $\mathbf{M_{12}}$

$$\mathbf{M_{12}} = \mathbf{T}^{-1} \begin{pmatrix} 1 & 0 \\ \\ 0 & -1 \end{pmatrix} \mathbf{T}$$

giving

$$(\mathbf{M_{12}})^n = \mathbf{T}^{-1} \begin{pmatrix} 1 & 0 \\ 0 & (-1)^n \end{pmatrix} \mathbf{T}.$$

Here $\mathbf{T}$ is the invertible matrix whose rows are the eigenvectors of $\mathbf{M_{12}}$. Since a general initial velocity vector $\mathbf{v^{(0)}}$ can be written as a linear combination of the normal modes

$$\mathbf{v^{(0)}} = \alpha_1 \mathbf{v_t} + \alpha_2 \mathbf{v_b},$$

we know that after one collision, the new velocity vector becomes

$$\mathbf{v^{(1)}} = \alpha_1 \mathbf{M v_t} + \alpha_2 \mathbf{M v_b} = \alpha_1 \mathbf{v_t} - \alpha_2 \mathbf{v_b},$$

while after two collisions, it is

$$\mathbf{v^{(2)}} = \alpha_1 \mathbf{M v_t} - \alpha_2 \mathbf{M v_b} = \alpha_1 \mathbf{v_t} + (-1)^2 \alpha_2 \mathbf{v_b}.$$

After n collisions, the velocity vector is

$$\mathbf{v^{(n)}} = \alpha_1 \mathbf{v_t} + (-1)^n \alpha_2 \mathbf{v_b}.$$

If we further make the assumption that the total momentum is zero, i.e. $P \equiv \sum_{i=1}^{N} m_i v_i = 0$, this is equivalent to setting $\alpha_1 = 0$, i.e. eliminating the uniform translation. Also, we can assume $\alpha_2 > 0$. Then we have the simple relation

$$\mathbf{v^{(n)}} = (-1)^n \mathbf{v^{(0)}}.$$

Thus, the velocities reverse sign upon collision, keeping their original magnitude, and all solutions are periodic of period 2. We summarize the eigenvalue distribution in the following:

Proposition 3 (Eigenvalue distribution for $\epsilon = 1$): *For the limit case $\epsilon = 1$, the eigenvalues of the products of the collision matrices $\mathbf{M_n}$ are $((-1)^n, 1)$. Thus, 75% are unity, while the remaining 25% are -1 as shown in figure 4.4.*

Proof:

1. $|\mathbf{M_{12}} - \lambda I| = \begin{vmatrix} -\lambda & 1 \\ 1 & -\lambda \end{vmatrix} = \lambda^2 - 1 = 0$

   $\lambda = \{\pm 1\}$

2. $|\mathbf{M_{12}^2} - \lambda I| = \begin{vmatrix} 1-\lambda & 0 \\ 0 & 1-\lambda \end{vmatrix} = (1-\lambda)^2 = 0$

   $\lambda = \{1, 1\}$

4.2.2 $\epsilon = 0$: Two beads with a wall

When $\epsilon = 0$, the system effectively becomes a wall with two equal masses ($m_1 = \infty, m_2 = 1, m_3 = 1$) as shown in figure 4.1. $\mathbf{M_{ij}}$ reduce to the following collision matrices:

$$\mathbf{M_{12}} = \begin{pmatrix} 1 & 0 & 0 \\ 2 & -1 & 0 \\ 0 & 0 & 1 \end{pmatrix}; \quad \mathbf{M_{23}} = \begin{pmatrix} 1 & 0 & 0 \\ 0 & 0 & 1 \\ 0 & 1 & 0 \end{pmatrix}; \quad \mathbf{M_{13}} = \begin{pmatrix} 1 & 0 & 0 \\ 0 & 1 & 0 \\ 2 & 0 & -1 \end{pmatrix}$$

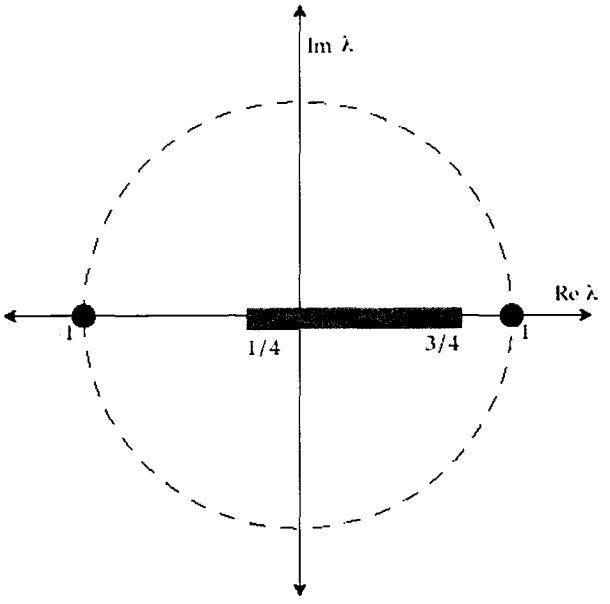

Figure 4.4: Eigenvalue distribution for the limiting case $\epsilon = 1$. In this case, 3/4 of the eigenvalues are $+1$ while the remaining 1/4 are -1.

In general, $\mathbf{M_{12}}$ and $\mathbf{M_{13}}$ represent the particle colliding with the wall (m_2 and m_3 respectively) ending with the same velocity magnitude, but opposite direction as it elastically reflects, hence

$$\mathbf{v}' = \begin{pmatrix} 0 \\ -v_2^{(0)} \\ v_3^{(0)} \end{pmatrix} = (\mathbf{M_{12}}) \begin{pmatrix} 0 \\ v_2^{(0)} \\ v_3^{(0)} \end{pmatrix}$$

$$\mathbf{v}' = \begin{pmatrix} 0 \\ v_2^{(0)} \\ -v_3^{(0)} \end{pmatrix} = (\mathbf{M_{13}}) \begin{pmatrix} 0 \\ v_2^{(0)} \\ v_3^{(0)} \end{pmatrix}.$$

The third collision matrix $\mathbf{M_{23}}$ represents a collision between the two equal masses, hence they simply exchange velocities. This gives

$$\mathbf{v}' = \begin{pmatrix} 0 \\ v_3^{(0)} \\ v_2^{(0)} \end{pmatrix} = (\mathbf{M_{23}}) \begin{pmatrix} 0 \\ v_2^{(0)} \\ v_3^{(0)} \end{pmatrix}.$$

If we again assume the total momentum is zero and the wall has no initial velocity, then since the second and third particles are equal in mass, the velocities of these latter particles must be equal and opposite:

$$P = m_1 v_1 + m_2 v_2 + m_3 v_3 = 0 + v - v = 0$$

which yields

$$\mathbf{v^{(0)}} = \begin{pmatrix} 0 \\ v \\ -v \end{pmatrix}$$

With this initial data, we separate the discussion into two distinct situations shown in figure 4.6, symmetric and asymmetric initial positions.

4.2.3 Symmetric initial positions

If masses m_2 and m_3 have initial positions that are symmetric about m_1 as shown in figure 4.6(a), this becomes the familiar two bead case (albeit a special case since there is

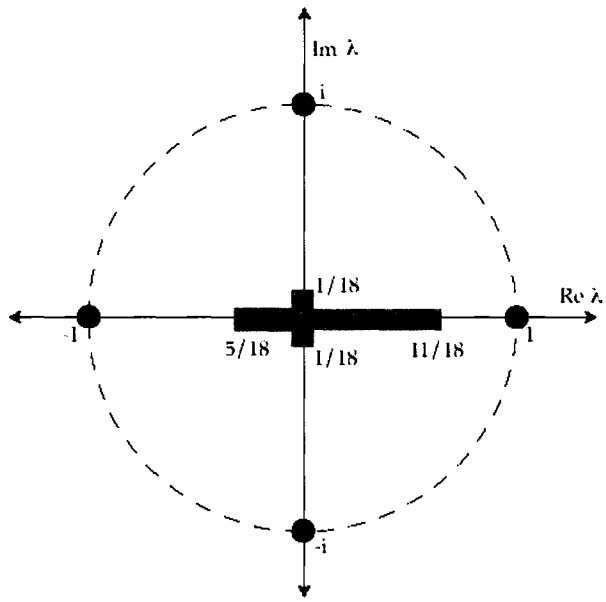

Figure 4.5: Eigenvalue distribution for the limiting case $\epsilon = 0$. In this case, 11/18 of the eigenvalues are $+1$, 5/18 are -1 1/18 are $+i$ and 1/18 are $-i$.

a triple collision). Either the first collision is between m_2 and m_3 opposite m_1 on the ring, or the triple collision at m_1 occurs first. Without loss of generality, assume the former occurs first. Then

$$\mathbf{v}^{(1)} = (\mathbf{M_{23}}) \begin{pmatrix} 0 \\ v \\ -v \end{pmatrix} = \begin{pmatrix} 0 \\ -v \\ v \end{pmatrix}.$$

Since the triple collision has all three particles colliding simulataneously with the m_1 (wall) particle having no velocity and the other two particles having opposite and equal velocities, this is the same as a M_{23} collision. Thus, the orbits are periodic and only

collide at these two locations. We can refer to this as a periodic orbit of *period 2*, since after every second collision, the system returns to it's initial conditions.

$$\mathbf{v}^{(2)} = (\mathbf{M_{23}})^2 \mathbf{v}^{(0)} = \mathbf{I}\mathbf{v}^{(0)} = \mathbf{v}^{(0)}.$$

4.2.4 Asymmetric initial positions

This case is shown in figure 4.6(b). Again assume that the first collision is between m_2 and m_3 (otherwise, the collision sequence would just start at a different place). If the wall is located at the top of the ring, as in figure 4.6, then m_2 and m_3 can either be on one side of the ring or on separate sides. If the initial positions are on the same side of the ring, then the second collision will be with the wall on that same side of the circle. The resulting collision sequence is $M_{12}M_{13}M_{23}M_{13}M_{12}M_{23}$. This results in the identity matrix, and with symmetry is equivalent to the collision sequence that results from all the masses starting on the other side of the ring. This yields

$$M_{12}M_{13}M_{23}M_{13}M_{12}M_{23} = M_{13}M_{12}M_{23}M_{12}M_{13}M_{23} = I.$$

If the initial positions are on opposite sides of the ring, then the second collision will occur with the wall on the same side as where the first collision occurred, or in other words, the side with the initial mass position closest to the wall. If m_2 is closest to the wall, then the resulting collision sequence is again $M_{12}M_{13}M_{23}M_{13}M_{12}M_{23}$. Conversely, if m_3 is the closest to the wall, then the resulting collision sequence is again $M_{13}M_{12}M_{23}M_{12}M_{13}M_{23}$.

Collision No.	Rel. Ang. 1	Rel. Ang. 2	Rel. Ang. 3	Comments
0	$\theta_1^{(0)}$	$\theta_2^{(0)}$	$\theta_3^{(0)}$	initial positions
1	$\theta_1^{(0)} + \frac{\theta_2^{(0)}}{2}$	0	$\theta_3^{(0)} + \frac{\theta_2^{(0)}}{2}$	first non-wall collision
2	0	$2\theta_1^{(0)} + \theta_2^{(0)}$	$\theta_3^{(0)} - \theta_1^{(0)}$	wall collision
3	$\theta_3^{(0)} - \theta_1^{(0)}$	$2\theta_1^{(0)} + \theta_2^{(0)}$	0	wall collision
4	$\theta_3^{(0)} + \frac{\theta_2^{(0)}}{2}$	0	$\theta_1^{(0)} + \frac{\theta_2^{(0)}}{2}$	second non-wall collision
5	$\theta_3^{(0)} - \theta_1^{(0)}$	$2\theta_1^{(0)} + \theta_2^{(0)}$	0	wall collision
6	0	$2\theta_1^{(0)} + \theta_2^{(0)}$	$\theta_3^{(0)} - \theta_1^{(0)}$	wall collision
7	$\theta_1^{(0)} + \frac{\theta_2^{(0)}}{2}$	0	$\theta_3^{(0)} + \frac{\theta_2^{(0)}}{2}$	first non-wall collision

Table 4.1: Scenario 1 positions

Collision No.	Rel. Ang. 1	Rel. Ang. 2	Rel. Ang. 3	Comments
0	$\theta_1^{(0)}$	$\theta_2^{(0)}$	$\theta_3^{(0)}$	initial positions
1	$\theta_1^{(0)} + \frac{\theta_2^{(0)}}{2}$	0	$\theta_3^{(0)} + \frac{\theta_2^{(0)}}{2}$	first non-wall collision
2	$\theta_1^{(0)} - \theta_3^{(0)}$	$2\theta_3^{(0)} + \theta_2^{(0)}$	0	wall collision
3	0	$2\theta_3^{(0)} + \theta_2^{(0)}$	$\theta_1^{(0)} - \theta_3^{(0)}$	wall collision
4	$\theta_3^{(0)} + \frac{\theta_2^{(0)}}{2}$	0	$\theta_1^{(0)} + \frac{\theta_2^{(0)}}{2}$	second non-wall collision
5	0	$2\theta_3^{(0)} + \theta_2^{(0)}$	$\theta_1^{(0)} - \theta_3^{(0)}$	wall collision
6	$\theta_1^{(0)} - \theta_3^{(0)}$	$2\theta_3^{(0)} + \theta_2^{(0)}$	0	wall collision
7	$\theta_1^{(0)} + \frac{\theta_2^{(0)}}{2}$	0	$\theta_3^{(0)} + \frac{\theta_2^{(0)}}{2}$	first non-wall collision

Table 4.2: Scenario 2 positions

Thus, the velocity vectors are periodic. Since, the velocities of m_2 and m_3 are opposite in direction, but equal in magnitude (v), it is simple to calculate the positions of each particle at each collision. Under the first scenario, the resulting positions are shown in table 4.1. The second scenario gives rise to the positions in table 4.2.

Thus, we see that the positions as well as the velocities are periodic for asymmetric cases too. The asymmetric initial positions just lead to orbits of period 6 versus orbits of period 2 for the symmetric initial positions. We summarize the eigenvalue distribution for this

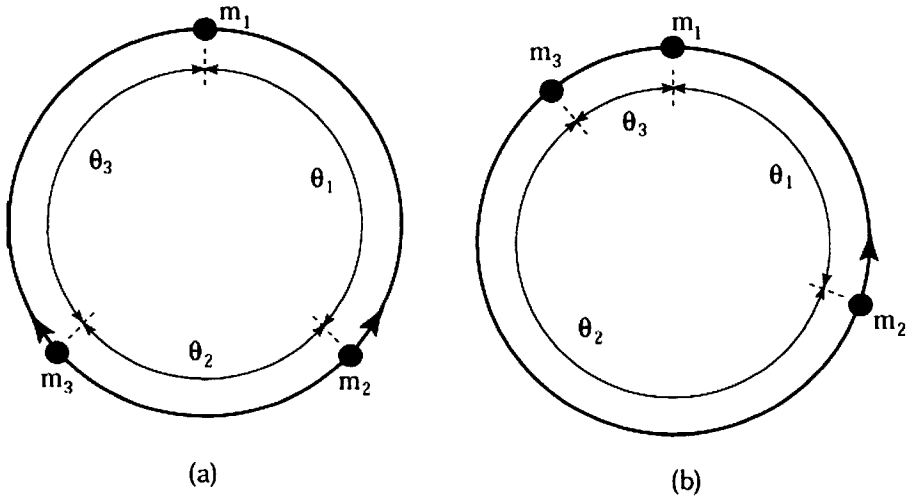

Figure 4.6: (a) Beads m_2 and m_3 are placed symmetrically ($\theta_1 = \theta_3$) with respect to m_1; (b) Beads m_2 and m_3 are placed asymmetrically ($\theta_1 \neq \theta_3$) with respect to m_1.

case as follows:

Proposition 4 (Eigenvalue distribution for $\epsilon = 0$): *For the limit case $\epsilon = 0$, the eigenvalues of the products of the collision matrices $\mathbf{M_n}$ are $(1, 1, -1)$ for n odd. For n even, they unfold as follows: $n = 2 : (1, i, -i)$; $n = 4 : (1, -1, -1)$; $n = 6 : (1, 1, 1)$, repeating in this same sequence. Thus, $11/18$ are unity, $5/18$ are -1, $1/18$ are i and $1/18$ are $-i$ as shown in figure 4.5.*

Proof:

$$1.\ |\mathbf{M_{23}} - \lambda I| = \begin{vmatrix} 1-\lambda & 0 & 0 \\ 0 & -\lambda & 1 \\ 0 & 1 & -\lambda \end{vmatrix} = \lambda^3 - \lambda^2 - \lambda + 1 = 0$$

$$\lambda = \{1, 1, -1\}$$

2. $|\mathbf{M_{13}} \cdot \mathbf{M_{23}} - \lambda I| = \begin{vmatrix} 1-\lambda & 0 & 0 \\ 0 & -\lambda & 1 \\ 2 & -1 & -\lambda \end{vmatrix} = \lambda^3 - \lambda^2 + \lambda - 1 = 0$

$\lambda = \{i, -i, 1\}$

3. $|\mathbf{M_{12}} \cdot \mathbf{M_{23}} - \lambda I| = \begin{vmatrix} 1-\lambda & 0 & 0 \\ 2 & -\lambda & -1 \\ 0 & 1 & -\lambda \end{vmatrix} = \lambda^3 - \lambda^2 + \lambda - 1 = 0$

$\lambda = \{i, -i, 1\}$

4. $|\mathbf{M_{12}} \cdot \mathbf{M_{13}} \cdot \mathbf{M_{23}} - \lambda I| = \begin{vmatrix} 1-\lambda & 0 & 0 \\ 2 & -\lambda & -1 \\ 2 & -1 & -\lambda \end{vmatrix} = \lambda^3 - \lambda^2 - \lambda + 1 = 0$

$\lambda = \{1, 1, -1\}$

5. $|\mathbf{M_{13}} \cdot \mathbf{M_{12}} \cdot \mathbf{M_{23}} - \lambda I| = \begin{vmatrix} 1-\lambda & 0 & 0 \\ 2 & -\lambda & -1 \\ 2 & -1 & -\lambda \end{vmatrix} = \lambda^3 - \lambda^2 - \lambda + 1 = 0$

$\lambda = \{1, 1, -1\}$

6. $|\mathbf{M_{23}} \cdot \mathbf{M_{12}} \cdot \mathbf{M_{13}} \cdot \mathbf{M_{23}} - \lambda I| = \begin{vmatrix} 1-\lambda & 0 & 0 \\ 2 & -1-\lambda & 0 \\ 2 & 0 & -1-\lambda \end{vmatrix}$

$= (1-\lambda)(1+\lambda)^2 = 0$

$\lambda = \{1, -1, -1\}$

7. $|\mathbf{M_{23}} \cdot \mathbf{M_{13}} \cdot \mathbf{M_{12}} \cdot \mathbf{M_{23}} - \lambda I| = \begin{vmatrix} 1-\lambda & 0 & 0 \\ 2 & -1-\lambda & 0 \\ 2 & 0 & -1-\lambda \end{vmatrix}$

$= (1-\lambda)(1+\lambda)^2 = 0$

$\lambda = \{1, -1, -1\}$

8. $|\mathbf{M_{12}} \cdot \mathbf{M_{23}} \cdot \mathbf{M_{12}} \cdot \mathbf{M_{13}} \cdot \mathbf{M_{23}} - \lambda I| = \begin{vmatrix} 1-\lambda & 0 & 0 \\ 0 & 1-\lambda & 0 \\ 2 & 0 & -1-\lambda \end{vmatrix}$

$= (1-\lambda)^2(-1-\lambda) = 0$

$\lambda = \{1, 1, -1\}$

9. $|\mathbf{M_{13}} \cdot \mathbf{M_{23}} \cdot \mathbf{M_{13}} \cdot \mathbf{M_{12}} \cdot \mathbf{M_{23}} - \lambda I| = \begin{vmatrix} 1-\lambda & 0 & 0 \\ 2 & -1-\lambda & 0 \\ 0 & 0 & 1-\lambda \end{vmatrix}$

$= (1-\lambda)^2(-1-\lambda) = 0$

$\lambda = \{1, 1, -1\}$

10. $|\mathbf{M_{13}} \cdot \mathbf{M_{12}} \cdot \mathbf{M_{23}} \cdot \mathbf{M_{12}} \cdot \mathbf{M_{13}} \cdot \mathbf{M_{23}} - \lambda I| = \begin{vmatrix} 1-\lambda & 0 & 0 \\ 0 & 1-\lambda & 0 \\ 0 & 0 & 1-\lambda \end{vmatrix}$

$= (1-\lambda)^3 = 0$

$\lambda = \{1, 1, 1\}$

11. $|\mathbf{M_{12}} \cdot \mathbf{M_{13}} \cdot \mathbf{M_{23}} \cdot \mathbf{M_{13}} \cdot \mathbf{M_{12}} \cdot \mathbf{M_{23}} - \lambda I| = \begin{vmatrix} 1-\lambda & 0 & 0 \\ 0 & 1-\lambda & 0 \\ 0 & 0 & 1-\lambda \end{vmatrix}$

$= (1-\lambda)^3 = 0$

$\lambda = \{1, 1, 1\}$

Finally, we can summarize here with the following:

Theorem 1. *For the two limiting cases $\epsilon = 0$ and $\epsilon = 1$ with P=0 and $v_1^{(0)} = 0$, all orbits are periodic. For $\epsilon = 0$, they are of period 2, whereas for $\epsilon = 1$ they are of period 2 if symmetrically placed about m_1, and period 6 otherwise.*

4.3 Numerical simulations

We summarize the conjectured eigenvalue distribution for the generic case of unequal masses in the diagram shown in figure 4.7. Half of the eigenvalues are unity, $\frac{1}{6}$ are -1, while the other $\frac{1}{3}$ are spread evenly in complex conjugate pairs around the unit circle. By contrast, the eigenvalue distributions for the limiting cases (shown in figures 4.4, 4.5) were discrete. The question we explore in this section is how the uniform spectrum of figures 4.3 and 4.7 collapses to the discrete spectral distributions in the limits $\epsilon \to 0$ and $\epsilon \to 1$. The collapse of the spectral distributions in these singular limits is shown to follow clear scaling behavior. In order to obtain accurate results, care must be taken to sample the available energy surfaces uniformly when compiling the collision sequences.

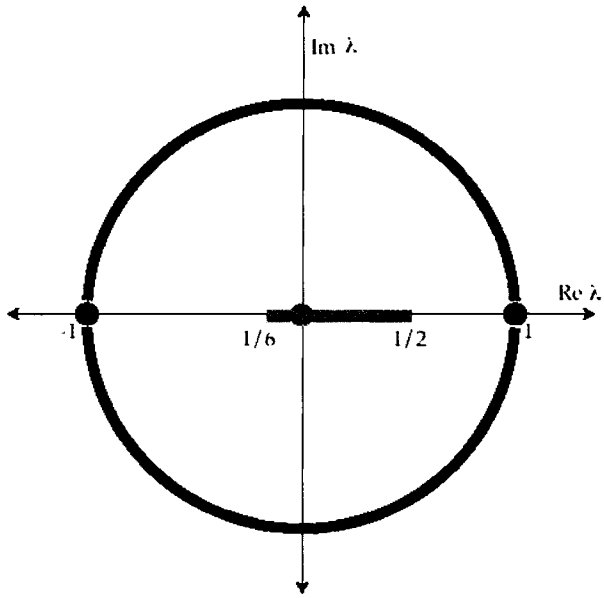

Figure 4.7: Generic spectral distribution associated with $\mathbf{M_n}$ for beads of unequal mass. Half of the eigenvalues are unity, $\frac{1}{6}$ are -1, while the other $\frac{1}{3}$ are spread evenly in complex conjugate pairs around the unit circle. These distributions are shown by the grey histogram bars.

4.3.1 Sampling of energy surface

For a fixed value of the energy, we take a single initial position for each of the particles as we sample over the available velocities. Energy conservation tells us

$$2E = m_1 v_1^2 + m_2 v_2^2 + m_3 v_3^2 = \frac{1}{\epsilon} v_1^2 + v_2^2 + (1-\epsilon) v_3^2, \tag{4.3}$$

and the conservation of momentum equation (while keeping zero momentum (P=0)) yields

$$v_1 = v_3(\epsilon^2 - \epsilon) - \epsilon v_2. \tag{4.4}$$

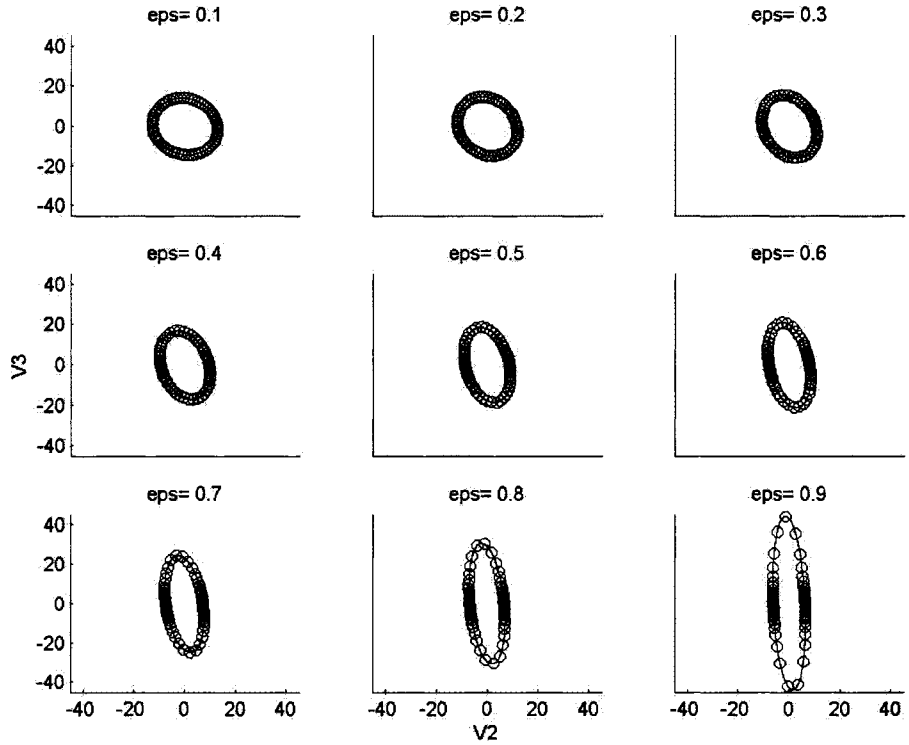

Figure 4.8: Sampling the energy surface for value E=100 and various ϵ. Each point corresponds to a value of (v_2, v_3).

Now, substituting (4.4) into (4.3) and using polar coordinates for the remaining velocities $(v_2 = rcos\theta, v_3 = rsin\theta)$ we obtain

$$2E = r^2[sin^2\theta(\epsilon^3 - 2\epsilon^2 + 1) - 2sin\theta cos\theta(\epsilon^2 - \epsilon) + (1 + \epsilon)cos^2\theta]. \tag{4.5}$$

For fixed values of ϵ, equation (4.5) is a two dimensional energy surface depicted in figure 4.8. This surface is sampled uniformly to generate initial velocity conditions. Thus, we take small step sizes $(\Delta\theta)$ on the energy surface and obtain the velocity distributions which we use at that energy level and value of ϵ.

4.3.2 The emergence of power-law scaling

If the energy level and ϵ values are fixed, a trajectory can be calculated out to a set number of collisions for each set of initial velocity conditions calculated as described above. These trajectories provide an eigenvalue spectrum which can be observed to collapse to the discrete values of the limiting cases ($\epsilon = 0$ and $\epsilon = 1$). This collapse is observed by the transition from uniform eigenvalue distributions to the emergence of Gaussian distributions of eigenvalues around the discrete values of the limiting cases (*i.e.* $1, \frac{\pi}{2}, \pi, \frac{3\pi}{2}$). The variances of these Gaussian distributions exhibit scaling behavior as ϵ approaches a limit. Figures 4.9 and 4.10 show the variances associated with the Gaussian distributions around the discrete spectral values in the limits $\epsilon \to 0$ and $\epsilon \to 1$ respectively.

Figure 4.9 shows the variances around the limiting discrete spectral values in figure 4.5 ($\epsilon \to 0$). These variances demonstrate power law scaling of the form $\sigma^2 \sim \alpha\epsilon^\beta$ where σ^2 is the variance associated with the Gaussian distribution centered around the mean. For the region around $\lambda = 1$, the log-log plots give $\beta \approx 1.5617$, and $\log(\alpha) \approx 0.106$. Similarly, around $\lambda = -1$, $\beta \approx 1.5743$, and $\log(\alpha) \approx 1.0222$. The regions around $\lambda = \pm i$ have identical scaling components of $\beta \approx 1.6273$, and $\log(\alpha) \approx 2.3918$.

This should be contrasted with the scaling around the discrete spectral values in the limit $\epsilon \to 1$ shown in figure 4.4. This regime shows a scaling law of the form $\sigma^2 \sim \beta \log(\epsilon)$. For the region around $\lambda = 1$, the semi-log plot gives $\beta \approx -169,146$, whereas around $\lambda = -1$, $\beta \approx -330,294$.

The following theorem summarizes these results.

Theorem 2. *In the limit as* $\epsilon \to 0$, *the eigenvalue spectrum collapses from uniform to discrete values,* $\lambda \in \{\pm 1, \pm i\}$, *according to power law scalings of the form* $\sigma^2 \sim \alpha\epsilon^{\beta}$. *In the limit as* $\epsilon \to 1$, *the eigenvalue spectrum collapses from uniform to discrete values,* $\lambda \in \{\pm 1\}$, *according to scaling laws of the form* $\sigma^2 \sim \beta \log(\epsilon)$.

4.4 Conclusions

For the generic cases of three unequal masses on a ring which are parametrically bounded by the cases of two beads on a ring with and without a wall, the eigenvalue spectrum generated by the long term dynamics is relatively uniform. This is characteristic of a spectral distribution generated by a chaotic billiard system in a right triangular domain. The boundary cases have a well defined discrete eigenvalue spectrum that is characteristic of the integrable billiard systems they represent. The collapse of the spectrum from uniform to discrete can be represented by scaling laws unique to each boundary case.

This is a simple case representing transition from chaos to an integrable system. Thus, it can be used as a good introduction to much more complicated dynamical systems.

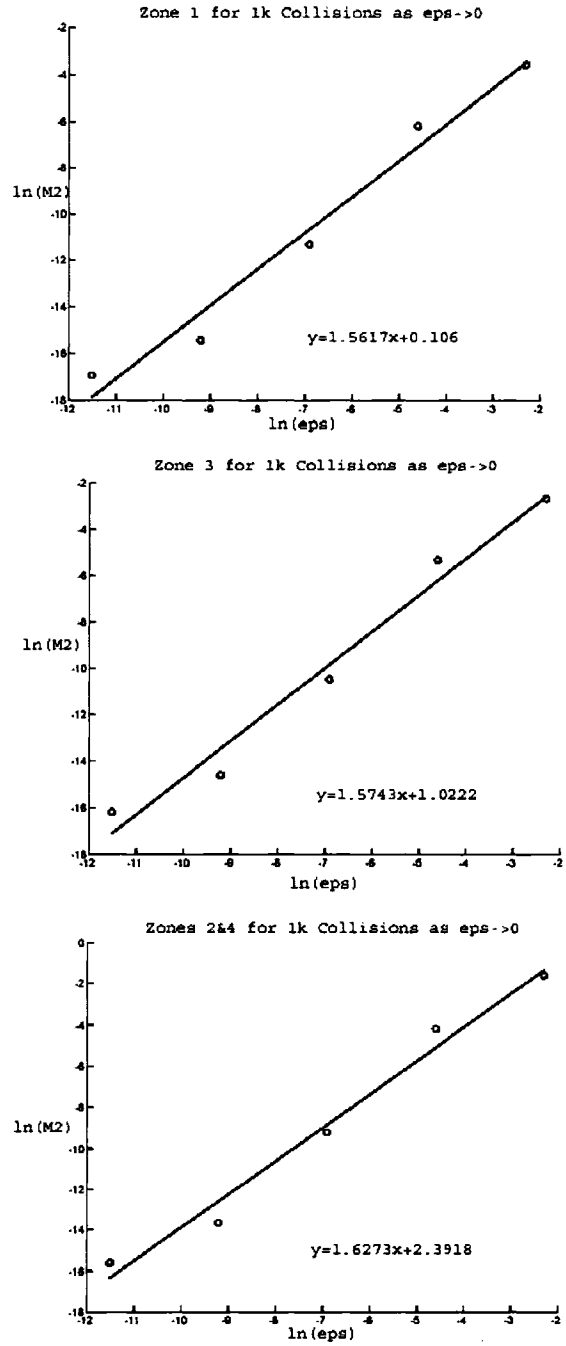

Figure 4.9: Scaling behavior in the limit $\epsilon \to 0$ showing $\sigma^2 \sim \alpha\epsilon^\beta$ where σ^2 is the variance associated with the Gaussian distribution centered around the mean. For Zone 1 ($\lambda = 1$), $\beta \approx 1.5617, \log(\alpha) \approx 0.106$. For Zone 3 ($\lambda = -1$), $\beta \approx 1.5743, \log(\alpha) \approx 1.0222$. For Zone 2 and 4 ($\lambda = \pm i$) have identical scaling exponents $\beta \approx 1.6273, \log(\alpha) \approx 2.3918$.

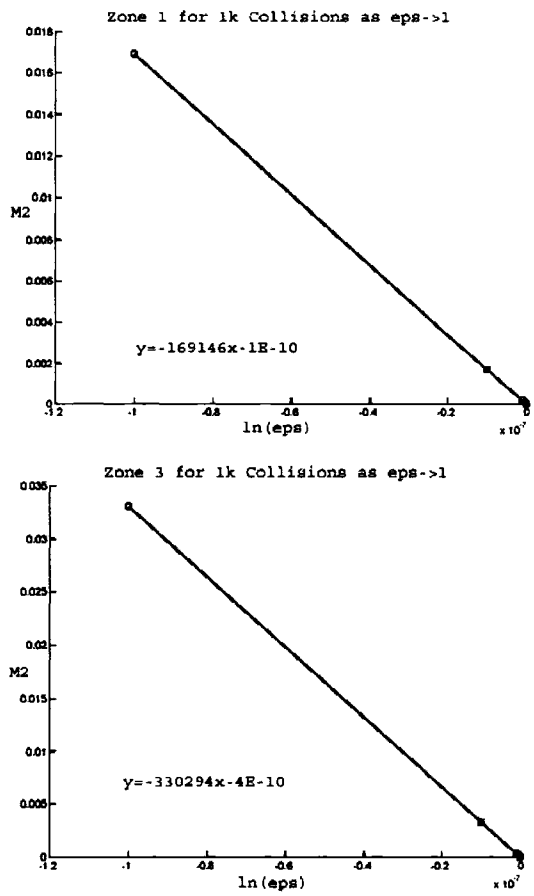

Figure 4.10: Scaling behavior in the limit $\epsilon \rightarrow 1$ showing $\sigma^2 \sim \beta \log(\epsilon)$ where σ^2 is the variance associated with the Gaussian distribution centered around the mean. For Zone 1 ($\lambda = 1$), $\beta \approx -169,146$. For Zone 3 ($\lambda = -1$), $\beta \approx -330,294$.

References

[1] J. S. Bendat and A. G. Piersol. *Random data: analysis and measurement procedures.* John Wiley & sons, 1986.

[2] G. E. P. Box and G. M. Jenkins. *Time Series Analysis.* Holden-Day, 1976.

[3] D. S. Broomhead and E. Gutkin. The dynamics of billiards with no-slip conditions. *Physica D*, 1993.

[4] B. Cipra, P. Dini, S. Kennedy, and A. Kolan. Stability of one-dimensional inelastic collision sequences of four balls. *Physica D*, 1999.

[5] B. Cipra, R. Hanson, and A. Kolan. Periodic trajectories in right triangles. *Phys. Rev. E*, 1995.

[6] P. D. Coddington. Analysis of the suitability of different random number generators. *J. Mod. Phys.*, 1994.

[7] P. Constantin, E. Grossman, and M. Mungan. Inelastic collisions of three particles on a line as a two-dimensional billard. *Physica D*, 1999.

[8] B. Cooley and P. K. Newton. Random number generation from chaotic impact collisions. *Reg. and Chaotic Dyn.*, 2004.

[9] B. Cooley and P. K. Newton. Iterated impact dynamics of n-beads on a ring. *Siam Review*, 2005.

[10] S. L. Glashow and L. Mittag. Three rods on a ring and the triangular billard. *J. Stat. Phys.*, 1997.

[11] E. Gutkin. Billards in polygons: Survey of recent results. *J. Stat. Phys.*, 1996.

[12] R. C. Hibbeler. *Engineering Mechanics, Dynamics.*

[13] D. W. Jepson. Dynamics of a simple many-body system of hard rods. *J. Math. Phys.*, 1965.

[14] H. Kantz and T. Schreiber. *Nonlinear time series analysis.* Cambridge University Press, 1997.

[15] A. Katok and B. Hasselblatt. *Introduction to the modern theory of dynamical systems.* Cambridge University Press, 1995.

[16] J. B. Keller. Impact with friction. *J. Appl. Mech.*, 1986.

[17] J. B. Keller. How many shuffles to mix a deck? *Siam Review*, 1995.

[18] V. K. Kozlov and D. V. Treshchëv. Billards: A genetic introduction to the dynamics of systems with impacts. *translation of mathematical monographs*, 1991.

[19] E. H. Lieb and D. C. Mattis. *Mathematical physics in one dimension: exactly soluble models of interacting particles.* Academic Press, 1966.

[20] S. McNamara and W. R. Young. Inelastic collapse and clumping in a one-dimensional granular medium. *Phys. Fluids*, 1992.

[21] S. McNamara and W. R. Young. Inelastic collapse in two-dimensions. *Phys. Rev. E*, 1994.

[22] T. J. Murphy. Dynamics of hard rods in one-dimension. *J. Stat. Phys.*, 1994.

[23] T. J. Murphy and E. G. D. Cohen. Maximum number of collisions among identical hard spheres. *J. Stat. Phys.*, 1993.

[24] K. Petersen. *Ergodic Theory.* Cambridge University Press, 1983.

[25] Alwyn Scott. *Encyclopedia of Nonlinear Science.* Routledge, 2005.

[26] M. B. Sevryuk. Estimate of the number of collisions of n elastic particles on a line. *translated from Teoreticheskaya i Matematicheskaya Fizika*, 1994.

[27] A. Shudo. Algorithmic complexity of the eigenvalue sequence of a nonintegrable hamiltonian system. *Phys. Rev. Lett.*, Oct. 30, 1989.

[28] J. L. Synge. Maximum number of collisions of elastic particles. *Proc. Roy. Soc. Lond. A*, 1972.

[29] L. Tonks. The complete equation of state of one, two, and three dimensional gases of hard spheres. *Phys. Rev.*, 1936.

[30] G. E. Uhlenbeck and L. S. Ornstein. On the theory of brownian motion. *Physical Rev.*, 1930.

[31] N. D. Whelan, D. A. Gootings, and J. K. Cannizzo. Two balls in one dimension with gravity. *Phys. Rev. A*, 1990.

[32] G. Zaslavsky. Chaotic dynamics and the origin of statistical laws. *Phys. Today*, 1999.

[33] T. Zhou and L. Kadanoff. Inelastic collapse of three particles. *Phys. Rev. E*, 1996.